

**Study on growth of Ga-polar untwinned
semi-polar (10-13) GaN templates
and (10-13) InGaN/GaN quantum wells**

HU Nan

胡楠

Doctoral Dissertation

Study on growth of Ga-polar untwinned semi-polar (10-13) GaN
templates and (10-13) InGaN/GaN quantum wells

Ga 極性非双晶半極性面 (10-13) GaN テンプレート及び (10-13)
InGaN/GaN 量子井戸構造の成長に関する研究

A DISSERTATION SUBMITTED TO DEPARTMENT OF
ELECTRONICS ENGINEERING
SCHOOL OF ENGINEERING
NAGOYA UNIVERSITY
FOR THE DEGREE OF
DOCTOR OF PHILOSOPHY

HU Nan

胡楠

Abstract

Nitride semiconductors based blue LEDs have reached very high efficiencies, even surpassing red arsenide based LEDs. However, the efficiencies of LEDs drop fast towards longer wavelengths. This is called “Green gap”. Polarization induced electrical fields along [0001] are thought as the main reason. To overcome this, semi-polar and non-polar orientations have been studied which feature lower fields. Until now, semi-polar LEDs still have lower efficiencies than common (0001) oriented LEDs.

So far, almost all the studied semi-polar orientations have negative polarization induced fields, which easily induces leaking hole states. This work focusses on the (10-13) orientation. (10-13) GaN based LEDs would have strongly reduced polarization induced electric fields across the active region, but a positive field and thus stronger bound hole states. Therefore, the semi-polar (10-13) orientation has the potential to finally deliver a more efficient green LED.

In this study, the basic building blocks for a (10-13) LEDs are tackled: first the development of high-quality (10-13) GaN templates on m-plane sapphire, and then the growth of high indium containing (10-13) InGaN/GaN quantum well on these templates.

To obtain high quality untwinned Ga-polar (10-13) GaN templates on m-plane sapphire, directional sputtering is combined by metal-organic vapor phase epitaxy (MOVPE). The directional sputtering is great at suppressing twinning, which otherwise easily occurs. There are two steps in directional sputtering, first sputtering of Al and then AlN. It turned out that Al sputtering time is very critical, the Al layer controls the

orientation of the resulting template. By controlling the thickness of Al layer, (10-10) plane, (10-13) plane, (10-14) plane and even (0001) plane GaN can be made. Since Al is easy to be oxidized, AlN layer is needed to be sputtered to protect the Al layer.

Then the sputtered wafers are put into MOVPE. First step is AlN overgrowth. Omitting AlN growth, the following (10-13) GaN would be twinned. The next step is GaN epitaxy which consists of two different conditions. 3 dimensional (3D) growth is to annihilate dislocations by bending on inclined sidewalls followed by 2 dimensional (2D) growth to smoothen the morphology. By controlling the parameters of 3D and 2D growth, less than 550 arcsec FWHM in X-ray rocking curve and less than 30 nm RMS for (10-13) GaN templates have been obtained.

High indium content InGaN quantum wells are an essential part for a green LED. The few reports in literature suggest low indium incorporation on (10-13). This study observed it too. However, higher indium incorporation have been realized using high growth rates.

Content

Abstract	i
Content	iii
List of Figures	v
List of Tables.....	viii
Chapter 1 Introduction.....	1
1.1 Nitride semiconductor and blue LED.....	1
1.2 Green gap and polarization.....	2
1.3 (10-13) orientation.....	6
1.4 Objective and overall structure of this thesis.....	7
1.5 Synthesis systems	8
1.6 Characterization systems	10
References	13
Chapter 2 Directional sputtering and MOVPE growth	18
2.1 Directional sputtering	19
2.2 Substrates.....	22
2.3 Advantage of directional sputtering	25
2.4 Summery	28
References	29
Chapter 3 Al layer sputtering	31
3.1 Time of Al sputtering	31
3.2 Temperature of Al sputtering	36
3.3 Origin of the different orientations.....	39
3.4 Impact of Al parameters on the final GaN layer	41
3.5 Summary	44
References	47
Chapter 4 AlN layer	49
4.1 Use of AlN layer.....	49
4.2 How AlN sputtering affects the initial Al layer.....	53
4.3 Optimization of AlN sputtering.....	55

4.3.1 Optimization of AlN sputtering by Al target.....	55
4.3.2 AlN target and low temperature annealing.....	58
4.4 AlN by MOVPE.....	61
4.5 Summary	62
References	64
Chapter 5 GaN layer.....	66
5.1 Introduction	66
5.2 3D growth and 2D growth.....	68
5.2.1 Optimization of 3D growth	72
5.2.2 Ratio of 3D growth time and 2D growth time.....	74
5.2.3 3D-2D sequences.....	76
5.2.4 AlN/GaN super lattices.....	77
5.3 Characterizations of GaN layer	78
5.3.1 X-ray measurements.....	78
5.3.2 TEM image.....	81
5.4 Summary	83
References	85
Chapter 6 (10-13) InGaN/GaN quantum wells.....	87
6.2 Growth of (10-13) InGaN/GaN quantum well	88
6.3 Characterization of (10-13) InGaN/GaN quantum wells	90
6.4 Summary	92
References	94
Chapter 7 Summary and Outlook.....	96
7.1 Summary	96
7.2 Outlook.....	98
References	100
Appendix	101
Achievements list	106
Acknowledgement.....	109

List of Figures

Figure 1.1 Wurtzite crystal structure of GaN [9].....	2
Figure 1.2 “Green gap” and efficiencies of semi-polar LEDs. Polar LEDs data are taken from [13-15] semi-polar LEDs data are taken from [16-30].....	3
Figure 1.3 Band structure of InGaN/GaN quantum wells with and without polarization [11].	4
Figure 1.4 (a) Polarization function of InGaN/GaN QWs with tilt angle of orientation (b) InGaN/GaN QWs with 25% indium incorporation ratio under different polarization fields [56] (c) PL spectra of (10-1±3) quantum wells [57].	5
Figure 1.5 (a) Sputter chamber and four targets (b) Plasma emission during sputtering	9
Figure 1.6 (a) Showerhead of MOVPE reactor used in this study (b) sketch of the MOVPE in-situ monitor.....	9
Figure 1.7 Omega-2Theta scan of (10-13) InGaN/GaN quantum wells around the 10-13 GaN reflection. The red curve is experiment data and the blue one is calculation data.	12
Figure 2.1 Schematic geometry of directional sputtering.....	20
Figure 2.2 Process flow of template preparation. Step 1 is Al sputtering and step 2 is AlN layer sputtering both with Al target. Step 3 and 4 are AlN and GaN epitaxy in MOVPE.....	21
Figure 2.3 In-plane alignments of (10-13) GaN unit-cells on m-plane sapphire.....	23
Figure 2.4 Top view of (10-13) GaN samples on (a) (001) Si substrate [1] and (b) m-plane sapphire. Microscope pictures of (10-13) GaN samples on (c) (001) Si substrate and (d) m-plane sapphire under 100 magnification.	24
Figure 2.5 X-ray rocking curves of (001) Si substrate sample and m-plane sapphire sample. (10-13 GaN reflection).....	25
Figure 2.6 (a) Orientation of GaN from ϕ -measurements of the skew symmetric GaN (0002) and sapphire (20-24) diffraction (b) and EBSD data on AlN and GaN (b), showing both AlN and GaN have the same surface orientation and are untwinned. (c) In-plane epitaxial relationship between GaN/AlN and m-sapphire	26
Figure 2.7 Side view of GaN layer along $[1-210]_{\text{GaN}}$ direction by HR-STEM result. Right side indicates the relation between Ga and N-planes along $[0001]$ direction for a side view along $[1-210]$	27
Figure 3.1 2θ - ω XRD measurements of samples after overgrown MOVPE (see Chapter 2.1) using different sputter times t_s for the Al layer. The transition is not sharp, and a slight variation in time dependency might be due to change of target. 2θ angles of each plane: (10-13) GaN at 63.42°, (10-14) GaN at 82.04°, (10-10) GaN at 32.39°, (20-20) GaN at 68.80, (30-30) GaN at 112.57. The samples are from 2s, 5s, 8s, 10s and 12s Al sputtering templates respectively.	32
Figure 3.2 Sketch of a four-layer (air-Al-sapphire-air) optical transmission system	33
Figure 3.3 Optical transmission spectra of sputtered Al samples on sapphires with different times in both (a) and (b). (a) Dot lines are calculated curves with different Al thicknesses by using n and k values of Al bulk. (b) Dash lines are also calculated curves with different Al thicknesses but using the ϵ values from [3], which were only available 2.4 nm and 6.2 nm but not for 0.8 nm or 10nm.	34
Figure 3.4 (a) XRR data and (b) growth rates of sputtered Al layer from optical transmission	

data and XRR data.	35
Figure 3.5 2θ - ω XRD measurements of MOVPE overgrown GaN samples on m-plane sapphire substrates under Al sputtering temperature. Under the same sputtering time, surface orientation change with the increased temperature. Al sputter temperatures of examples in this figure are 150°C, 380°C and 620°C respectively.	37
Figure 3.6 Assumption of Al atoms configurations in (a) low temperature mode and (b) high temperature mode.	38
Figure 3.7 Surface morphologies of (a) 500°C Al sputtering sample and (b) 700°C Al sputtering sample.	38
Figure 3.8 Crystallographic relationship of (10-13) and (10-10) AlN on (10-10) m-plane sapphire. For (10-13) AlN, two m-plane sapphire surface unit is need while only one is needed for (10-10) AlN.	40
Figure 3.9 XRD FWHM along the two directions of GaN (a) and tilt angle (b) of the GaN towards [0001] as functions of Al sputter temperature.	42
Figure 3.10 XRD diffraction of a (10-13) GaN layer. (a) wide 2θ - ω scan along $[1-210]_{\text{GaN}}$ direction (b) Symmetric (10-13) rocking curves of the layer scanned along $[30-3-2]_{\text{GaN}}$ and $[1-210]_{\text{GaN}}$ directions.	43
Figure 4.1 Sketch of shadow effect.	49
Figure 4.2 Structures and manufacture flow of each samples. (a) for sample (a), (b) for sample (b) and (c) and (c) for sample (f).	50
Figure 4.3 X-ray phi scan of 0min and 4 min MOVPE AlN buffer layer (without sputtered AlN layer) and subsequent GaN growth. The peaks are the 0002 GaN reflection from the (10-13) GaN layer.	52
Figure 4.4 (a) particles hit on solid material, (b) sample after Al sputtering, (c) sample after nitrogen plasma treatment.	53
Figure 4.5 (a) sketches of each samples. (b) Optical transmission spectra of Al layers sputtered for 8s, Al for 8s followed by 2s or 10s of sputtered AlN, and for 10s of AlN. The minimum values of 8s followed by 2s or 10s of sputtered AlN (arrow position) are shifted from 8s sputtered Al but are also quite different form only sputtering pure AlN.	54
Figure 4.6 Optical microscope pictures of GaN layers on sputtered AlN layers with different sputtering power.	56
Figure 4.7 FWHM of X-ray rocking curves of GaN layers with sputtered AlN layers in different sputtering power. (10-13 GaN reflection).	56
Figure 4.8 Optical microscope pictures of GaN layer with sputtered AlN layers in different sputtering time.	57
Figure 4.9 FWHM of X-ray rocking curves of GaN layers with sputtered AlN layers in different sputtering time. (10-13 GaN reflection)	57
Figure 4.10 ω - 2θ scan of 3:7 N ₂ : Ar ratio sputtered AlN buffer layer sample.	60
Figure 4.11 (a) Structure and manufacture flow the annealed sample. (b) X-ray rocking curves of (10-13) GaN samples with annealing of sputtered AlN layer.	61
Figure 4.12 X-ray (a) rocking curves of (10-13) AlN buffer layer after MOVPE epitaxy and (b) ω - 2θ scan after final GaN growth.	62
Figure 5.1 Morphology by (a) SEM, (b) OM and (c) AFM scan (10 μm \times 10 μm)	66
Figure 5.2 OM pictures of different V/III ratio GaN samples.	67

Figure 5.3 Schematic diagrams of (a) 3D growth mode and (b) 2D growth mode. Red lines stand for threading dislocations.	69
Figure 5.4 Schematics of the semi-polar (10-13) GaN epitaxial structures with three different epitaxy layers. Samples A, B, and C consists of a 2D growth layer, 3D growth layer, and 2D+3D mixed layer, respectively.....	69
Figure 5.5 OM images of the GaN surface of (a) sample A, (b) sample B and (c) sample C. And AFM images of the GaN surface of (d) sample A, (e) sample B and (f) sample C.	71
Figure 5.6 (a) FWHM values (left axis) and RMS values of 10×10 μm (right axis) of 3D growth (10-13) GaN layer with different V/III ratios. AFM images are shown in (b).	73
Figure 5.7 Reflectance curve of in-situ monitor and OM pictures of the different growing step.	75
Figure 5.8 X-ray rocking curves and OM pictures of different 3D growth and 2D growth ratio. (a) and (c) from 26min 3D growth + 11min 2D growth one. (b) and (d) from 34min 3D growth + 6min 2D growth one.	76
Figure 5.9 Sketch of 3D-2D loops.....	77
Figure 5.10 (a) Sketch of sample with AlN/GaN super lattices. (b) and (c) are AFM images of (10-13) GaN samples o/w AlN/GaN super lattices.	78
Figure 5.11 X-ray rocking curve measurement on different points of sample.	79
Figure 5.12 Tilt angle from X-ray rocking curve omega scans.....	80
Figure 5.13 X-ray scanned from different directions.....	80
Figure 5.14 TEM cross section scan from (1-210) orientation, the very visible interface is the AlN to GaN interface, i.e. the surface at the beginning of 3D growth.	81
Figure 5.15 Side view of sapphire substrate and (10-13) AlN layer interface by HR-STEM. (a) is annular dark-field image. While (b), (c) and (d) are fourier transformed images of the AlN area, black area and sapphire area, respectively.	83
Figure 6.1 Indium content of each quantum wells on each orientation from literature.....	88
Figure 6.2 Indium content in quantum wells on both (10-13) plane and c-plane templates. (a) low growth rate mode, (b) high growth rate mode.....	90
Figure 6.3 X-ray RSM of the asymmetric 10-15 GaN reflection of a (10-13) QW.....	91
Figure 6.4 PL spectra of one (10-13) and one (0001) InGaN/GaN quantum wells grown with high growth rate.	91
Figure 6.5 Relationship between PL wavelength and PL FWHM. Blue star is the data from literature [4].....	92

List of Tables

Table 1.1 EQE of each LED with different wavelength from literatures	4
Table 2.1 Previous reports of (10-1±3) GaN	18
Table 2.2 Parameters of whole process.....	22
Table 3.1 Lattice mismatch of m-plane sapphire with respect to (10-1L) AlN.....	40
Table 3.2 Samples made by different Al sputtering parameters	45
Table 4.1 Twinned status of (10-13) GaN layer on different AlN buffer layers	50
Table 4.2 X-ray omega scan results of sputtered c-plane AlN.....	58
Table 4.3 X-ray omega scan results of final (10-13) GaN of with.....	59
Table 4.4 Results of all experiments in this chapter	63
Table 5.1 Growth condition information of V/III ratio GaN samples in Figure 5.2.....	68
Table 5.2 Growth condition information of 3D/2D samples in Figure 5.41	70
Table 5.3 X-ray and RMS results of 2D, 3D and mixed 3D+2D (10-13) GaN samples1	71
Table 5.4 Growth conditions for optimization of 3D-GaN growth1	72
Table 5.5 Parameters of 3D growth and 2D growth after optimization1	76
Table 5.6 X-ray (rocking curve) results of loop samples1	77
Table 5.7 Properties of samples w/o SL buffer layers1	78
Table 5.8 Methods tried to improve the quality of (10-13) GaN Layer1	84
Table 6.1 Growth parameters of InGaN/GaN quantum well	89
Table 6.2 Properties of (10-13) InGaN/GaN quantum wells	93

Chapter 1 Introduction

1.1 Nitride semiconductor and blue LED

The advent of blue light-emitting-diodes (LEDs) at the beginning of 1990s made a big contribution towards energy-saving and a more environment-friendly society. This major breakthrough was enabled by nitride semiconductors InGaN/GaN. These advances to enable GaN LEDs were made by three dedicated Japanese scientists-Isamu Akasaki, Hiroshi Amano, and Shuji Nakamura, who were consequently awarded the 2014 Nobel Prize in Physics “for the invention of efficient blue light-emitting diodes, which have enabled bright and energy-saving white light sources” [1-4]. Their research also initiated the third generation semiconductors. The 2010ies saw a surge in the use of GaN-based LEDs for a wide variety of applications as diverse as traffic lights, TVs, monitors, cell phone display and general lighting. LEDs have become ubiquitous in this modern age. In fact, LEDs are superior to traditional lighting sources in almost all aspects, like efficiency, energy-saving, compactness, device lifetime, safety, cost-effectiveness and above all, eco-friendliness because they do not contain any harmful substances such as mercury [5-9].

This progress relied on metal-organic vapor phase epitaxy (MOVPE) to make the complex layer structures inside these devices. At typical MOVPE growth conditions, GaN crystallizes in the most thermodynamically stable form into the wurtzite structure. As depicted in Figure 1.1, the wurtzite crystallographic structure can be seen as two

hexagonal close-packed sub-lattices, which are shifted with respect to each other along c-axis by $3/8$ of the cell height. Locally, each Ga/N atom is surrounded by 4 atoms of the other element that are arranged at the edges of a tetrahedron.

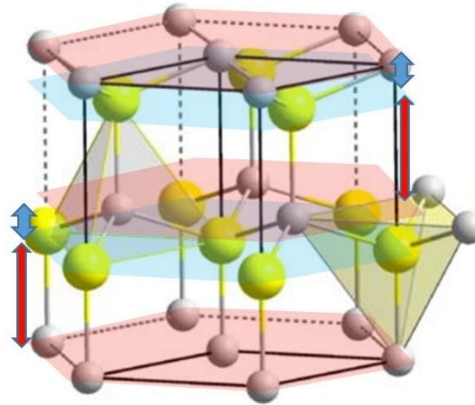


Figure 1.1 Wurtzite crystal structure of GaN [9]

In the GaN crystal, the Ga atom has a very different electronegativity value from the N atom. Since the wurtzite unit cell is lacking inversion symmetry, there is strong spontaneous (and if strained also piezoelectric) polarization along the $[0001]$ direction of GaN [10].

1.2 Green gap and polarization

The efficiency of nitride semiconductor based blue LEDs has been very high. The external quantum efficiency (EQE) of the InGaN LEDs are listed in Table 1.1. But at longer wavelengths, like green and yellow, the EQE of nitride LEDs decreases rapidly (see Figure 1.2 and Table 1.1). Until now, green LEDs still have low efficiencies. This decrease of efficiency is called “green gap”

What’s the reason of this “green gap”? One reason is the polarization. The

radiative recombination rate in InGaN quantum wells (QWs) grown along [0001] is heavily affected by a strong electric field caused by piezoelectric and spontaneous polarization. The resulting red shift of emission is called quantum-confined Stark effect (QCSE) [11, 12]. Figure 1.3 shows the influence of the polarization induced fields on the band structure of an InGaN/GaN QW. Compared to the non-polar case, the energy bands of the polar QWs are tilted by polarization. Then two things happen. First, the wave function maximum of the holes ground state moves away from the maximum of the wave function of the electron ground state. This separation reduces the overlap between the wave functions and hence decreases the radiative recombination rate. Second, the energy gap between electrons and holes is reduced i.e. the luminescence emission shifts to red.

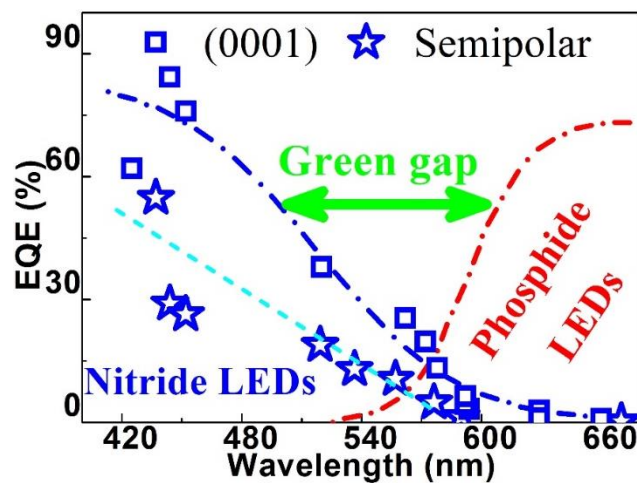


Figure 1.2 “Green gap” and efficiencies of semi-polar LEDs. Polar LEDs data are taken from [13-15] semi-polar LEDs data are taken from [16-30].

To emit at longer wavelengths, more indium is needed. Thus a green LED needs more indium than a blue one. More indium means more strain in the QW, which means a stronger QCSE. While the red shift helps for a green LED, the polarization induced

reduction of radiative efficiency is the dominating effect. So the polarization field is a reason for the lower efficiency of green LEDs.

Table 1.1 EQE of each LED with different wavelength from literatures

C-plane LEDs								
Wavelength (nm)	425	444	452	520	562	572	578	592
EQE (%)	62	84.3	76	38	25.5	19.8	13.3	6.4
Semi-polar plane LEDs								
Wavelength (nm)	437	444	452	519	536	557	576	590
EQE (%)	54.8	29	26.4	18.9	13	10.6	4.9	1.3

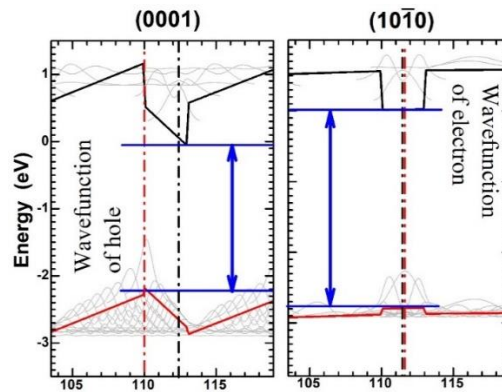


Figure 1.3 Band structure of InGaN/GaN quantum wells with and without polarization [11].

Polarization fields can be reduced if the devices are not oriented along the [0001] direction but tilted, resulting in so-called semi-polar surface orientations (for reduced fields), and non-polar for even completely suppressed fields [31-36]. Figure 1.4 shows sketches of several semi- and non-polar orientations. Among the semi- and non-polar orientations, (10-11), (11-22), (20-21), and (10-10) orientations have been commonly studied. (10-11) GaN layers are always grown on (001) Si by selected area growth [37-

39]. (11-22) orientation, which has the highest efficiency in semi-polar LEDs, can be obtained on m-plane sapphire or (113) Si by selected area growth [40]. (20-21) GaN can be achieved on patterned (22-43) sapphire [41-43]. Nonpolar (10-10) GaN layers have been obtained on (100) LiAlO₂ [44], (10-10) ZnO [45], (10-10) SiC [46, 47] and (112) Si [48] substrates. Also, patterned a-plane sapphire substrates were used, where (10-10) GaN grew on c-plane sidewalls of the patterns [49-50]. Planar growth of (10-10) GaN was realized on m-plane sapphire by different buffer layers, such as low-temperature AlN layer [51, 52], Al₄C₃ layer [53] and low-temperature GaN layers [54].

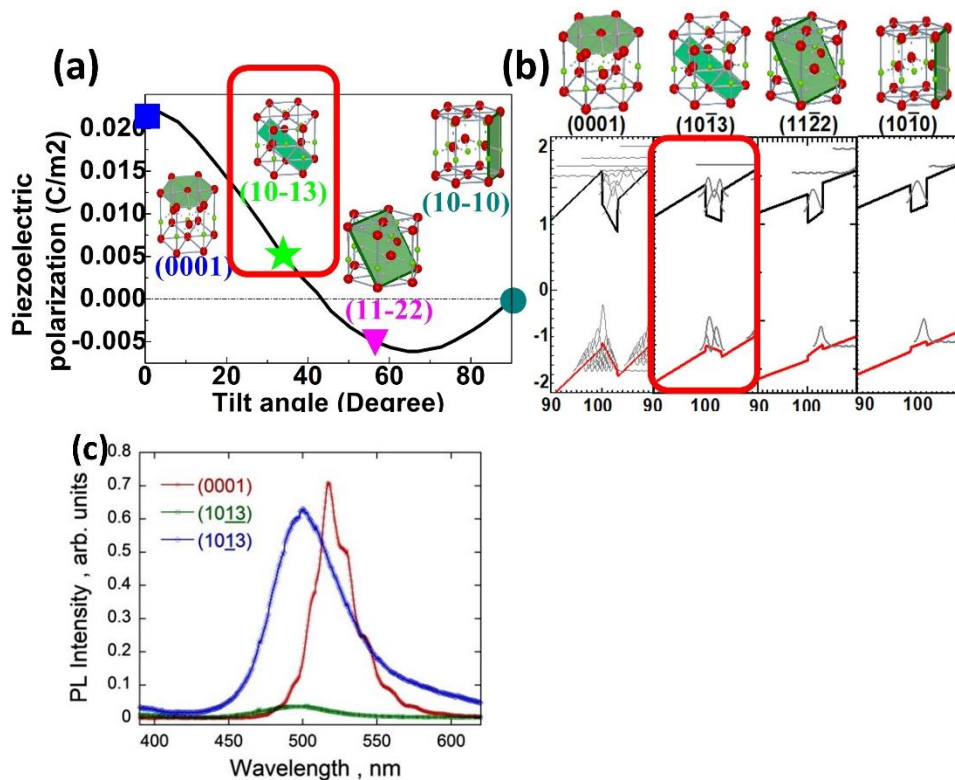


Figure 1.4 (a) Polarization function of InGaN/GaN QWs with tilt angle of orientation (b) InGaN/GaN QWs with 25% indium incorporation ratio under different polarization fields [56] (c) PL spectra of (10-1±3) quantum wells [57].

Apart from optical devices, the different impurities incorporation behaviors on

non- and semi-polar orientations [55] can benefit electronic devices as well. Furthermore, the reduced or absent polarization fields might motivate different approaches for normally-off high power transistors.

For green LEDs, researchers put attention on semi-polar orientations due to an increase of the radiative recombination rate via less tilted bands. Despite large efforts, the efficiencies of semi-polar LEDs are lower than (0001) (or “c-plane”) LEDs until now, as shown by the star symbols in Figure 1.2 and Table 1.1.

1.3 (10-13) orientation

What’s the reason of low efficiencies of semi-polar LEDs? Besides difference of crystalline quality between semi-polar GaN templates and c-plane GaN templates, and probably different point defects. The so-far investigated orientations are the key point.

Figure 1.4 (a) shows the polarization induced by InGaN/GaN QWs with 25% indium content for different orientations. The polarization fields across the QWs can be positive or negative. The commonly studied semi-polar orientations mentioned before and so on have negative polarization.

Figure 1.4 (b) shows the calculated band edges of InGaN/GaN quantum wells of an LED structure with different orientations at zero bias, i.e. photoluminescence conditions [56]. (Zero bias, because the software cannot calculate forward currents correctly.) In case of the (0001) orientation, the polarization field is the strongest and the energy bands are tilted heavily. Despite a small valence band offset, there are many confined holes states. For the (11-22) and (10-10) orientations, the polarization field is

weak or even absent. The energy bands are only tilted due to doping. Due to the small valence band offset, the hole states are little confined and leak out. This reduces the overlap with the electrons, despite the low polarization field. This may be one of the reasons for low efficiencies of the so-far studied semi-polar LEDs.

Based on the above analyses, an orientation which has a weak but positive polarization is desired. The (10-13) orientation can fulfill this. As seen in Figure 1.4 (b), its polarization is weaker than the (0001) orientation and its holes states are better confined than for the negative semi-polar orientations. In addition, it has good lattice match with m-plane sapphire, a common used substrate. Therefore, it can be a promising candidate for green LEDs.

Additionally, Figure 1.4 (c) indicates that Ga-polar (10-13) orientation is much better for LEDs than N-polar (10-1-3) orientation since the direction of polarization field.

1.4 Objective and overall structure of this thesis

The objective of this research is to obtain high quality untwinned Ga-polar (10-13) GaN template and (10-13) InGaN/GaN quantum wells.

Directional sputtering is used to achieve this. It includes Al sputtering and AlN sputtering. After sputtering, an AlN buffer layer and a GaN layer are grown by MOVPE. Each step is optimized in this study.

Chapter 2 introduces the typical procedure of making (10-13) GaN, including directional sputtering and MOVPE growth and how this relates to the substrate.

Chapter 3 focusses on the Al layer. It is made by directional sputtering. Although it is ultrathin, different orientations could be got by changing the Al sputtering condition. Thus, some effort was spent to determine the thickness of the Al layer. Optimization of the Al sputtering for (10-13) orientation is also covered.

Chapter 4 addresses the AlN layers. There are two AlN layers. One is made by directional sputtering, the other one is made by MOVPE. The AlN is a key point of to obtain an untwinned crystal. Furthermore, AlN sputtering affects the previous sputtered Al layer.

Chapter 5 studies the GaN layer, which is grown by MOVPE. The aim is to get both good crystalline quality and a smooth surface of (10-13) semi-polar GaN layer. To achieve the aim, two step (3 dimensional growth and 2 dimensional growth) growth is applied.

Chapter 6 is about (10-13) InGaN/GaN quantum wells, which are grown on the optimized (10-13) GaN templates. The main focus is achieving a high indium content suitable for a green LED. After optimizing growth rate of InGaN layer, 17% indium content (10-13) quantum wells were obtained.

1.5 Synthesis systems

Sputter and MOVPE have been used to synthesize (10-13) GaN templates and InGaN/GaN quantum wells.

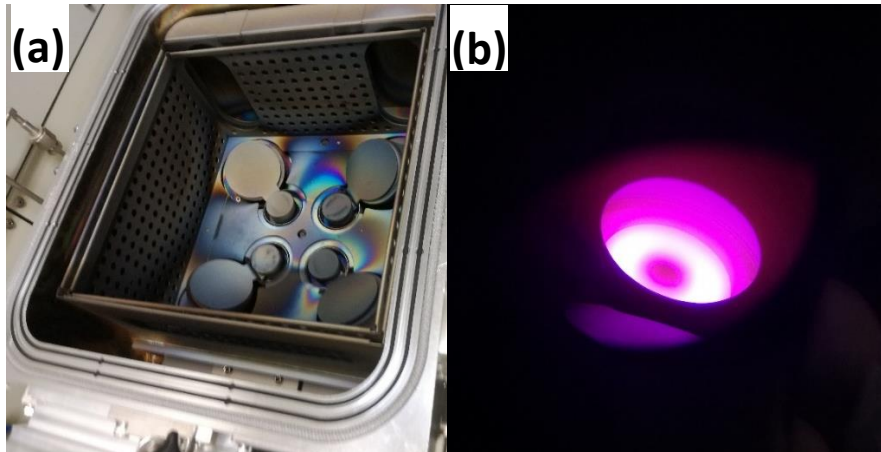


Figure 1.5 (a) Sputter chamber and four targets (b) Plasma emission during sputtering

The sputter system is an ULVAC ACS-4000. It has four targets, as shown in Figure 1.5(a). Three of them have radio frequency (RF) power sources, one has a direct current (DC) power source. Three gases could be used: Ar, N₂, and O₂. The upper limit of the heater is 800°C. Since the thermocouple does not touch the sample holder, the temperature control of the radiative heating requires a strict attention to heater power setting etc. In the directional sputtering experiments, 5N Al target and DC power source are used. The working gases are 5N Ar and purified N₂. Figure 1.5(b) shows the plasma during Al sputtering.

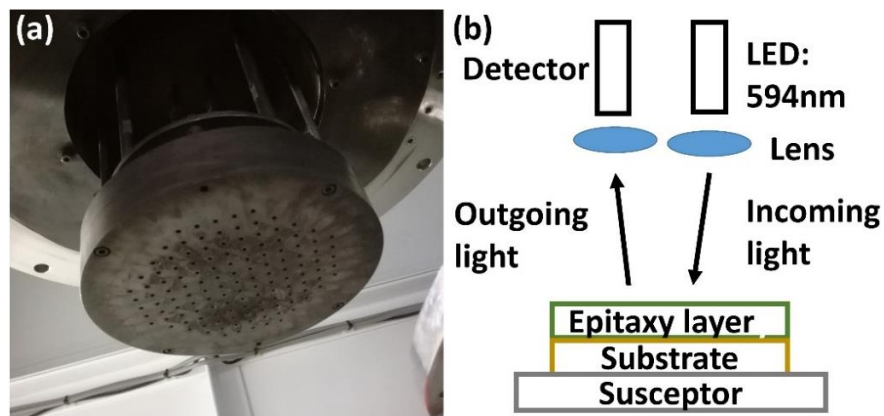


Figure 1.6 (a) Showerhead of MOVPE reactor used in this study¹¹ (b) sketch of the MOVPE in-situ monitor

The MOVPE reactor is a vertical EpiQuest 3x2” close-coupled showerhead reactor. The AlN layer, the GaN layer, and the InGaN/GaN quantum wells were deposited in it. The showerhead is shown in Figure 1.6 (a). The gap between the showerhead and susceptor is 17 mm. A homemade in-situ monitor is inserted on top of one of the holes of the showerhead. Sketch of it is shown in Figure 1.6 (b). The wavelength of LED signal is 594 nm. The light is detected with a CCD, which detects the reflected light of the LED from sample surface together with the black-body radiation of sample and susceptor at high temperature ($>400^{\circ}\text{C}$). The signal recording is then synchronized to the rotations of susceptor to monitor three wafers simultaneously.

For MOVPE, ammonia (NH_3) is used with Trimethylaluminum (TMAI) for AlN deposition and Trimethylgallium (TMGa) for GaN growth. Precursors of for the InGaN layer are Triethylgallium (TEGa) and Trimethylindium (TMIn). Pressure of each bubbler is 101 kPa. The metal-organic are kept in baths at 20°C for TMAI, TMIn and TEGa and at 3°C for TMGa.

1.6 Characterization systems

An Olympus-BX51M optical microscope (OM) is used to quickly measure sample morphology by interference contrast.

The surface topography is examined in detail by atomic force microscope (AFM) in tapping mode (Nanocute, SII NanoTech). Root-mean-square (RMS) value is used to estimate roughness of samples.

Additionally a scanning electron microscope (SEM) (Hitachi SU-70) is used to

measure the morphology of sample. With an attached electron backscatter diffraction (EBSD) (AZtec EBSD system from Oxford instruments) one could measure the surface orientation of the samples (by fitting the Kikuchi line patterns to a given crystal structure). For (10-13) AlN/GaN samples, carbon coating is often needed to avoid charging up in SEM.

Polarity and dislocations of the samples have been measured externally by high resolution scanning transmission electron microscope (HR-STEM) at Evans Analytical Group.

Optical transmission measurements are performed using a Shimadzu UV-2700 UV-VIS spectrophotometer in the 200-900 nm wavelength range. This instrument is mainly used to measure the thickness of the sputtered Al layer described in Chapter 3.1.

Photoluminescence (PL) spectrum is used to characterize the InGaN/GaN quantum wells. In this study, a 325nm He-Cd continuous-wave laser is used at room temperature. Its power is 15mW while beam diameter is less than 1.2mm².

Since orientation also needs to be assessed together with crystalline quality, X-ray diffraction (XRD) is the most often used measurement method in this study. Our XRD machine (PANalytical X'pert) has one X-ray source (CuK α 1 source) and three detectors (open detector, analyser crystal detector, and PixCel 2D detector). To obtain the crystalline quality, an open detector omega scan is used to measure (10-13) semi-polar samples. Since they have a two-fold symmetry, the [0001] direction must be known first. For (10-13) GaN one does an open detector phi scan at of the skew-symmetric 0002 reflection, i.e. at a tilt (chi) angle of 32.04° (tilt angle of (0001) for the (10-13)

GaN orientation) and incident and exit beam at 17.28° . By rotating the sample by 360° (phi scan) one detects a signal when the [0002] direction is 90° to the beam direction. In case of twinning, two peaks separated by 180° are observed. The omega full-width at half maximum (FWHM) of the 0002 reflection and the 10-13 reflection along and perpendicular to [11-20] direction are used as indicator for crystalline quality.

To obtain the thickness of sputtered Al layers also X-ray reflection (XRR) is measured at glancing incidence.

Finally the indium content of InGaN/GaN quantum wells was characterized. For this a wide omega-2Theta scan around the 10-13 reflection was measured, as well as reciprocal space maps around the 10-15 reflection. The satellite peaks of the omega-2Theta scan are compared to a calculated scan to obtain thickness and indium content. Since a semi-polar layer has up to four degrees of strain relaxation, the method from [58] is used to calculate (10-13) InGaN/GaN quantum wells. Figure 1.7 shows an example of both measurement and calculation data.

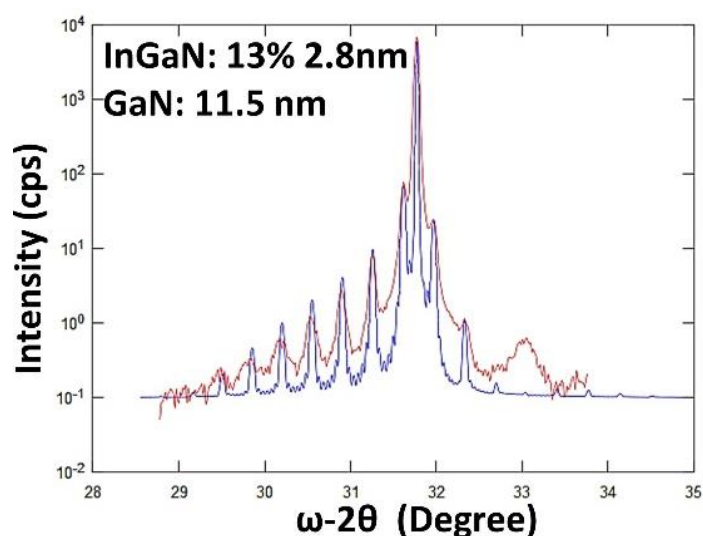


Figure 1.7 Omega-2Theta scan of (10-13) InGaN/GaN quantum wells around the 10-13 GaN reflection. The red curve is experiment data and the blue one is calculation data.

References

- [1] H. Amano, Rev. Mod. Phys. **87**, 1133 (2015).
- [2] I. Akasaki, Rev. Mod. Phys. **87**, 1119 (2015).
- [3] S. Nakamura, Rev. Mod. Phys. **87**, 1139 (2015).
- [4] K.L. Choy, Progress Mater. Sc. **48**, 57 (2013).
- [5] N. Motegi, Y. Kashimoto, K. Nagatani, S. Takahashi, T. Kondo, Y. Mizusawa and I. Nakayama, J. Vac. Sci. Technol. B **12**, 1906 (1995).
- [6] T.Q. Li, S. Noda, Y. Tsuji, T. Osawa and H. Komiya, J. Vac. Sci. Technol. A **20**, 583 (2002).
- [7] I. Goldfrab, J. Pelleg, L. Zevin and N. Croitoru, Thin Solid Films **200**, 117 (1991).
- [8] M. Kobayashi and Y. Doi, Thin Solid Films **54**, 67 (1978).
- [9] http://en.wikipedia.org/wiki/wurtzite_crystal_structure
- [10] T. Langer, H. Pietscher, F. A. Ketzer, H. Jönen, U. Rossow, D. Menzel and A. Hangleiter, Phys. Rev. B **90**, 205302 (2014).
- [11] J. J. Huang, H. C. Kuo and S. C. Shen, Nitride Semiconductor Light-Emitting Diodes (LEDs): Materials, Technologies and Applications, pp. 129-133, Woodhead Publishing, 2014.
- [12] M. A. Maur, A. Pecchia, G. Penazzi, W. Rodrigues and Aldo Di Carlo Phys. Rev. Lett. **116**, 027401 (2016).
- [13] K. A. Bulashevich, A. V. Kulik and S. Y. Karpov, Phys. Status Solidi A, **212**, 914 (2015).
- [14] D. Schiavon, M. Binder, M. Peter, B. Galler, P. Drechsel and F. Scholz, Phys. Status

Solids B **250**, 283 (2013).

[15] A. Chakraborty, B. A. Haskell, S. Keller, J. S. Speck, S. P. DenBaars, S. Nakamura and U. K. Mishra, *Appl. Phys. Lett.* **85**, 5143 (2004).

[16] S. Jung, Y. Chang, K. H. Bang, H. G. Kim, Y. H. Choi, S. M. Hwang and K. H. Baik, *Semicond. Sci. Technol.* **27**, 024017 (2012).

[17] K. Okamoto, H. Ohta, D. Nakagawa, M. Sonobe, J. Ichihara and H. Takasu, *Jpn. J. Appl. Phys.* **45**, L1197 (2006).

[18] M. C. Schmidt, K. C. Kim, H. Sato, N. Fellows, H. Masui, S. Nakamura, S. P. DenBaars and J. S. Speck, *Jpn. J. Appl. Phys.* **46**, L126 (2007).

[19] Y. D. Lin, A. Chakraborty, S. Brinkley, H. C. Kuo, T. Melo, K. Fujito, J. S. Speck, S. P. DenBaars and S. Nakamura, *Appl. Phys. Lett.* **94**, 261108 (2009).

[20] T. Yokogawa and A. Inoue, *Proc. SPIE* **9003**, 900316 (2014).

[21] H. Sato, A. Tyagi, H. Zhong, N. Fellows, R. B. Chung, M. Saito, K. Fujito, J. S. Speck, S. P. DenBaars and S. Nakamura, *Phys. Status Solidi (RRL)* **1**, 162 (2007).

[22] I. L. Koslow, M. T. Hardy, P. Shan Hsu, P. Y. Dang, F. Wu, A. Romanov, Y. R. Wu, E. C. Young, S. Nakamura, J. S. Speck and S. P. DenBaars, *Appl. Phys. Lett.* **101**, 121106 (2012).

[23] Y. Wang, R. Shimma, T. Yamamoto, H. Hayashi, K. Shiohama, K. Kurihara, R. Hasegawa and K. Ohkawa, *J. Cryst. Growth* **416**, 164 (2015).

[24] H. Zhong, A. Tyagi, N. N. Fellows, F. Wu, R. B. Chung, M. Saito, K. Fujito, J. S. Speck, S. P. DenBaars and S. Nakamura, *Appl. Phys. Lett.* **90**, 233504 (2007).

[25] Y. Zhao, J. Sonoda, C. C. Pan, S. Brinkley, I. Koslow, K. Fujito, H. Ohta, S. P. Den

- Baars and S. Nakamura, *Appl. Phys. Express* **3**, 102101 (2010).
- [26] S. Yamamoto, Y. Zhao, C. C. Pan, R. B. Chung, K. Fujito, J. Sonoda, S. P. DenBaars and S. Nakamura, *Appl. Phys. Express* **3**, 122102 (2010).
- [27] I. L. Koslow, J. Sonoda, R. B. Chung, C. C. Pan, S. Brinkley, H. Ohta, S. Nakamura and S. P. DenBaars, *Jpn. J. Appl. Phys.* **49**, 080203 (2010).
- [28] H. Yamada, K. Iso, M. Saito, H. Masui, K. Fujito, S. P. DenBaars and S. Nakamura, *Appl. Phys. Express* **1**, 041101 (2008).
- [29] D. V. Dinh, M. Akhter, S. Presa, G. Kozlowski, D. O'Mahony, P. P. Maaskant, F. Brunner, M. Caliebe, M. Weyers, F. Scholz, B. Corbett and P. J. Parbrook, *Phys. Status Solidi A* **212**, 2196 (2015).
- [30] S. H. Park, *J. Appl. Phys.* **91**, 9904 (2002).
- [31] T. Takeuchi, H. Amano and I. Akasaki, *Jpn. J. Appl. Phys.* **39**, 413 (2000).
- [32] K. Kojima, M. Funato, Y. Kawakami, S. Masui, S. Nagahama and T. Mukai, *Appl. Phys. Lett.* **91**, 255107 (2007).
- [33] M. Kubota, K. Okamoto, T. Tanaka and H. Ohta, *Appl. Phys. Express* **1**, 011102 (2008).
- [34] C. Chitnis, V. Chen, M. Adivarahan, E. Shatalov, V. Kuokstis, J. Mandaili, J. Yang and M. A. Khan, *Appl. Phys. Lett.* **84**, 3663 (2004).
- [35] T. Fujiwara, R. Yeluri, D. Denninghoff, J. Lu, S. Keller, J.S. Speck, S. P. DenBaars and U. K. Mishra, *Appl. Phys. Express* **4**, 096501 (2011).
- [36] S. C. Cruz, S. Keller, T. E. Mates, U. K. Mishra and S. P. DenBaars, *J. Cryst. Growth* **311**, 3817 (2009).

- [37] Y. Honda, N. Kameshiro, M. Yamaguchi and N. Sawaki, *J. Cryst. Growth* **242**, 82 (2002).
- [38] M. Kushimoto, Y. Honda and H. Amano, *Jpn. J. Appl. Phys.* **55**, 05FA10 (2016).
- [39] M. Kushimoto, T. Tanikawa, Y. Honda and H. Amano, *Appl. Phys. Express* **8**, 022702 (2015).
- [40] M. Pristovsek, M. Frentrup, Y. Han and C. J. Humphreys, *Phys. Status Solidi B*, **253**, 61 (2016).
- [41] N. Okada, H. Oshita, K. Yamane and K. Tadatomo, *Appl. Phys. Lett.* **99**, 242103 (2011).
- [42] B. Leung, D. Wang, Y. S. Kuo, K. Xiong, J. Song, D. Chen, S. H. Park, S. Y. Hong, J. W. Choi and J. Han, *Appl. Phys. Lett.* **104**, 262105 (2014).
- [43] J. Song, J. Choi, K. Xiong, Y. Xie, J. J. Cha and J. Han, *ACS Appl. Mater. Interfaces* **9**, 14088 (2017).
- [44] P. Waltereit, O. Brandt, A. Trampert, H. T. Grahn, J. Menniger, M. Ramsteiner, M. Reiche and K. H. Ploog, *Nature* **406**, 865 (2000).
- [44] A. Kobayashi, S. Kawano, Y. Kawaguchi, J. Ohta and H. Fujioka, *Appl. Phys. Lett.* **90**, 041908 (2007).
- [45] N. F. Gardner, J. C. Kim, J. J. Wierer, Y. C. Shen and M. R. Krames, *Appl. Phys. Lett.* **86**, 111101 (2005).
- [46] B. Imer, F. Wu, M. D. Craven, J. S. Speck and S. P. DenBaars, *Jpn. J. Appl. Phys.* **45**, 8644 (2006).
- [47] X. Ni, M. Wu, J. Lee, X. Li, A. A. Baski, Ü. Özgür and H. Morkoç, *Appl. Phys.*

Lett. **95**, 111102 (2009).

[48] N. Okada, Y. Kawashima and K. Tadatomo, Appl. Phys. Express **1**, 1111011 (2008).

[49] K. Okuno, Y. Saito, S. Boyama, N. Nakada, S. Nitta, R. G. Tohmon and N. Shibata, Appl. Phys. Express **2**, 3 (2009)

[50] N. Okada, Y. Kawashima and K. Tadatomo, Phys. Status Solidi A **206**, 1164 (2009)

[51] R. Armitage and H. Hirayama, Appl. Phys. Lett. **92**, 1 (2009).

[52] D. V. Dinh, H. Amano and M. Pristovsek, J. Cryst. Growth **502**, 14 (2018).

[53] H. Sasaki, H. Sunakawa, N. Sumi, K. Yamamoto and A. Usui, J. Cryst. Growth **311**, 2910 (2009).

[54] H. J. Lee, K. Fujii, T. Goto, T. Yao and J. Chang, Appl. Phys. Lett. **98**, 071904 (2011).

[55] M. Pristovsek, C. J. Humphreys, S. Bauer, M. Knab, K. Thonke, G. Kozlowski, D. O'Mahony, P. Maaskanta and B. Corbett, Jpn. J. Appl. Phys. **55**, 05FJ10 (2016).

[56] Calculated by Prof. Markus Pristovsek (Designated professor at International Research Section, iMaSS) and Dr. Duc Van Dinh (Researcher at International Research Section, iMaSS)

[57] D. D. Koleske, S. R. Lee, M. H. Crawford, M. E. Coltrin and P. T. Fini, Sandia Report, SAND2013-5065 (2013).

[58] F. Oehler, M. E. Vickers, M. J. Kappers and R. A. Oliver, J. Appl. Phys. **114**, 053520 (2013).

Chapter 2 Directional sputtering and MOVPE growth

There are very few reports on the preparation of Ga-polar (10-13) GaN [1-4]. Single phase N-polar (10-1-3) GaN has been grown on (110) spinel by hydride vapor phase epitaxy (HVPE) [5]. A few more reports exist on N-polar (10-1-3) GaN on m-plane sapphire because it is almost lattice matched to m-plane sapphire [6, 7]. However, the (10-10) sapphire surface has the same bond configuration along $[1-210]_{\text{sapphire}}$ and $[-12-10]_{\text{sapphire}}$ directions, thus, there are two possible orientations for the [0001] direction of (10-1 \pm 3) GaN [4]. This leads to an inherent twinning of (10-1 \pm 3) GaN on m-plane sapphire, which is hard to overcome [8]. Furthermore, N-polar (10-1-3) GaN layers are usually obtained in MOVPE due to sapphire nitridation, with one irreproducible exception [2]. Table 2.1 shows the results from reports.

Table 2.1 Previous reports of (10-1 \pm 3) GaN

Polarity	N-polar	N-polar	N-polar	Ga-polar
Phase	Single	Single*	Twinned/single	Single
Substrate	Spinel	M-plane sapphire	M-plane sapphire	(100) Si
Growth method	HVPE	HVPE	MOVPE	Directional sputtering + MOVPE

*Not checked in some reports.

Directional sputtering is the method to realize untwinned Ga-polar (10-13) GaN. In this chapter, parameters and substrate of directional sputtering will be introduced. Several measurements also will confirm that the samples by directional sputtering and MOVPE on m-plane sapphire are really untwinned Ga-polar (10-13) GaN.

2.1 Directional sputtering

Sputtering is a common used method for thin film deposition [9]. It also has been used in nitride semiconductors for long time [10]. For example, pulsed sputtering is used to fabricate GaN-based LEDs, HEMTs and MISFETs [11]. High-quality AlN thin film can be made by AlN sputtering followed by high temperature face-to-face annealing [12, 13]. Directional sputtering method, which is named by its inventors, was firstly used to deposit semi-polar AlN and GaN on (100) Si substrates by Dr. Hojun Lee (Amano lab, Nagoya University) [3]. (10-13) and (10-15) orientations could be obtained via this method at that time.

The directional sputtering was performed using a direct current power source magnetron sputtering system. Sputtering target was a two-inch 5 N aluminum target while 5N argon or purified N₂ were used as sputtering gas. The m-plane sapphire substrates were used as received.

The substrates were loaded into the sputtering chamber so that the [1-210]_{sapphire} direction pointed towards the Al target, which put the incident angle of Al target at 35° off the normal axis (Figure 2.1). This range of angles is close to the angle of 32.04° between the (0001) and (10-13) planes of GaN. The distance to the target was about 250 mm, which is fixed by the machine.

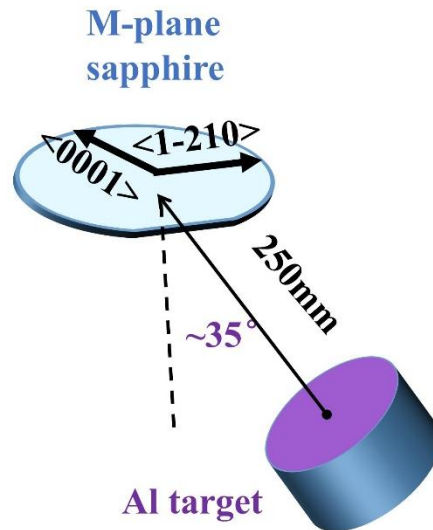


Figure 2.1 Schematic geometry of directional sputtering.

First, a very thin layer of Al was sputtered (about 1 nm, see Chapter 3.1) on the m-plane sapphire substrate with argon plasma at 300°C and 0.55 Pa chamber pressure. By changing the Al sputtering parameters, other orientations can also be obtained, such as the (10-10) orientation (see Chapter 3). Afterwards, a 5-10 nm thick AlN layer was sputtered at 650°C using nitrogen plasma at a chamber pressure of 0.2 Pa. High temperatures help to improve the AlN quality [14, 15]. Thus the chamber temperature was heat up to almost the upper limit of the machine after Al sputtering. However, the melting point of Al metal is about 660°C. To protect the Al layer from melting at high temperature during the ramping to the AlN sputtering step, nitrogen plasma is used to nitride the wafer surface at 300°C after Al sputtering before heating up.

After sputtering, the samples were loaded into MOVPE reactor to grow AlN and then GaN. TMAI, TMGa and NH₃ were used as precursors. The carrier gas was hydrogen while the total flow rate was 15000sccm. The surface was stabilized by NH₃ during the ramping up to 1250°C, with an NH₃ partial pressure of 700 Pa and a total H₂

pressure of 5 kPa. After temperature stabilization, about 50-100 nm of AlN was grown with a V/III ratio of 80 and an NH₃ partial pressure of 34 Pa. The temperature was then reduced to 1100°C, and the pressure was set to 10 kPa. GaN layers were usually grown for 1 hour with a growth rate of about 10μm/h and V/III ratios <150. The growth condition information is listed in Table 2.2. More on the GaN growth will be in Chapter 5.

Figure 2.2 shows the whole process of semi-polar templates manufacture. Step 1 and step 2 are done in sputtering chamber, and are called directional sputtering. Step 3 and step 4 are done in MOVPE.

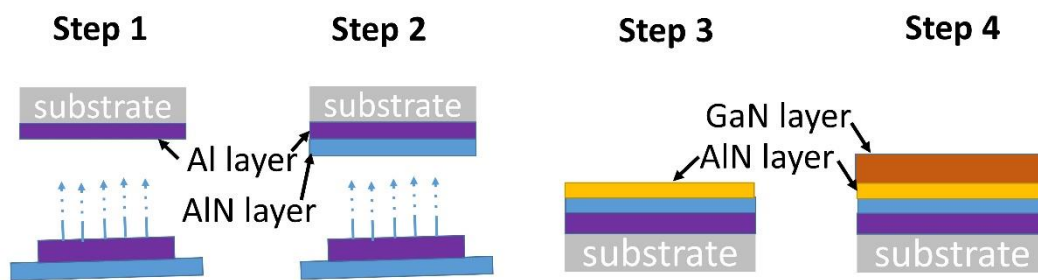


Figure 2.2 Process flow of template preparation. Step 1 is Al sputtering and step 2 is AlN layer sputtering both with Al target. Step 3 and 4 are AlN and GaN epitaxy in MOVPE.

Growth parameters are shown in Table 2.2. Several parameters of GaN growth are indicated a range, since different parameters have different effects. Chapter 5 will explain this in detail. Both Figure 2.2 and Table 2.2 just show the basic process of samples. To improve the quality, some techniques have been applied, such as annealing and short period AlN/GaN superlattices. These techniques will also be discussed in following chapters.

Table 2.2 Parameters of whole process

Directional sputtering			
Step	Al sputtering	AlN sputtering	
Target	Al target (2inch, round)	Al target (2inch, round)	
Sputter time	0-15s 5-8s for (10-13) orientation	60s	
Flow	Ar, 3570 μ mol/min	N ₂ , 2230 μ mol/min	
Chamber pressure	0.55Pa	0.2Pa	
Sputter power	DC, 275W	DC, 275W	
Growth temperature	200-700°C 250-550°C for (10-13) orientation	650°C	
MOVPE growth			
Step	AlN deposition	GaN deposition*	GaN deposition**
Precursors	TMAI, NH ₃	TMGa, NH ₃	TMGa, NH ₃
Chamber pressure	5kPa	5-10kPa	10kPa
Carrier gas	H ₂	H ₂	H ₂
Total flow	15000sccm	15000sccm	15000sccm
V/III ratio	80	10-150	28.6
NH ₃ partial pressure	34Pa	136Pa	202Pa
MO partial pressure	0.43Pa	3.53-7.05Pa	7.05Pa
Growth temperature	1250°C	1080-1180°C	1100°C
Growth time	10min	20-60min	60min

* Overview of GaN growth conditions in this thesis. ** GaN growth conditions (From Chapter 2-4) before 2D-3D growth optimization (Chapter 5).

2.2 Substrates

Before this work, untwinned (10-13) GaN layers were reported on (001) Si by directional sputtering [3]. The FWHM of the X-ray rocking curve of these layers is relatively broad, i.e., more than 2000 arcsec. Even after epitaxial lateral overgrowth the FWHM was still 1000 arcsec [4]. Furthermore, cracking of the layers is a challenge due to the large mismatch in thermal expansion coefficient between Si and GaN and the anisotropic strain relaxation mechanism of semi-polar GaN.

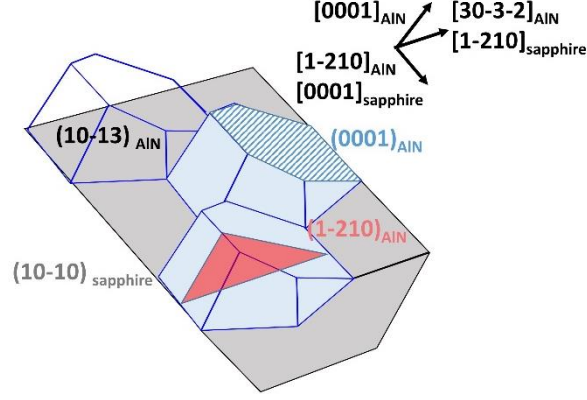


Figure 2.3 In-plane alignments of (10-13) GaN unit-cells on m-plane sapphire.

M-plane sapphire was used instead of Si wafers in this work since m-plane sapphire and (10-13) AlN (or GaN) have lower lattice mismatch. Figure 2.3 shows surface unit cells of (10-13) AlN on indicate the crystallographic alignment since AlN buffer layer touch the m-plane sapphire substrates directly in this study. The crystal relationship between m-plane sapphire and AlN is best matched at $[11-20]_{\text{AlN}} // [0001]_{\text{Al}_2\text{O}_3}$ and $[30-3-2]_{\text{AlN}} // [1-210]_{\text{Al}_2\text{O}_3}$. The resulting mismatch for the tensile stressed AlN epitaxy layer is

$$f_{[0001]}^{\text{Al}_2\text{O}_3} = \frac{4 \cdot a_{\text{AlN}} - c_{\text{Al}_2\text{O}_3}}{c_{\text{Al}_2\text{O}_3}} = 4.7\%$$

Perpendicular, along the $[1-210]_{\text{sapphire}}$ direction, the lattice mismatch is given by the tilt of the (10-1L) orientated unit cells:

$$f_{[1-210]}^{\text{Al}_2\text{O}_3} = \frac{\frac{3}{2} \cdot dc' - 2 \cdot a_{\text{Al}_2\text{O}_3}}{2 \cdot a_{\text{Al}_2\text{O}_3}}$$

The translation period along the tilted AlN c-axis is given by

$$dc' = \sqrt{\frac{3 \cdot a_{\text{AlN}}^2}{4} \cdot L^2 + c_{\text{AlN}}^2} \quad (|L| \leq 2)$$

and

$$dc' = \sqrt{3 \cdot a_{\text{AlN}}^2 + \frac{4 \cdot c_{\text{AlN}}^2}{L^2}} \quad (|L| \geq 2)$$

For (10-13) AlN the unit cell is compressively strained by -0.8%. This is the lowest lattice mismatch along $[1-210]_{\text{sapphire}}$ for all (10-1L) AlN orientations [7]. Based on the lattice mismatch values, m-plane sapphire should be an excellent substrate for (10-13) AlN/GaN.

Experimental results confirmed this. Both (001) Si and m-plane sapphire were used to produce semi-polar GaN templates by directional sputtering and MOVPE growth using exactly the same conditions. Figure 2.4 (a) and (b) show the result. The optical microscope images (Figure 2.4 (c) and (d)) show obvious crack lines on the (001) Si substrate sample but not on the m-plane sapphire sample.

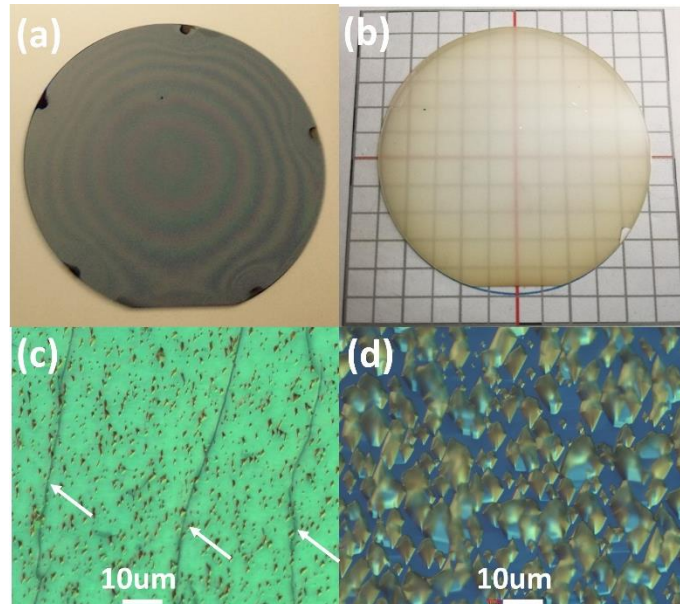


Figure 2.4 Top view of (10-13) GaN samples on (a) (001) Si substrate [1] and (b) m-plane sapphire. Microscope pictures of (10-13) GaN samples on (c) (001) Si substrate and (d) m-plane sapphire under 100 magnification.

X-ray diffraction was also measured for these two samples. The rocking curves of

(10-13) reflection of these two samples in Figure 2.5 show a much narrower FWHM (about 800 arcsec) for then m-plane sample than the (001) Si substrate sample (about 2800 arcsec).

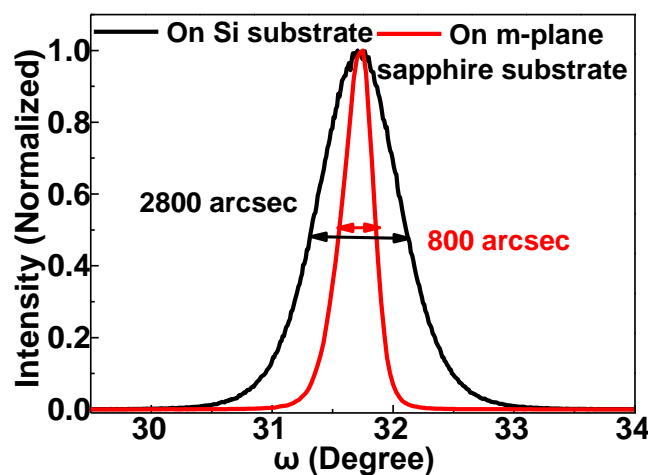


Figure 2.5 X-ray rocking curves of (001) Si substrate sample and m-plane sapphire sample. (10-13 GaN reflection)

Both lattice mismatch analysis and experimental results demonstrate that m-plane is a better substrate of (10-13) GaN/AlN than (001) Si wafer.

2.3 Advantage of directional sputtering

It is necessary to verify that the samples on m-plane sapphire substrate are untwinned as well as Ga-polar (10-13) orientation. For this, the samples were measured by XRD, EBSD and STEM.

The surface orientation of the AlN and GaN layers was measured by XRD and EBSD. The data are summarized in Figure 2.6. Only a single peak appears for GaN in XRD for an azimuthal scan of the skew-symmetric (0002) diffraction (Figure 2.6 (a)), i.e. there is no twinning. This is confirmed by the EBSD data in Figure 2.6 (b), which

only shows a single hexagon for the (10-13) GaN diffraction. (Twinning would show up as a second hexagon rotated by 30° .) Apparently, the directional sputtering of the initial layer provided enough selectivity to suppress the twin, which is very likely, since directional sputtering selects even one of four orientation on Si (001) [4, 13, 14]. The selection mechanism is probably related to shadowing, i.e. columnar growth towards the direction of the sputter target, which reduces the rate of columns not pointing in other directions.

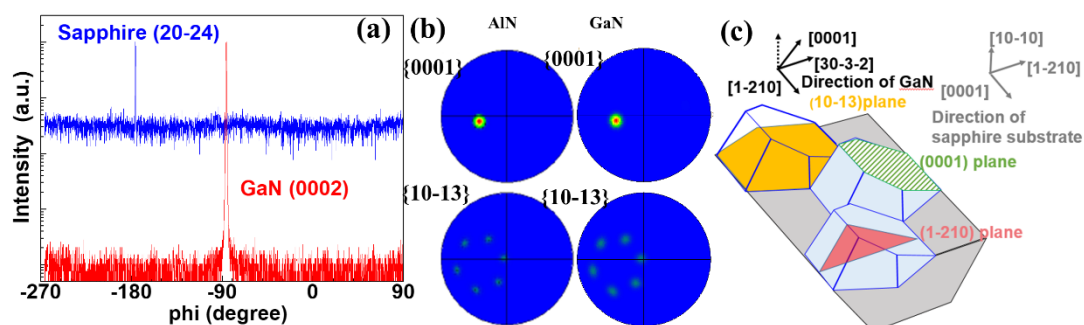


Figure 2.6 (a) Orientation of GaN from ϕ -measurements of the skew symmetric GaN (0002) and sapphire (20-24) diffraction (b) and EBSD data on AlN and GaN (b), showing both AlN and GaN have the same surface orientation and are untwinned. (c) In-plane epitaxial relationship between GaN/AlN and m-sapphire

The substrate is important though. If the sapphire is rotated so that $[0001]_{\text{sapphire}}$ points to the target, (11-22) despite a tilt of (0001) GaN plane of 58° can be obtained. This is somewhat expected, since also (11-22) matches interface m-plane sapphire. (See Appendix 1) With other alignments multiple orientations are got, usually dominated by twinned (0001) together with semi-polar or non-polar contributions. Since the (11-22) plane has been widely studied [16-19] and has negative polarization in InGaN/GaN QWs, it was not further studied in this work.

Azimuthal scans confirm that $[1-210]_{\text{GaN}}$ is parallel to $[0001]_{\text{sapphire}}$. This alignment (as shown in Figure 2.6(c)) is expected, since it minimizes the strain between m-plane sapphire and (10-13) surface unit cells. The lattice mismatch between $[30-3-2]_{\text{AlN}}$ and $[1-210]_{\text{sapphire}}$ is -0.83% while it is -4.23% along $[1-210]_{\text{AlN}}$ and $[0001]_{\text{sapphire}}$ over four AlN lattice units .

To determine the polarity of the samples, a side view of (1-210) GaN was measured roughly 200 nm above the sapphire interface by HR-STEM. The Ga atom planes in Figure 2.7 are close to the N planes along the $[000-1]_{\text{GaN}}$, which indicates that the $[0001]$ direction was tilted by 32.04° to the surface normal. This confirms Ga-polar (10-13) GaN. Most likely the initial Al starting layer from directional sputtering favored the metal-polar orientation.

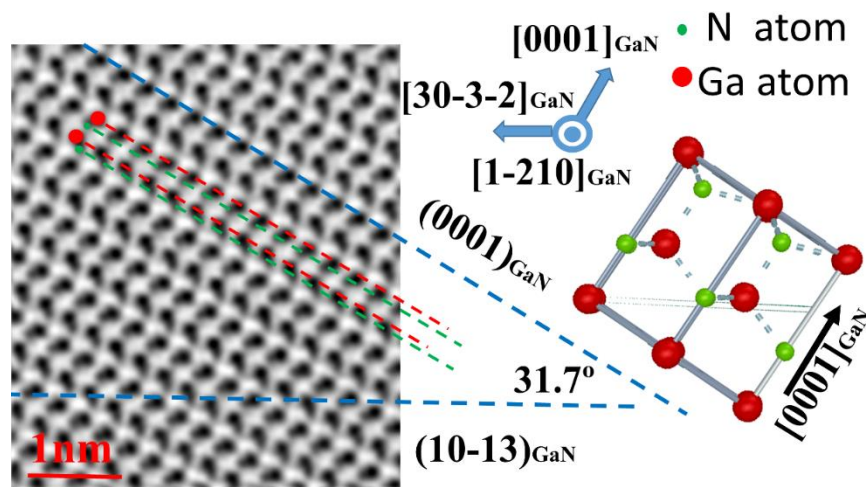


Figure 2.7 Side view of GaN layer along $[1-210]_{\text{GaN}}$ direction by HR-STEM result. Right side indicates the relation between Ga and N-planes along $[0001]$ direction for a side view along $[1-210]$.

By XRD, EBSD and STEM measurements, it can be seen that the sample made by directional sputtering method is true untwinned Ga-polar (10-13) GaN.

2.4 Summery

In this chapter, directional sputtering has been introduced. In this technique, substrates should be loaded in the chamber by fixed direction and should not be rotated. For (100) Si, [110] direction should be towards target while for (10-10) plane sapphire, the [1-210] direction should point towards the target. The directional sputtering includes two steps, Al sputtering and AlN sputtering. Al targets are used in both steps. The difference is that Ar is used for Al sputtering but N₂ for AlN sputtering. (100) Si and (10-10) m-plane sapphire could be used as substrates in directional sputtering to grow (10-13) semi-polar GaN. (10-10) m-plane sapphire is better than (001) Si in (10-13) semi-polar GaN deposition from lattice mismatch analysis, which is confirmed by XRD rocking curve results. Afterwards, XRD, EBSD and TEM were used to check the sample on m-plane sapphire. The results confirmed untwinned Ga-polar (10-13) GaN.

References

- [1] H. J. Lee, S. Y. Bae, K. Lekhal, K. T. Mitsunari, A. Tamura, Y. Honda and H. Amano, *J. Cryst. Growth*, **454**, 114 (2016).
- [2] J. Bläsing, V. Holý, A. Dadgar, A. P. Veit, J. Christen, S. Ploch, M. Frentrup, T. Wernicke, M. Kneissl and A. Krost, *J. Phys. D Appl. Phys.* **46**, 125308 (2013).
- [3] T. Mitsunari, H. J. Lee, Y. Honda and H. Amano, *J. Cryst. Growth*, **431**, 60 (2015).
- [4] H. J. Lee, S. Y. Bae, K. Lekhal, A. Tamura, T. Suzuki, M. Kushimoto, Y. Honda and H. Amano, *J. Cryst. Growth*, **468**, 547 (2017),
- [5] T. J. Baker, B. A. Haskell, F. Wu, P. T. Fini, J. S. Speck and S. Nakamura, *Jpn. J. Appl. Phys.* **44**, L920 (2005).
- [6] R. Sharma, P. M. Pattison, H. Masui, H. R. M. Farrell, T. J. Baker, B. A. Haskell, F. Wu, S. P. DenBaars, J. S. Speck and S. Nakamura, *Appl. Phys. Lett.* **87**, 231110 (2005)
- [7] M. Frentrup, S. Ploch, M. Pristovsek and M. Kneissl, *Phys. Status Solidi B* **248**, 583 (2011).
- [8] M. Jue, H. Yoon, H. Lee, S. Lee and C. Kim, *Appl. Phys. Lett.* **104**, 092110 (2014).
- [9] E. Kay, *J. Appl. Phys.* **32**, S99 (1961).
- [10] H. J. Hovel and J. J. Cuomo, *Appl. Phys. Lett.* **20**, 71 (1972).
- [11] J. W. Shon, J. Ohta, K. Ueno, A. Kobayashi and H. Fujioka, *Sci. Rep.* **4**, 5325 (2015).
- [12] H. Miyake, C. H. Lin, K. Tokoro and K. Hiramatsu, *J. Cryst. Growth* **456**, 155 (2016).
- [13] D. V. Dinh, N. Hu, Y. Honda, H. Amano and M. Pristovsek, *J. Cryst. Growth* **498**,

377 (2018).

[14] A. Dadgar, A. Krost, J. Christen, B. Bastek, F. Bertram, A. Krtschil, T. Hempel, J.

Bläsing, U. Haboeck and A. Hoffmann, *J. Crys. Growth*, **297**, 306 (2006).

[15] M. Sakaia, H. Ishikawa, T. Egawa, T. Jimbo, M. Umeno, T. Shibata, K. Asai, S.

Sumiya, Y. Kuraoka, M. Tanaka and O. Oda, *J. Crys. Growth*, **244**, 6 (2002).

[16] T. J. Baker, B. A. Haskell, F. Wu, J. S. Speck and S. Nakamura, *Jpn. J. Appl. Phys.*

45, L154 (2006).

[17] M. J. Kappers, J. L. Hollander, C. McAleese, C. F. Johnston, R. F. Broom, J.

Barnard, M. Vickers and C. J. Humphreys, *J. Cryst. Growth* **300**, 155 (2007).

[18] S. Jang, H. Kim, D. Soo Kim, S. M. Hwang, J. Kim and K. H. Baik, *Appl. Phys.*

Lett. **103**, 162103 (2013).

[19] M. Pristovsek, M. Frentrup, Y. Han and C. J. Humphreys, *Phys. Status Solidi B*,

253, 61 (2016).

Chapter 3 Al layer sputtering

Al sputtering is the first step in directional sputtering. The sputtering time of the Al layer is short, always less than 15s. So its thickness is quite thin. However, it acts an important role in the whole process. (10-13), (10-14), (10-10) and even (0001) plane GaN/AlN could be obtained by only changing the parameter of Al sputtering. This work is the first time study on its impact.

In this chapter, time and temperature of Al sputtering are studied. They are two key parameters of Al sputtering. During optimizing of these two parameters, they were found could control the orientations of following AlN/GaN epitaxy layers. Optical transmission method is used to measure the thickness of the Al layer and X-ray reflection. Since the aim is to grow (10-13) GaN templates, the impact of Al sputtering on the final (10-13) GaN is also studied.

3.1 Time of Al sputtering

The initial Al layer decides the surface orientations of the following AlN/GaN layers. Figure 3.1 shows 2θ - ω scans of samples after MOVPE growth with increasing Al sputtering time (t_s). The samples were made as Figure 2.2 and Table 2.2. Only time of Al sputtering (Step 1 in Figure 2.2 and Table 2.2) was changed on different samples. Temperature of Al sputtering was 380°C. If t_s is very short (0-3 s), (10-10) GaN is obtained. For t_s of 5-8s, (10-13) GaN is achieved. If t_s is further increased, the growth orientation further tilts to (10-14). The transitions between these regimes are not sharp, and additional phases might appear: m-plane mixed with (10-13) plane, or (10-13) plane

mixed with (10-14) plane.

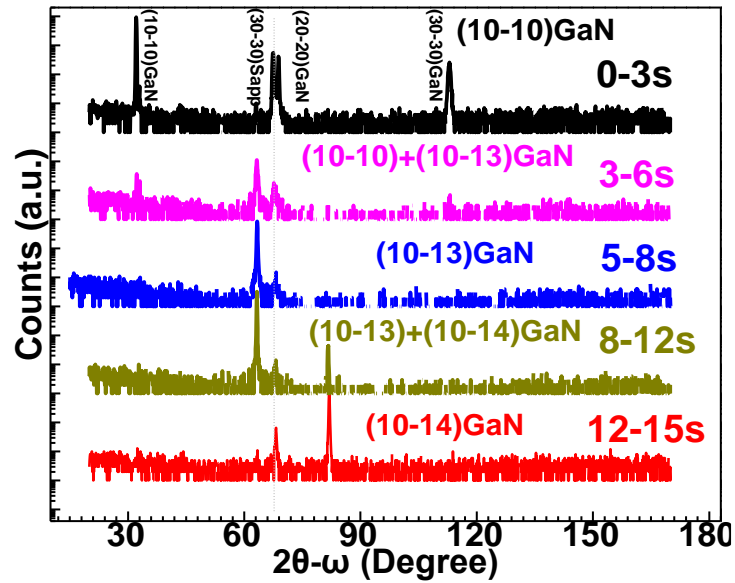


Figure 3.1 2θ - ω XRD measurements of samples after overgrown MOVPE (see Chapter 2.1) using different sputter times t_s for the Al layer. The transition is not sharp, and a slight variation in time dependency might be due to change of target. 2θ angles of each plane: (10-13) GaN at 63.42° , (10-14) GaN at 82.04° , (10-10) GaN at 32.39° , (20-20) GaN at 68.80° , (30-30) GaN at 112.57° . The samples are from 2s, 5s, 8s, 10s and 12s Al sputtering templates respectively.

For further discussion it is necessary to know the thickness of the initial Al layer.

Al has a very high refractive index (n) and extinction coefficient (k). Thus, the thickness of very thin Al layers can be measured by optical transmission. For this, four Al samples have been sputtered on sapphire with increasing sputtering time (8, 15, 30, and 60s) and measured with optical transmission.

Expected transmission spectra for different thicknesses of Al layers were also calculated. For the calculation, a four-layer stack (air-Al-sapphire-air) model was used. Figure 3.2 shows this stack.

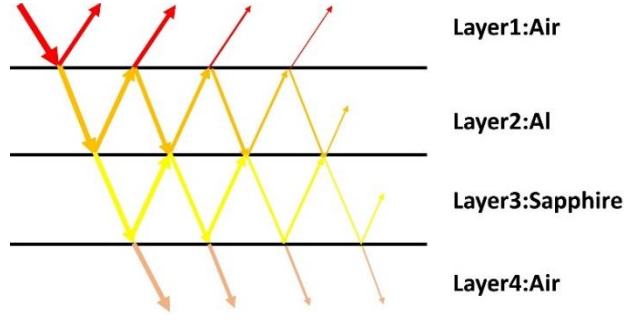


Figure 3.2 Sketch of a four-layer (air-Al-sapphire-air) optical transmission system

In this model, light reflects and transmits in Al layer and sapphire layer at each interface. To calculate the final outgoing light the following formulae is used, which is obtained by solving Maxwell's equation [1].

$$\alpha_1 = 2\pi k_1 d / \lambda \quad \gamma_1 = 2\pi n_1 d_1 / \lambda \quad \alpha_2 = 2\pi k_2 d_2 / \lambda$$

$$g_1 = \frac{n_0^2 - n_1^2 - k_1^2}{(n_0 + n_1)^2 + k_1^2} \quad g_2 = \frac{n_1^2 - n_2^2 + k_1^2 - k_2^2}{(n_1 + n_2)^2 + (k_1 + k_2)^2}$$

$$h_1 = \frac{2n_0 k_1}{(n_0 + n_1)^2 + k_1^2} \quad h_2 = \frac{2(n_1 k_2 - n_2 k_1)}{(n_1 + n_2)^2 + (k_1 + k_2)^2}$$

$$C = 2(g_1 g_2 - h_1 h_2) \quad D = 2(g_1 h_2 + g_2 h_1)$$

$$T' = \frac{n_2}{n_0} \frac{\{(1 + g_1)^2 + h_1^2\} \{(1 + g_2)^2 + h_2^2\}}{\exp(2\alpha_1) + (g_1^2 + h_1^2)(g_2^2 + h_2^2) \exp(-2\alpha_1) + C \cos 2\gamma_1 + D \sin 2\gamma_1}$$

$$T = T' \exp(2\alpha_2 d_2) \left(1 - \frac{(n_2 - 1)^2 + (k_2 - 1)^2}{(n_2 + 1)^2 + (k_2 + 1)^2}\right)$$

For Al, the n_1 and k_1 values from Reference 2 were used, while parameters of sapphire are essentially constant ($n_2=1.75$, $k_2=0$) over our measurement range. And d_1 is thickness of Al layer while thickness of sapphire d_2 is constant, 3.8×10^5 nm. Additionally, dielectric functions in Reference 3 were also used to the calculation.

Firstly, n and k values could be got by the following equations:

$$\varepsilon_1 = n^2 - k^2 \quad \varepsilon_2 = 2nk$$

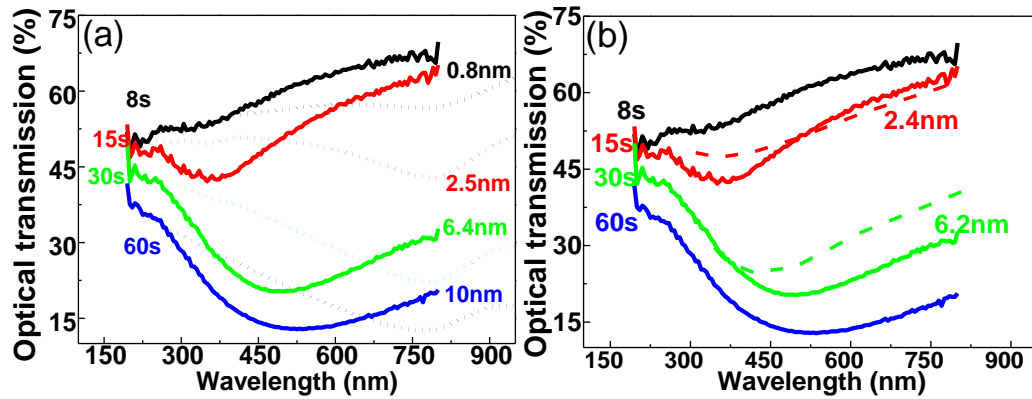


Figure 3.3 Optical transmission spectra of sputtered Al samples on sapphires with different times in both (a) and (b). (a) Dot lines are calculated curves with different Al thicknesses by using n and k values of Al bulk. (b) Dash lines are also calculated curves with different Al thicknesses but using the ε values from [3], which were only available 2.4 nm and 6.2 nm but not for 0.8 nm or 10nm.

Both measured data and calculated data are compared in Figure 3.3. Calculated transmission spectra have a similar shape and minimum position in wavelength (around 780 nm), as shown in Figure 3.3 (a). But the minimum value of the measured curves is shifted from 780 nm to much shorter wavelengths, with a larger shift for thinner layers (horizontal arrows). Such a thickness dependency in the dielectric function of Al has previously been reported for very thin Al films (<10 nm) [3], and was attributed to confinement effects (like change in mean free path and effective mass) or plasmonic effect. However, Reference 3 also showed that the dielectric functions of layers with the same thickness may even change for different growth conditions. Unfortunately literature values were not measured for all layers thicknesses (especially not below 2.4 nm), but the values for 2.4 nm and 6.2nm come very close to the measured transmission of our samples. As shown in Figure 3.3 (b), the optical transmission curves

calculated by the parameters from [3] are much closer to measured curves than the curves calculated by the parameters of Al bulk. And the thickness values from literature are close to the thickness values matched by minimum in Figure 3.3 (a). Therefore, the general shapes in the calculation by the bulk Al dielectric function could be used to get an approximate thickness.

From the simulation, thicknesses for 8, 15, 30 and 60s sputtered Al layers are 0.8nm, 2.5nm, 6.5nm and 10nm, respectively. For thicker Al layers, the thicknesses was also calculated by XRR. For the 8s and 15s Al samples no clear oscillations were observed, as shown in Figure 3.4 (a). For the 30s and 60s Al sputtered samples, there are at least two oscillation, which give thicknesses of 7 and 11.7nm respectively, which are only 10% thicker than the thicknesses of 6.4 and 10nm estimated from the optical measurements. Therefore it is confident that the optical thickness is within 10% of the actual thickness also for the thinner samples.

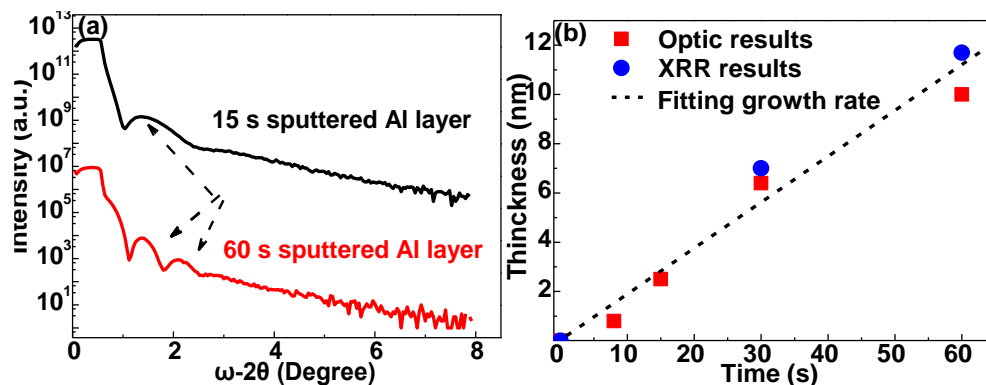


Figure 3.4 (a) XRR data and (b) growth rates of sputtered Al layer from optical transmission data and XRR data.

Furthermore, the purpose of the optical transmission measurements is to get the approximate thickness of the sputtered Al layers. The match criterion is only the

minimum. Despite that, it should be noted that the results of optical transmission method agrees with the results by XRR method of thicker layers with only about 10% difference. This indicates that the results from the optical transmission measurements are also reliable. The oxidation and roughness of Al layers could also influence the optical transmission but only a little. Since it is not the main part in this work, the simulation of oxidation and roughness of Al layers are shown in Appendix 2.

Therefore, less than 0.5nm Al was formed on the sapphire for very short Al sputtering time (<3s), which yield the (10-10) orientation. And for the (10-13) orientation only 1-2 monolayers (0.5-0.7 nm) are needed. The growth rate of sputtered Al could be calculated by the thickness data. It's about 0.18nm/s by optic transmission method and XRR method, as shown in Figure 3.4 (b).

To the Al layer, the limit of the quantitative analysis has been reached, since a four-layer stack to a five-layer stack (air-AlN-Al-sapphire-air) cannot be solved analytically any more. Moreover, one must then properly deal with an Al dielectric function strongly changing by thickness as discussed above.

3.2 Temperature of Al sputtering

Except the time of Al sputtering, temperature of Al sputtering should also be considered. Samples were manufactured at different Al sputtering temperatures with the same sputtering time of 8s. Afterwards, AlN and GaN with same growth parameters were deposited on these templates. The samples were made as Figure 2.2 and Table 2.2. Figure 3.5 displays XRD results of the samples after GaN deposition.

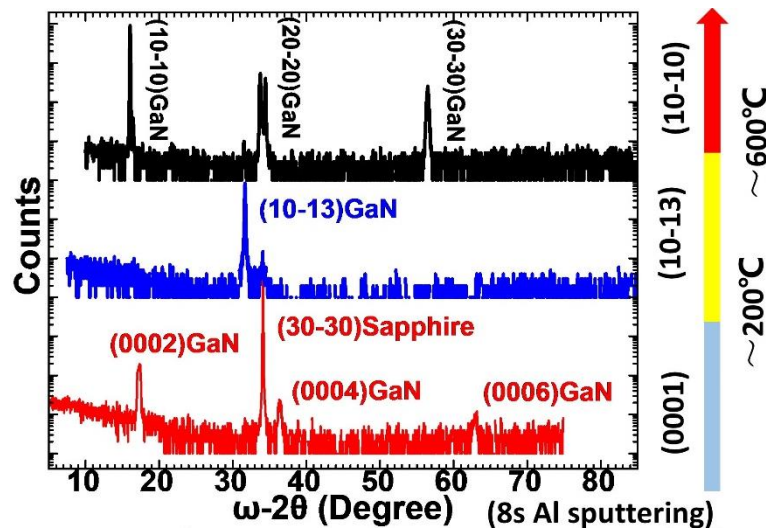


Figure 3.5 2θ - ω XRD measurements of MOVPE overgrown GaN samples on m-plane sapphire substrates under Al sputtering temperature. Under the same sputtering time, surface orientation change with the increased temperature. Al sputter temperatures of examples in this figure are 150°C, 380°C and 620°C respectively.

From the XRD results, it can be seen that (0001), (10-13) and (10-10) orientations appear separately with increasing temperature of Al sputtering. Under 200°C, (0001) GaN could be got. From 200°C to 600°C, (10-13) GaN arises. If increasing the temperature further, (10-10) GaN could be obtain. It needs to be emphasized that, the transition is not sharp, and a slight variation in time dependency might be due to change of target either. Compared with the Al sputtering time dependency, the (10-10) and (10-13) orientations could be found in the temperature series but not the (10-14) orientation. And there are no mixed orientations in these samples, indicating sharper transitions happen at different temperatures.

The melting point of Al metal is about 660°C [4]. The transition between (10-13) orientation and (10-10) orientation is about 600°C, close to the melting point of Al metal. Likely Al atoms can migrate longer on the substrate surface at 600°C and cluster together to minimize surface energy [5, 6].

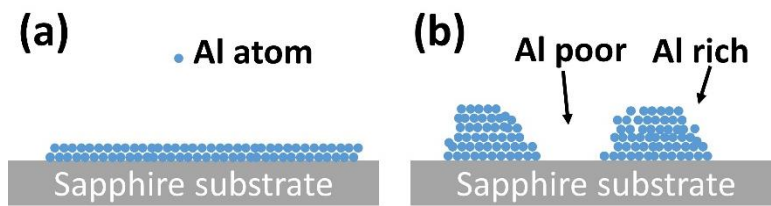


Figure 3.6 Assumption of Al atoms configurations in (a) low temperature mode and (b) high temperature mode.

Figure 3.6 shows this assumption. In Figure 3.6 (a), atoms arrange homogeneously in low temperature. The (10-13) orientation in Figure 3.5 corresponds to this model. In Figure 3.6 (b), atoms form into clusters which only occupy little area of the substrate surface (Al-rich areas). In other areas, (Al-poor areas), there are almost no Al atoms. As shown for the Al sputter time series, (10-10) GaN arises on the Al-poor areas. Hence, high temperature Al sputtering is like short 0-3s Al sputtering.

To verify this assumption, the surface of two sputtering samples was measured by SEM. The samples were sputtered with 8s Al and 8s AlN. The difference is that one Al sputtering was 500°C (lower than 600°C) and the other was 700°C (higher than 600°C), while the AlN sputtering was the same for both samples. The surface morphology is shown in Figure 3.7.

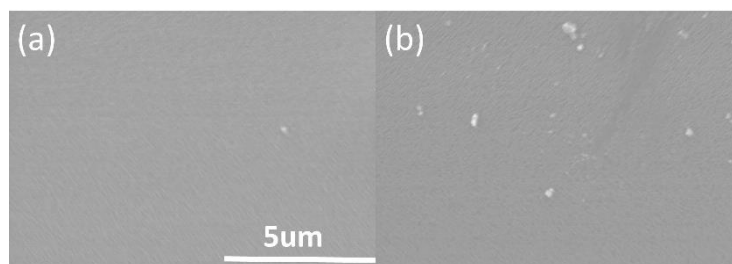


Figure 3.7 Surface morphologies of (a) 500°C Al sputtering sample and (b) 700°C Al sputtering sample.

There is almost nothing on the 500°C Al sputtering sample while many clusters

exist on the 700°C Al sputtering sample. The diameters of these clusters are 100-200nm. Just from the morphology, the measured figure could match to the assumption of all Al clustering.

3.3 Origin of the different orientations

Sections 3.1 and 3.2 show that the (10-10), (10-13), (10-14) and (0001) orientations could occur by different Al sputtering condition. Now it's time to discuss about why these orientations occur.

Among the observed orientations, (10-13) AlN has the best lattice match to m-plane sapphire, followed by (10-10) AlN and (10-14) AlN (Table 3.1). Apart from the lattice matching, other factors contribute to the total energy, which is the sum of the elastic energy, the surface energy, and the interfacial energy [7]. The difference of the elastic energy depends on the lattice mismatch along $[11-20]_{\text{sapphire}}$ direction which is estimated to be about -4.1% for the (10-10) orientation and -0.8% for the (10-13) orientation. (in the other direction, the mismatch is the same for all orientations.) As approximation of the surface energies of the (10-10) and (10-13) orientation, the number of dangling bonds (DB) per surface area was used. These values are 11.34 nm^{-2} for the (10-10) surface and 13.89 nm^{-2} for the (10-13) surface [8]. This would also favor the (10-13) orientation. More sophisticated calculations show that (10-10) GaN/AlN has a lower surface energy due to relaxation and surface reconstruction [9, 10]. However, the unknown interface energy of sapphire with or without Al layer is more important in our case.

Table 3.1 Lattice mismatch of m-plane sapphire with respect to (10-1L) AlN

	(10-10)AlN	(10-13)AlN	(10-14)AlN
Lattice mismatch	-4.1%	-0.8%	-7.0%
	$[11-20]_{\text{sapp}}//[0001]_{\text{AlN}}$	$[11-20]_{\text{sapp}}/[30-3-2]_{\text{AlN}}$	$[11-20]_{\text{sapp}}/[20-2-1]_{\text{AlN}}$
	+4.7%	+4.7%	+4.7%
	$[0001]_{\text{sapp}}/[11-20]_{\text{AlN}}$	$[0001]_{\text{sapp}}/[11-20]_{\text{AlN}}$	$[0001]_{\text{sapp}}/[11-20]_{\text{AlN}}$

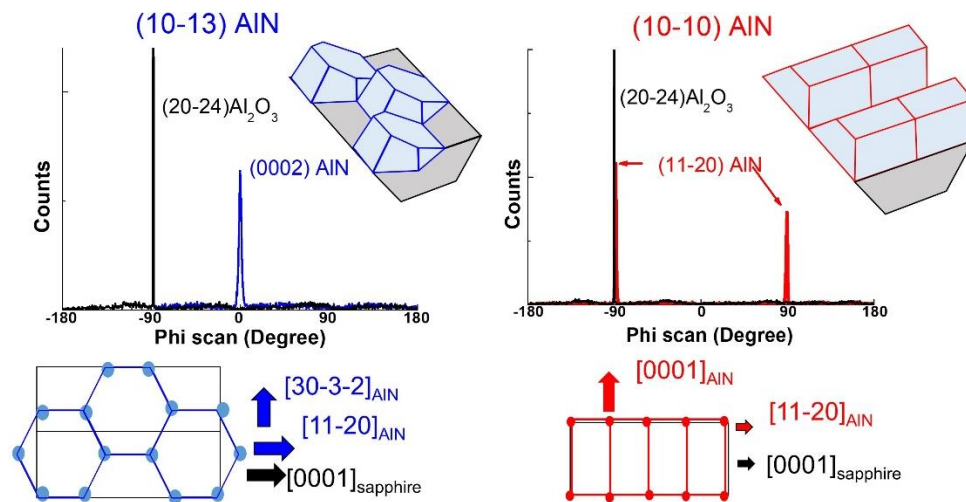


Figure 3.8 Crystallographic relationship of (10-13) and (10-10) AlN on (10-10) m-plane sapphire. For (10-13) AlN, two m-plane sapphire surface unit is need while only one is needed for (10-10) AlN.

Beyond equilibrium, kinetics may also cause in the formation of (10-10) AlN without a closed Al layer despite strain. To obtain the low -0.8% mismatch with (10-13) AlN, the Al atoms need to arrange themselves over two m-plane sapphire surface unit cells, while only ordering along one surface unit cell is needed to match (10-10) AlN [11]. Figure 3.8 demonstrates this. In other words, the AlN species need to migrate less on m-plane sapphire to form (10-10) AlN while more rearrangement is needed for (10-13) AlN. Thus, it is assumed that the Al layer supports migration in initial part during directional sputtering. The enhanced migration favors (10-13) while conditions without Al mediated migration results in (10-10) AlN.

By increasing the Al thickness, the AlN layer gradually loses contact with m-plane sapphire substrate. Without any ordering from the interface, the AlN layer wants to orient itself into (0001), since this orientation is obtained when sputtering at room temperature [12], such as (10-14) orientation. The lattice mismatch of (10-14) AlN/m-plane sapphire is -7.0% along $[11-20]_{\text{sapphire}}$ (Table 3.1). Consequently, the FWHM of X-ray rocking curve is always much larger for (10-14) (more than 2500 arcsec) than for (10-13) (550 arcsec) due to the larger mismatch [13]. However, neither (10-11) AlN, nor any other (10-1*L*) orientations were observed, since these layers have too large lattice mismatch to the m-plane sapphire surfaces.

If Al layer is deposited at too high temperature ($>600^{\circ}\text{C}$), the Al atoms form clusters to decrease surface energy (Al-rich areas). There are very little even none Al atoms at Al-poor areas. The condition is like the short time (0-3s) mode. If Al layer is deposited at too low temperature, the Al atoms do not have enough energy to interact with each other with the sapphire at all and amorphous Al is obtained. On it the fastest growing orientation low energy surface dominates, which is the (0001) orientation. Due to the amorphous starting orientation, such layers are highly defective.

3.4 Impact of Al parameters on the final GaN layer

Although several orientations could be obtained by changing Al sputtering parameters, the (10-13) orientation is the target of this study. Optimization for this orientation is necessary and is studied in this section since it is the main aim of this study.

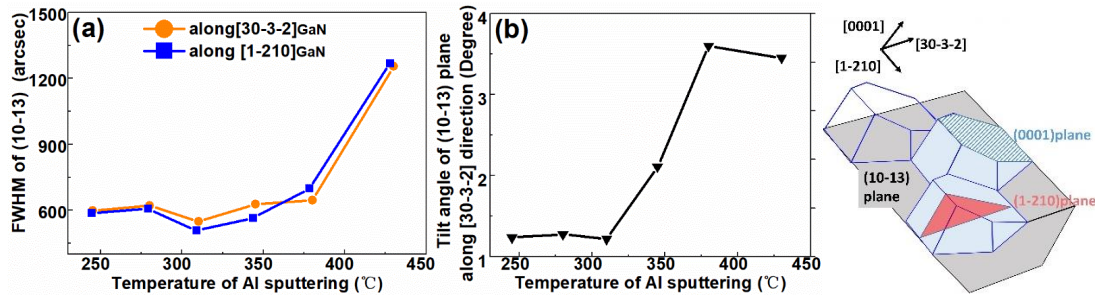


Figure 3.9 XRD FWHM along the two directions of GaN (a) and tilt angle (b) of the GaN towards [0001] as functions of Al sputter temperature. Sputtering time was fixed as 8s for each sample.

Figure 3.9 shows the impact of sputtering temperature of the initial Al layer, while the growth conditions of all subsequent layers were kept the same as Figure 2.2 and Table 2.2. Both FWHM and tilt angle have at their minimum at around 300°C. Sputtering the Al layer above 400°C results in a wider-FWHM (10-13) GaN. At low temperatures, the (0001) orientation occurs, and at above 600°C (10-10) occurs, as mentioned before.

Since higher temperatures are better for the sputtering of AlN, a two-temperature method was used. First the Al layer was sputtered at 300°C and then the temperature was ramped to about 650°C to sputter the AlN layer. The sputtering temperature of the AlN sputter had little impact on the quality of the overgrown GaN layer, and the temperature was rather limited by the heating power of the sputter system.

Figure 3.10 shows XRD data of the 310°C Al sputtering sample, which has the narrowest FWHM. Wide range 2θ - ω measurements in Figure 3.10 (a) shows only the (10-13) diffraction of GaN and AlN close to the (30-30) sapphire diffraction, demonstrating that a pure single phase (10-13) GaN was obtained. Moreover, a (10-13) AlN peak from the initial buffer layer was never reported using directional sputtering

on Si [14, 15]. This underlines that the quality of the AlN layer on m-sapphire is vastly superior, even though the FWHM values are still more than 4000 arcsec in both directions. Figure 3.10 (b) shows the rocking curves of the symmetric (10-13) GaN diffraction along the two main axis. The FWHM values are 550 arcsec along $[30-32]_{\text{GaN}}$ and even 500 arcsec in $[1-210]_{\text{GaN}}$ direction. These are a big improvement compared with previous work on Si (001) [15]. These small FWHM values also compare favorable among other hetero-epitaxial semi-polar GaN orientations on sapphire. For comparison, the best value for N-polar (10-1-3) GaN was on double epitaxial overgrowth with values of 381 arcsec and 582 arcsec along $[30-3-2]_{\text{GaN}}$ and $[1-210]_{\text{GaN}}$ and non-ELOG (epitaxial lateral overgrowth) values of 750 arcsec and 1180 arcsec [16]. Also (11-22) GaN typically reports broader FWHM on m-plane sapphire [17].

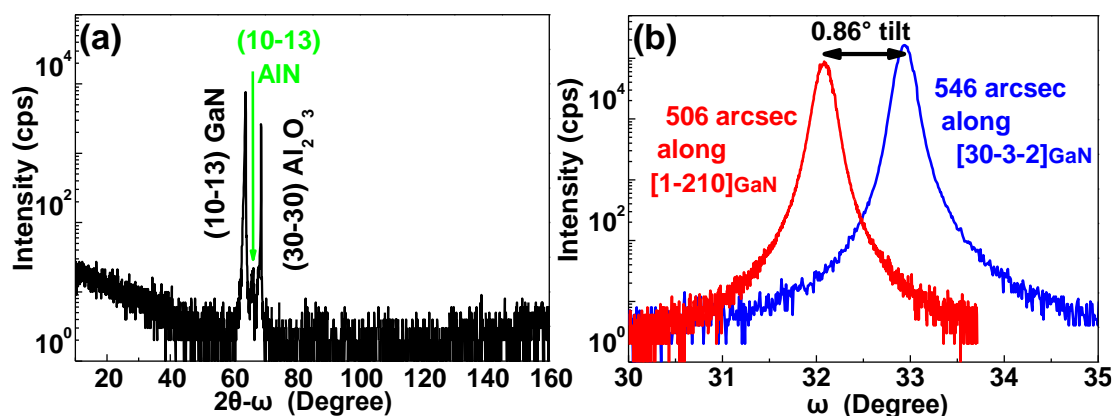


Figure 3.10 XRD diffraction of a (10-13) GaN layer. (a) wide $2\theta-\omega$ scan along $[1-210]_{\text{GaN}}$ direction (b) Symmetric (10-13) rocking curves of the layer scanned along $[30-3-2]_{\text{GaN}}$ and $[1-210]_{\text{GaN}}$ directions.

The (10-13) GaN diffraction along $[30-32]_{\text{GaN}}$ is tilted by 0.86° with respect to its theoretical position. This tilt is not due to strain. Moreover, a tilt towards the $[0001]$ direction is often observed in semi-polar layers, especially after an AlN/GaN hetero-interface. It originates from the annihilation of defects (especially basal-plane stacking

faults) at the hetero-interface between AlN and GaN. However, in our case also the directional sputtering as well as the strain may contribute to an initial tilt. (Especially since the tilt increases for longer sputtering times.)

3.5 Summary

The sputtering of the initial Al layer is studied in this chapter. Its sputter time is short and the Al layer is very thin, but it acts as an important role. (10-13), (10-14), (10-10) and even (0001) oriented AlN/GaN can be obtained on m-plane sapphire by changing time and temperature of the Al sputtering. The first three orientations are more or less lattice matched to m-plane sapphire. (The (11-22) AlN orientation would also match well with m-plane sapphire, but it is suppressed by the directional sputtering, i.e. orienting the samples 90° to its [0001] direction.) Conditions like high temperature (leading to Al clusters and bare sapphire) or short Al sputter time, result in no Al layer or ultrathin Al and form a (10-10) AlN since the Al atoms are not enough for migrating to two m-plane surface unit cells needed to form (10-13). If the Al thickness is just right, there are enough Al atoms to support migration of AlN over two m-plane surface unit cells and the low energy (10-13) orientation forms. If the Al thickness was increased further, the AlN could tilt larger to the most stable orientation which is (0001) orientation. The (10-14) orientation also occurs with thicker Al layers, and even the (10-14) still has good match with m-plane sapphire substrate. If the Al layer is too thick, the following epitaxy layer would lose its contact from substrate. In this condition, AlN would grow with (0001) orientation. The relationships are listed in

Table 3.2. The boundaries are somewhat gradually, so mixed orientations can happen.

Table 3.2 Samples made by different Al sputtering parameters

Sputter temperature: 380°C					
Sputter time	0-3s	3-6s	5-8s	8-12s	12-15s
Orientation	(10-10)	(10-10)	(10-13)	(10-13)	(10-14)
		+(10-13)		+(10-14)	
Sputter time: 8s					
Sputter temperature	RT-200°C	200-600°C	>600°C		
Orientation	(0001)	(10-13)	(10-10)		

Both (10-10) and (10-13) AlN surface unit cells could match to m-plane sapphire substrate well. The difference is that one m-plane sapphire unit cell is needed to match (10-10) AlN but two for (10-13) AlN. So more Al atoms should be sputtered for (10-13) orientations. That means longer Al sputtering time. By increasing the Al thickness (Al sputtering time), the AlN layer gradually loses its contact with m-plane sapphire substrate. The AlN layer wants to orientate itself into (0001), such as (10-14) orientation. If Al layer is deposited at too high temperature (>600°C), the Al atoms form clusters to decrease surface energy (Al rich area). There are very little even non Al atoms at Al poor area. The condition is like the short time (0-3s) mode. If Al layer is deposited at too low temperature, the Al atoms do not have enough energy to interact with each other with the sapphire at all and the result is amorphous Al. On it the fastest growing

orientation with low energy surface dominates, which is the (0001) orientation.

Thickness of Al layer for (10-13) orientation is only about 0.8nm.

As a final step the Al sputtering was optimized for (10-13) orientation. The appropriate condition was 0.8 nm of Al sputtering at 300°C. After optimization, the X-ray rocking curve FWHM is less than 550 arcsec along both $[30-3-2]_{\text{GaN}}$ direction and $[1-210]_{\text{GaN}}$ direction. And the tilt angle along $[30-3-2]_{\text{GaN}}$ direction is less than 1°.

References

- [1] S. G. Tomlin, *J. Phys. D, Appl. Phys.* **1**, 1667 (1968)
- [2] A. D. Rakić, *Appl. Optics*, **34**, 4755 (1995).
- [3] H. V. Nguyen, I. An and R. W. Collins, *Phys. Rev. B*, **47**, 3947 (1993).
- [4] <https://en.wikipedia.org/wiki/Aluminium>
- [5] S. R. Coon, W. F. Calaway, M. J. Pellin, G. A. Curlee and J. M. White, *Nucl. Instrum. Methods Phys. Res. Sect. B*, **82**, 329 (1993).
- [6] T. H. Van Steenkiste, J. R. Smith and R. E. Teets, *Surf. Coat. Technol*, **154**, 237 (2002).
- [7] P. Vennéguès, T. Zhu, D. Martin and N. Grandjean, *J. Appl. Phys.* **108**, 113521 (2010).
- [8] K. Hiramatsu, K. Nishiyama, A. Motogaito, H. Miyake, Y. Iyechika and T. Maeda, *Phys. Status Solidi A* **176**, 535 (1999).
- [9] J. E. Northrup and J. Neugebauer, *Phys. Rev. B* **53**, R10477 (1996).
- [10] L. Lymperakis and J. Neugebauer, *Phys. Rev. B* **79**, 241308 (2009).
- [11] A. Mogilatenko, H. Kirmse, J. Stellmach, M. Frentrup, F. Mehnke, T. Wernicke and M. Weyers, *J. Cryst. Growth*, **400**, 54 (2014).
- [12] T. Mitsunari, H. J. Lee, Y. Honda and H. Amano, *J. Cryst. Growth* **431**, 60 (2015).
- [13] N. Hu, D. V. Dinh, M. Pristovsek, Y. Honda and H. Amano, *J. Cryst. Growth* **507**, 205 (2018).
- [14] H. J. Lee, S. Y. Bae, K. Lekhal, A. Tamura, T. Suzuki, M. Kushimoto, Y. Honda and H. Amano, *J. Cryst. Growth* **468**, 547 (2017).

- [15] T. J. Baker, B. A. Haskell, F. Wu, P. T. Fini, J. S. Speck and S. Nakamura, *Jpn. J. Appl. Phys.* **44**, L920 (2005).
- [16] J. Yang, T. Wei, Z. Huo, Y. Zhang, Q. Hu, X. Wei, B. Sun, R. Duan and J. Wang, *Cryst. Eng. Comm.* **16**, 4562 (2014).
- [17] M. Pristovsek, M. Frentrup, Y. Han and C. J. Humphreys, *Phys. Status Solidi B*, **253**, 61 (2016).

Chapter 4 AlN layer

This chapter is about the AlN layers which provides templates for the final GaN layer. There are two AlN steps in the normal procedure. One is by sputtering, and the other is by MOVPE. First, the use of AlN layer is studied. Then the conditions of AlN sputtering will be discussed. Some methods are tried to improve quality of sputtered AlN, like annealing after AlN sputtering.

4.1 Use of AlN layer

As shown in Chapter 2 and Figure 2.6, untwinned (10-13) GaN samples could be obtained. Apparently the directional sputtering is essential, since otherwise often a twinned crystal is observed [1-4]. So which thing or which step kills the twinning grains? At the beginning, the shadow effect [5] was assumed as the main reason which prevents twinning. First, outgoing sputtering particles come to rest at random positions on the substrate, as Figure 4.1 (a). Then some areas will be higher than others. The higher areas can catch more particles, as shown in Figure 4.1 (b). Gradually, columns along c-direction (the most stable one) will be formed pointing to the direction which the particles fly in (Figure 4.1 (c)).

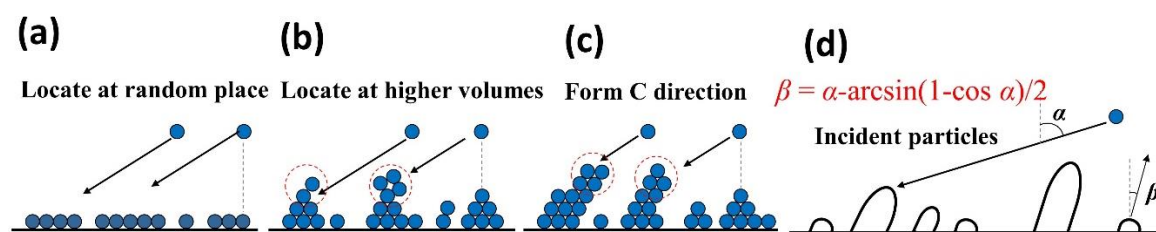


Figure 4.1 Sketch of shadow effect.

there is still a little AlN on the 0s sputtered AlN sample. Because the Al film is easily oxidized in the air, it is exposed shortly to N₂ plasma after Al sputtering. Some AlN forms during this step (as discussed in the next section).

Sample (a) was grown as Figure 4.2 (a), “0s sputter AlN+ 0min MOVPE AlN”. Sample (b) “0s sputter AlN+ 4min MOVPE AlN” and (c) “0s sputter AlN+ 8min MOVPE AlN” were made as Figure 4.2 (b). Sample (d) “60s sputter AlN+ 4min MOVPE AlN” and (e) “60s sputter AlN+ 8min MOVPE AlN” were deposited as Figure 2.2. And Sample (f) “90min sputter AlN+ 0min MOVPE AlN” was manufactured as Figure 4.2 (c). Afterward, GaN layers were grown by same condition except (f). Then the twinning was measured by X-ray diffraction phi scans of 0002 reflection. If there is only one reflection in reflection in 360° the layer is untwinned. If there is twinning, there would be two reflections separated by 180°, see Figure 4.3 for an example. From Table 4.1, it can be seen that twinning occurs at three conditions: “0s sputtered AlN+0 min MOVPE AlN” one, “0s sputtered AlN and 4 min MOVPE AlN” one and “90min sputter AlN+ 0min MOVPE AlN”. Among them, last two are slightly twinned. (Intensity of twinned grains less than 1% of intensity of main grains in X-ray phi scan)

The growth rate of sputtered AlN layer is very low. Thus, 8 min MOVPE AlN is much thicker than 60s sputtered AlN (which is less than 2 nm from extrapolating from thicker layers.). So the twinning occurs if AlN layers are thinner than untwinned conditions. In addition, there is also difference between two twinned samples.

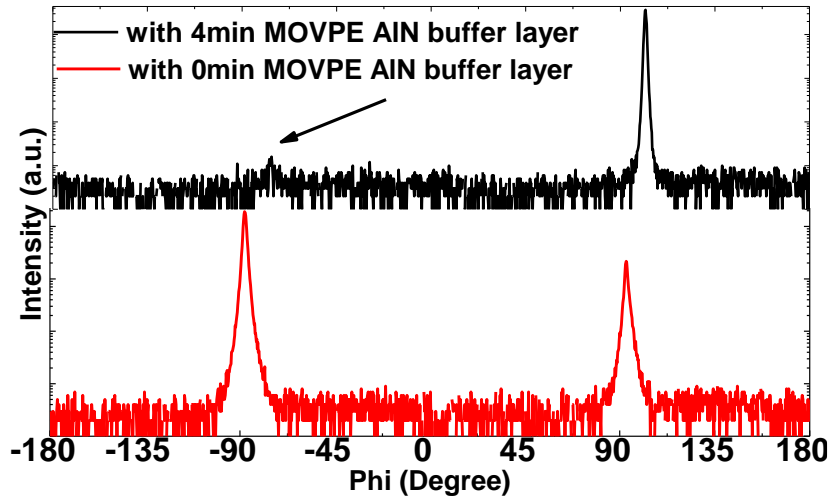


Figure 4.3 X-ray phi scan of 0min and 4 min MOVPE AlN buffer layer (without sputtered AlN layer) and subsequent GaN growth. The peaks are the 0002 GaN reflection from the (10-13) GaN layer.

Figure 4.3 shows the X-ray phi scan results of the skew-symmetric 0002 reflection of (10-13) GaN for the layer with 0 min and 4 min MOVPE AlN growth. Twinning is obvious for the 0 min MOVPE AlN layer, while it is magnitudes lower (logarithmic scale in Figure 4.3) in the 4 min MOVPE AlN layer sample.

To check whether the sputtered layer has twinning or not, a thick AlN layer was sputtered under typical conditions (but an AlN sputter time of 90 min). The result was only slightly twinned. Hence, experiments results indicate that twinning is only related to the thickness of AlN layer but no relation with growth method.

From these results, it can be seen that there is no twinning with thick enough AlN buffer layer. In other words, AlN layer eliminates the twinning. Other discussion about twinning is in Appendix 3.

4.2 How AlN sputtering affects the initial Al layer

In the previous chapter it has been found that the time of Al sputtering is short and the sputtered Al is thin. So it is easily affected by the following AlN sputtering.

So what happens in sputtering process. There are several kinds products from sputtering process, including: negative/positive/neutral particles and ultraviolet (UV) radiation. Energies of them range from 10 to 150 eV [6-8]. Among the outgoing particles and photons, negative particles have highest energy. When the 30-150 eV particles hit on solid materials, three phenomena can happen: reflection, injection, and sputtering, as shown in Figure 4.4 (a) [9]. In AlN sputtering, nitrogen plasma is used in AlN sputtering. In nitrogen plasma, N-ions have highest energy, while the AlN molecules will be much lower. When N-ions hit the Al layer, they can react with Al to AlN, as shown in Figure 4.4 (b) and (c).

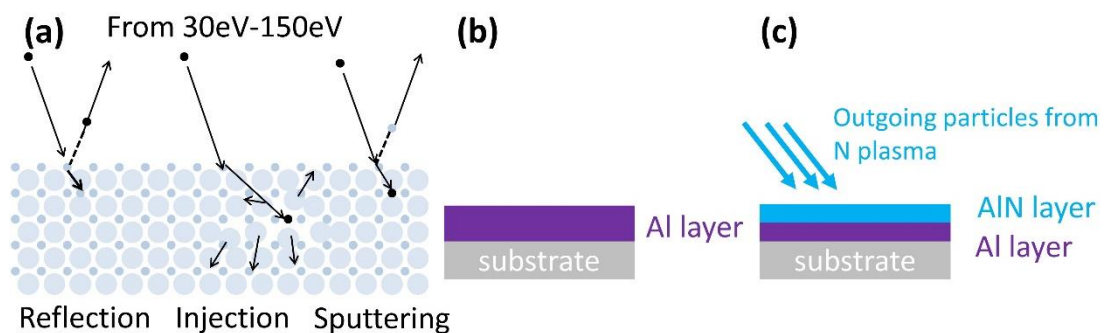


Figure 4.4 (a) particles hit on solid material, (b) sample after Al sputtering, (c) sample after nitrogen plasma treatment.

To verify this, optical transmission measurement was used again. Four samples are compared: 8s Al only, 8s Al+2s AlN, 8s Al+10s AlN, and 10s AlN only, with other

sputtering conditions as the AlN step in Table 2.2. The structures are shown in Figure 4.5 (a).

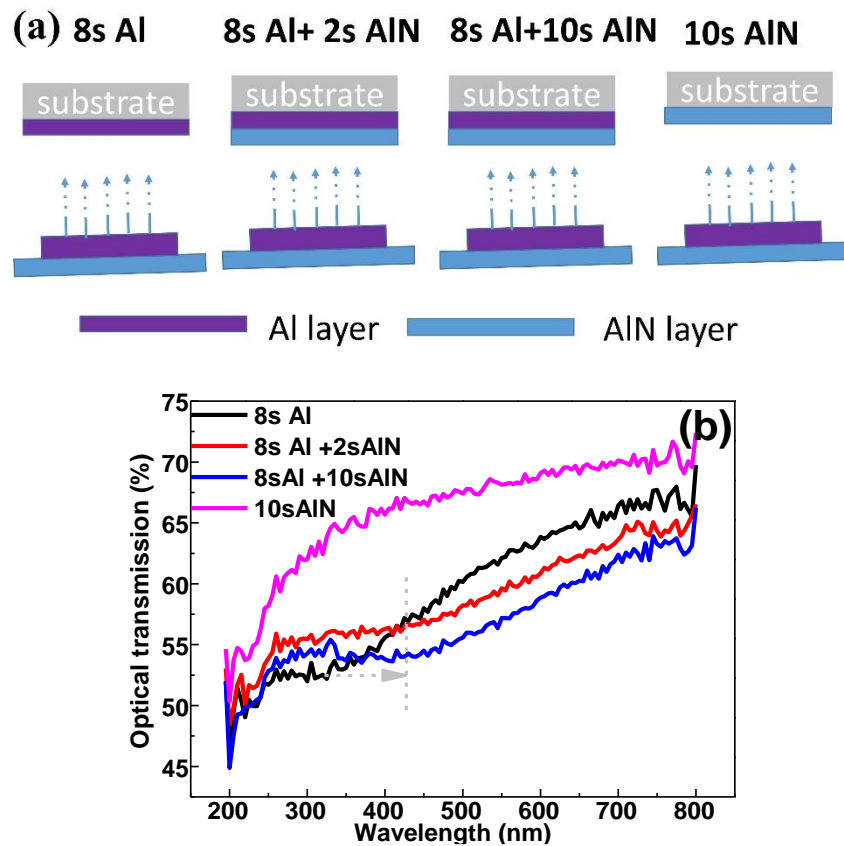


Figure 4.5 (a) sketches of each samples. (b) Optical transmission spectra of Al layers sputtered for 8s, Al for 8s followed by 2s or 10s of sputtered AlN, and for 10s of AlN. The minimum values of 8s followed by 2s or 10s of sputtered AlN (arrow position) are shifted from 8s sputtered Al but are also quite different form only sputtering pure AlN.

The optical transmission results are shown in Figure 4.5. Short AlN sputtering effects the optical transmission spectra a lot. Samples with both (Al+AlN) show very different spectra both from pure Al sample and pure AlN samples. Even after sputtering 2s AlN on 8s Al, the resulting transmission spectrum is different from the transmission spectrum with 8s Al. Nevertheless, the transmission spectra after sputtering 2s and 10s AlN on 8s Al are almost the same, i.e. they have the same AlN thickness. The high energy negative nitrogen ions convert the Al layer largely to AlN, since the energy of

negative outgoing particles in sputtering can exceed 150 eV [10]. In other words, many nitrogen atoms implant into the Al layer and bond with Al atoms forming AlN while the actual amount of sputtered AlN is much smaller. So the AlN part in the “8s Al+2s AlN” sample is almost the same thickness as in the “8s Al+10s AlN” sample. In addition, most converting happens at the very beginning time of AlN sputtering since “8s Al+2s AlN” sample has almost the same shape as the “8s Al+10s AlN” one.

After analysis and optical transmission measurement, it can be seen that some of the Al atoms have been converted into AlN at very beginning part of AlN sputtering step. Still some Al atoms survive, and give the templates after sputtering a slightly brown color. But these Al atoms will also be converted into AlN in temperature stabilization part of MOVPE growth by supporting NH₃. Chapter 5.3.2 will also talk about this by TEM image.

4.3 Optimization of AlN sputtering

There are in principle two ways of sputtering AlN, either using elements like Al target with N₂ plasma or with an AlN target and Ar/N mixture. This section will talk about both of them.

4.3.1 Optimization of AlN sputtering by Al target

AlN sputtering by Al target is the standard procedure. For AlN deposition, high temperature is preferred, for example 1200°C in MOVPE AlN growth [10, 11] and 2100-2300°C in thermal sublimation AlN [12, 13]. So the temperature of AlN

sputtering is set to almost max of our machine, 650°C. But this is still low for AlN deposition and thus the crystalline quality is poor. However, removing defects is difficult. Therefore, it is best to start as perfect as possible. Pure N₂ was used with an Al target.

Thus only time and power dependency samples were made for optimization. Other steps (Al sputtering before AlN sputtering and MOVPE growth after AlN sputtering) are the same as Figure 2.2 and Table 2.2. X-ray and optical microscope were used to characterize the final GaN layer.

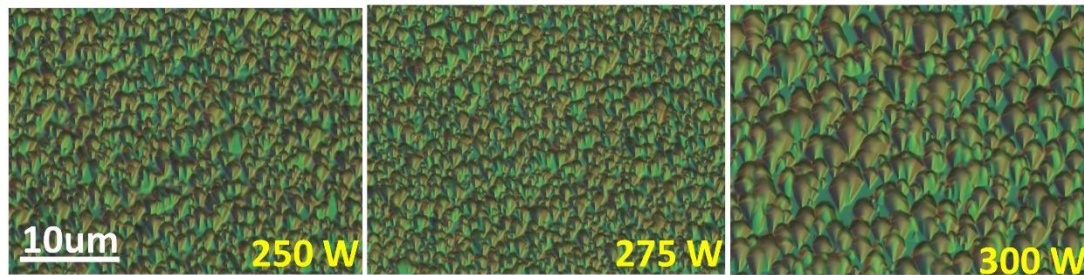


Figure 4.6 Optical microscope pictures of GaN layers on sputtered AlN layers with different sputtering power.

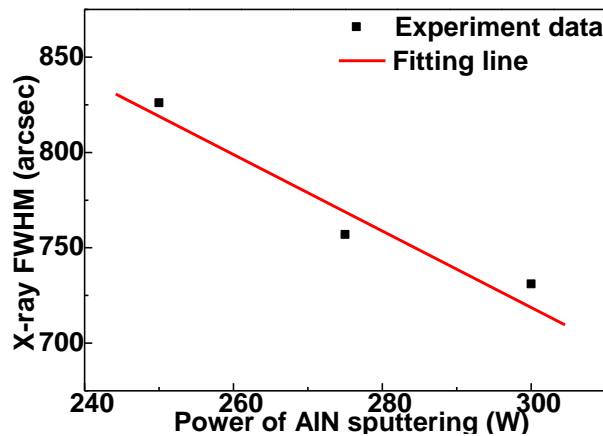


Figure 4.7 FWHM of 10-13 GaN reflection X-ray rocking curves of GaN layers with sputtered AlN layers in different sputtering power. The sputtering time is 60s.

Figure 4.6 (OM pictures) and 4.7 (data of X-ray rocking curve) show the results of power dependency of AlN sputtering. It can be seen that by using higher AlN sputtering power, larger grains are obtained, as well as a better quality of final GaN

layer. The maximum power of our machine is 300W. But for stable plasma and less stress, a little lower power of 275 W was used in our normal procedure.



Figure 4.8 Optical microscope pictures of GaN layer with sputtered AlN layers in different sputtering time.

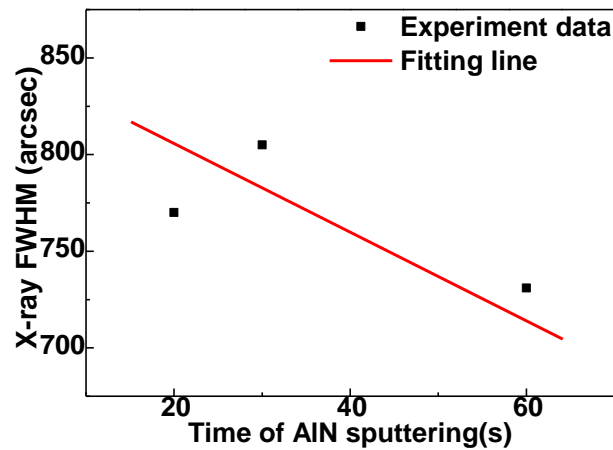


Figure 4.9 FWHM of 10-13 GaN reflection X-ray rocking curves of GaN layers with sputtered AlN layers in different sputtering time. The sputtering power is 275W.

Figure 4.8 (OM pictures) and 4.9 (GaN X-ray rocking curve FWHM) show the results of time dependency of AlN sputtering. Similar to before, bigger grain relate with smaller FWHM. The best result is around 60 s. Since sputtered AlN is relatively poor quality, the sputtering time should not be long. But if the time is too short, the AlN layer is too think to properly orientate the following layers. So the AlN sputtering time is set as 60s.

These are the optimization of AlN sputtering.

4.3.2 AlN target and low temperature annealing

As mentioned before, high temperature is needed for AlN growth. The sputtering machine could not arrive high enough temperature so that the quality of sputtered AlN layer is not good. To solve this, high temperature annealing is applied to improve sputtered AlN [14]. In the literature, AlN target is used to deposit c-plane AlN on c-plane sapphire. The FWHM of 0002 AlN reflection is 532 arcsec before annealing and 49 arcsec after annealing. So this method was tried in this study based on great effect.

The first step is to repeat the result in (0001) AlN layers. In this experiment, AlN layers, the only layer, were sputtered by AlN target on c-plane sapphire. RF power source was used and the power was set as 200W. Sputtering temperature was 650°C. Sputtering was 1 hour so that the AlN layer is thick enough for XRD measurements. The working gas was mixed Ar and N₂. Then ratio of Ar and N₂ was changed to look for the appropriate condition. Ratios and XRD results are listed in Table 4.2. The 0002 AlN reflection was measured by XRD.

Table 4.2 X-ray omega scan results of sputtered c-plane AlN

	N ₂ :Ar ratio	FWHM (arcsec)
High	3:1	5468
Low	1:3	980
	1:4	790

From the XRD results, it can be seen that low N₂: Ar ratios are good for AlN sputtering in our machine, which is different from the literature [14]. The FWHM value

of low N₂: Ar ratio is 790 arcsec, a little bigger than the literature but the difference could be accepted. However, c-plane AlN is not the aim. Therefore, low N₂: Ar ratios condition were applied to semi-polar AlN sputtering. The procedure was the same as Figure 2.2 and Table 2.2 except for the AlN step. The first is Al sputtering on m-plane sapphire substrates by Al target. Then AlN target was used to sputter the AlN layer (after rotating the sample towards it). The condition is the same as c-plane AlN sputtering mentioned before except the N₂: Ar ratio. Sputtering time of AlN is set as 60s, same as with the Al target. Afterwards, the templates were put into MOVPE for following AlN and GaN epitaxy. In this experiment, N₂: Ar ratio condition in AlN sputtering was also changed. But in XRD measurement, 10-13 GaN reflection was used to check the properties since the sputtered AlN layer is too thin to measure. The results are shown in Table 4.3 and Figure 4.10.

Table 4.3 XRD omega scan results of final (10-13) GaN of with different N₂: Ar ratio in AlN sputtering by AlN target

N ₂ :Ar ratio	FWHM along [11-20] _{GaN} (arcsec)	FWHM along [30-3-2] _{GaN} (arcsec)
1:9	854	787
2:8	850	730
3:7	727	791

Table 4.3 shows that higher N₂: Ar ratios sputtered AlN buffer layer sample is a little better than lower N₂: Ar ratio ones. But the differences are rather small. Additionally, all of them are not good as the sample with the standard procedure using an Al target. And there is no AlN peak in ω -2 θ scan in Figure 4.10, which is seen in

good samples.

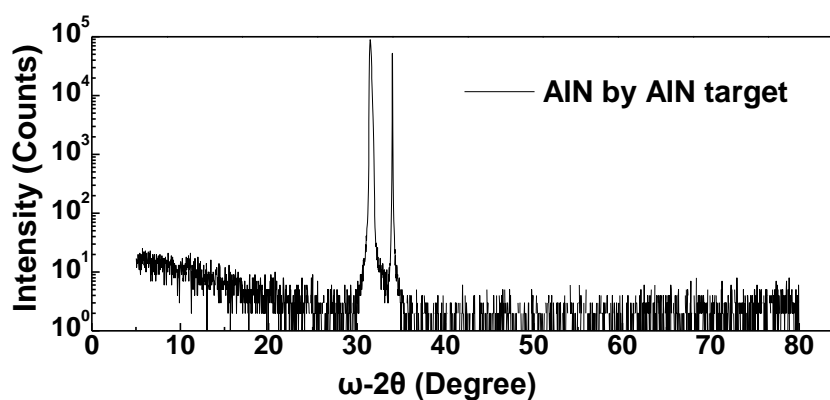


Figure 4.10 ω -2 θ scan of 3:7 N₂: Ar ratio sputtered AlN buffer layer sample.

From the literature, the FWHM value of sputtered c-plane AlN by AlN target was 530 arcsec. If the AlN buffer layer for (10-13) GaN could arrive this level, it would help to improve the GaN quality much; but then the 0002 reflection is only sensitive to c-component dislocations, while the 10-13 reflection sees each kinds of dislocations. However, either Al or AlN targets the 10-13 reflection ends up above 10000 arcsec for sputtered layers.

High temperature annealing of (0001) AlN has shown tremendous improvements. An annealing step was added between AlN sputtering and MOVPE AlN growth. It was done in MOVPE chamber for 10 min in NH₃ atmosphere, since the upper limit temperature of our MOVPE machine is only 1320°C. After annealing, AlN and GaN growth were continued without taking out or cooling down to room temperature, as shown in Figure 4.11(a). Then XRD was used to check the 10-13 GaN reflection.

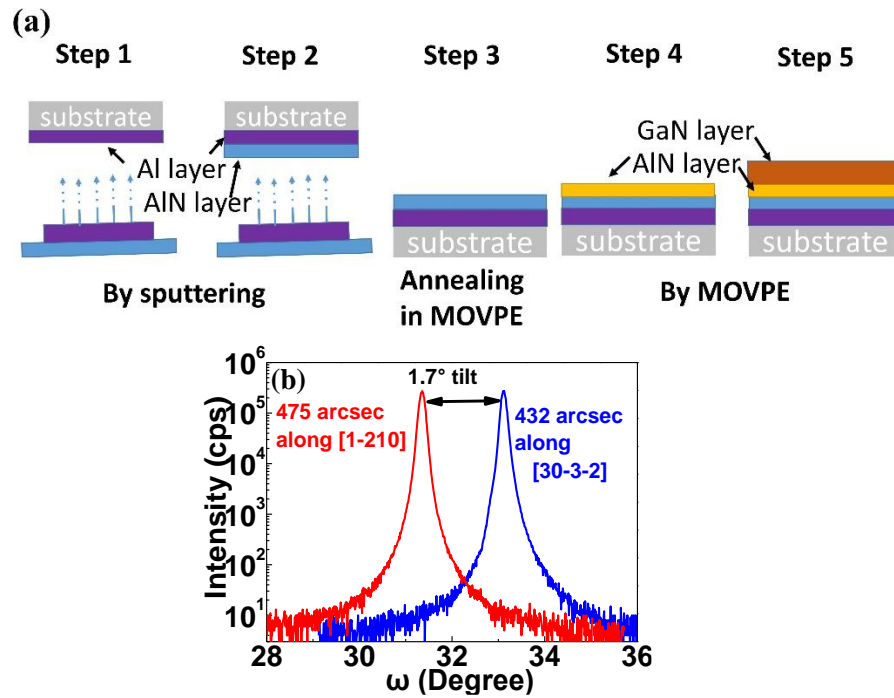


Figure 4.11 (a) Structure and manufacture flow the annealed sample. (b) X-ray rocking curves of (10-13) GaN samples with annealing of sputtered AlN layer.

As shown in Figure 4.11, the sample with annealing of sputtered AlN layer has narrower X-ray rocking curve than the sample by normal procedure in Figure 3.10. That means even low temperature anneal to sputtering AlN buffer layer could improve the quality of the following GaN epitaxy layer.

4.4 AlN by MOVPE

Since sputtered AlN layer does not have good quality, MOVPE is used to epitaxy an AlN layer with better quality (and higher growth rate). In addition, MOVPE overgrowth seems to strongly reduce the twinning. As said before, less than 10 nm of sputtered AlN is too thin to be measured by XRD. But after MOVPE growth, the AlN peak could be found in the X-ray scan.

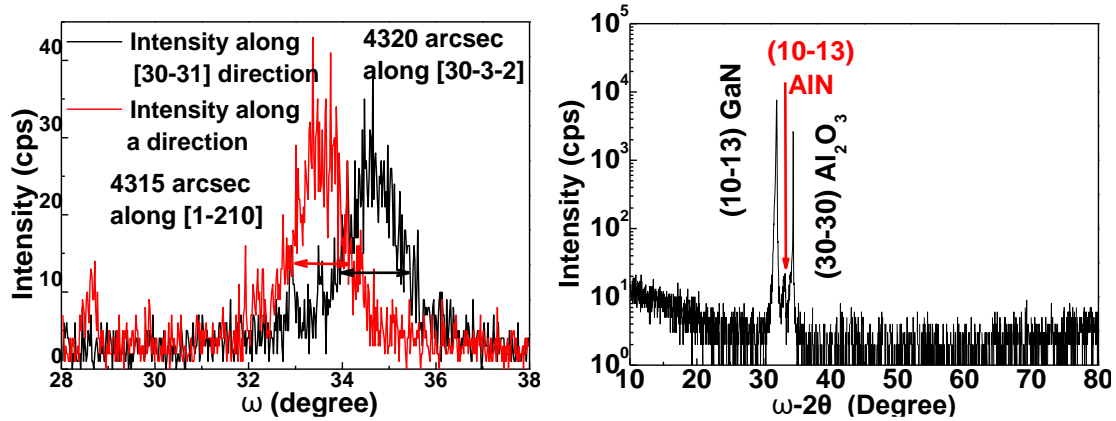


Figure 4.12 X-ray (a) rocking curves of (10-13) AlN buffer layer after MOVPE epitaxy and (b) ω - 2θ scan after final GaN growth.

Figure 4.12 (a) shows the X-ray rocking curves of (10-13) AlN buffer layers of the sample in Figure 3.10. They are relatively wide along both directions (although one has to consider that the AlN is less than 100 nm thick). If the AlN buffer is good enough, a 10-13 AlN reflection peak could also be observed in the ω - 2θ scan, like shown in Figure 4.12 (b).

4.5 Summary

In this chapter, the AlN buffer layer is studied. There are two AlN growth steps, AlN by sputtering and AlN by MOVPE. Apart from providing the metal-polar orientation for the following GaN layer, the AlN layer eliminates the twinning. At the beginning, the shadow effect during AlN sputtering is thought as main reason. But after more experiments, clearly a certain AlN thickness is needed, either by sputtering or MOVPE. More experiments (different thicknesses of AlN by sputtering and MOVPE respectively) are needed to clarify it.

Two techniques from literature are tried to improve the AlN quality: AlN sputtering by AlN target, and annealing of the sputtered layers prior to growth.

Sputtering by AlN target did not help but annealing even at 1320°C showed some improvement. The FWHM of X-ray rocking curves of AlN layer is still very wide even after MOVPE. A better AlN buffer layer is would be very much desired.

The results of the experiments in this chapter are listed in Table 4.4.

Table 4.4 Results of all experiments in this chapter

Use of AlN layer	
Thick AlN buffer layer	None or thin AlN buffer layer
Unwinned	Twinned (following GaN layer)
Parameters of AlN sputtering by Al target after optimization	
Time	Power
60s	275W
Techniques tried to improve the quality	
AlN target	Low temperature annealing
No improvement	Improvement

References

- [1] T. J. Baker, B. A. Haskell, F. Wu, P. T. Fini, J. S. Speck and S. Nakamura, *Jpn. J. Appl. Phys.* **44**, L920 (2005).
- [2] T. J. Baker, B. A. Haskell, F. Wu, J. S. Speck and S. Nakamura, *Jpn. J. Appl. Phys.* **45**, L154 (2006).
- [3] T. Wernicke, C. Netzel, M. Weyers and M. Kneissl, *Phys. Status Solidi C* **5**, 1815 (2008).
- [4] M. Frentrup, S. Ploch, M. Pristovsek and M. Kneissl, *Phys. Status Solidi B* **248**, 583 (2011).
- [5] L. Abelmann and C. Lodder. *Thin Solid Films* **305**, 1 (1997).
- [6] K. Tominaga, M. Chong and Y. Shintani, *J. Vac. Sci. Technol. A* **12**, 1435 (1994).
- [7] A. Plagemann, K. Ellmer and K. Wiesemann, *J. Vac. Sci. Technol. A* **25**, 1341 (2007).
- [8] Y. Takagi, Y. Sakashita, H. Toyoda and H. Sugai, *Vacuum* **80**, 581 (2006).
- [9] D. M. Sun and G. K. Xi, *Surface and interface of solid materials*, Anhui educational press, (1996) (in Chinese)
- [9] B. Demaurex, S. D. Wolf, A. Descoedres, Z. C. Holman and C. Ballif. *Appl. Phys. Lett.* **101**, 171604 (2012).
- [10] F. Brunner, H. Protzmann, M. Heuken, A. Knauer, M. Weyers and M. Kneissl, *Phys. Stat. Sol. C* **5**, 1799 (2008)
- [11] N. Fujimoto, T. Kitano, G. Narita, N. Okada, K. Balakrishnan, M. Iwaya, S. Kamiyama, H. Amano, I. Akasaki, K. Shimono, T. Noro, T. Takagi and A. Bandoh,

Phys. Stat. Sol. C **3**, 1617 (2006).

[12] R. Schlessler, R. Dalmau and Z.Sitar, J. Crys. Growth, **241**, 416 (2002).

[13] Z. G. Herro, D. Zhuang, R. Schlessler, R. Collazo and Z. Sitar, J. Crys. Growth, **286**, 205 (2010).

[14] H. Miyake, C. H. Lin, K. Tokoro and K. Hiramatsu, J. Cryst. Growth, **456**, 155 (2016).

Chapter 5 GaN layer

GaN growth has been studied in this chapter. After optimization of Al and AlN buffer layers, the X-ray rocking curve FWHM of the (10-13) GaN layer has become as narrow as 550 arcsec with the initial set of GaN growth conditions. However, the morphology was very rough so this chapter discusses how to achieve a GaN layer which is both of good crystalline quality and smooth surface morphology.

5.1 Introduction

After optimization of sputtering and AlN sequence, less than 550 arcsec FWHM (in X-ray rocking curve of 10-13 GaN reflection) (10-13) GaN sample could be obtained. This is a narrow FWHM for any hetero-epitaxial semi-polar GaN layer. However, the morphology of these samples is very rough (Figure 5.1). From SEM, AFM, and optical microscopy the surface is very rough on small and large scales, with RMS values larger than 100 nm.

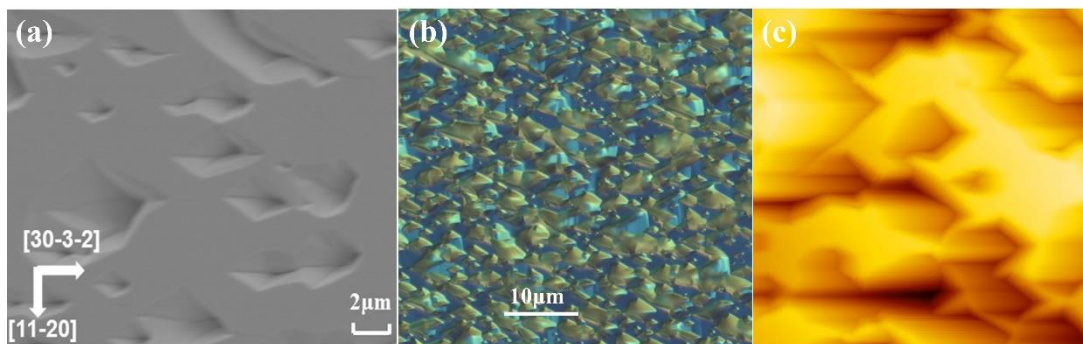


Figure 5.1 Morphology by (a) SEM, (b) OM and (c) AFM scan (10 μm × 10 μm)

Quantum wells could not be grown on such a rough template. Smoothing is needed. To smoothen semi-polar GaN one needs to find conditions that reduce the

growth along [0001] relative to other directions. One parameter is the V/III ratio [1]. A V/III ratio dependency was manufactured as the conditions in Table 2.2 by reducing only the NH_3 flow during the GaN step. The manufacture flow is as Figure 2.2. Figure 5.2 shows the resulting morphologies at different V/III ratios. With decreasing V/III ratio, the morphologies changed from big islands (33), belts (14.4) to flat (12.6 and 10). TMGa supply, growth temperature, chamber pressure and total flow were kept the same. All the 4 samples have almost the same growth rate ($10.07\mu\text{m/h}$ for sample A, $10.19\mu\text{m/h}$ for sample B, $10.22\mu\text{m/h}$ for sample C and $10.03\mu\text{m/h}$ for sample D). Growth time was also kept the same, and thus thickness is also the same (about $10\mu\text{m}$). Under these conditions, the factor which changed morphology is the reduction of NH_3 on the surface.

At the lowest V/III ratio the surface is smooth. However, a V/III ratio of 10 is very low for nitride growth by MOVPE and thus much carbon is incorporated even in the semi-polar GaN layer: the samples look deep yellow. Moreover, the crystalline quality of the low V/III ratio sample is bad, the FWHM of X-ray rocking curve is larger than 2000 arcsec.

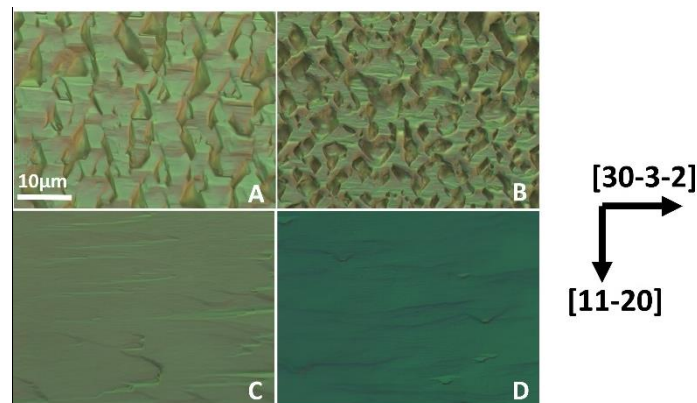


Figure 5.2 OM pictures of different V/III ratio GaN samples.

Table 5.1 Growth condition information of V/III ratio GaN samples in Figure 5.2

Sample	A	B	C	D
Precursors	TMGa, NH ₃	TMGa, NH ₃	TMGa, NH ₃	TMGa, NH ₃
Chamber pressure	10kPa	10kPa	10kPa	10kPa
Carrier gas	H ₂	H ₂	H ₂	H ₂
Total flow	15000sccm	15000sccm	15000sccm	15000sccm
V/III ratio	33	14.4	12.6	10
NH ₃ partial pressure	236Pa	101Pa	89Pa	70.5Pa
TMGa partial pressure	7.05Pa	7.05Pa	7.05Pa	7.05Pa
Growth temperature	1100°C	1100°C	1100°C	1100°C
Growth time	60min	60min	60min	60min

Consequently the main task in this chapter is to get both good crystalline quality and smooth surface (10-13) GaN.

5.2 3D growth and 2D growth

To achieve the aim, three dimension (3D) growth (islanding growth) and two dimensional (2D) growth (islands coalescence and smoothing) could be considered [2]. In 3D growth mode, the crystal grows along one certain orientation not perpendicular to the surface. This orientation is the (0001) in this case, which has higher growth rate than the others. So the grains grow like peaks and the morphology is rough. Thus, in 3D growth mode the morphology is rough and the grains have large surface. So dislocations can easily find a surface close to them, and they can bend out of the crystal to decrease the potential energy. The rougher the morphology is, the easier for dislocations to encounter a surface and bend out, and hence the less dislocations and the better the crystalline quality. So the property of 3D growth is good crystalline quality but rough morphology. Figure 5.3 (a) shows schematic diagram of 3D growth.

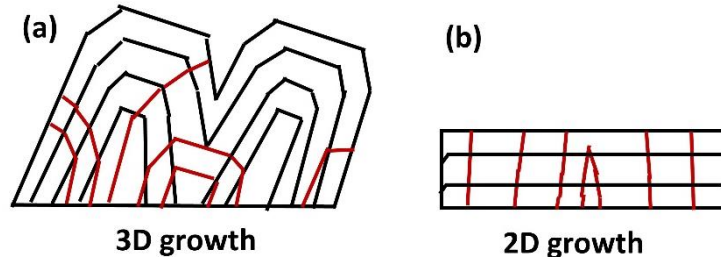


Figure 5.3 Schematic diagrams of (a) 3D growth mode and (b) 2D growth mode. Red lines stand for threading dislocations.

Compared with 3D growth mode, 2D growth mode is different. In 2D growth mode, there is no preferential orientation is perpendicular to the surface. So the crystal grows like laterally layer by layer. In this mode, the morphology is smooth. But it is hard for dislocations to meet each other and be annihilated. They rather progress in a straight line, as shown in Figure 5.3 (b). Accordingly the crystalline quality is not improved during 2D growth.

To show this for (10-13) GaN, three samples were made. Sample A only has 2D growth mode GaN layer, sample B only has 3D growth mode GaN layer, and sample C has both 3D growth followed by 2D growth, as shown in Figure 5.4. Growth conditions of GaN layers are shown in Table 5.2. And other layers were made as in Table 2.2.

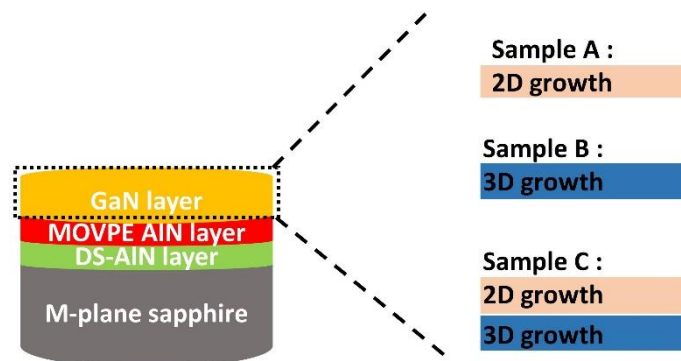


Figure 5.4 Schematics of the semi-polar (10-13) GaN epitaxial structures with three different epitaxy layers. Samples A, B, and C consists of a 2D growth layer, 3D growth layer, and 2D+3D mixed layer, respectively

Table 5.2 Growth condition information of 3D/2D samples in Figure 5.4.

Sample	A	B	C
Precursors	TMGa, NH ₃	TMGa, NH ₃	First grow as
Chamber pressure	5kPa	10kPa	condition B
Carrier gas	H ₂	H ₂	followed by
Total flow	15000sccm	15000sccm	growing as
V/III ratio	5.7	95.5	condition A
NH ₃ partial pressure	20.2Pa	673.3Pa	
TMGa partial pressure	3.53Pa	7.05Pa	
Growth temperature	1080°C	1180°C	
Growth time	8min	29min	

As shown in Figure 5.5 (a), there are almost no slate-like facets on the 2D grown layer. Since it is grown in 2D mode, a high density of threading dislocations (TDs) is contained in this sample which cause small hillocks and a wide XRD FWHM (Table 5.3). Sample B has the roughest morphology, the surface is full of features (Figure 5.5 (b)), but the X-ray rocking curve FWHM is narrow. At higher magnification in AFM a lot of tilted facets appear. The reason is that c direction has the highest growth rate and thus produces most. Figure 5.5 (c) shows the outcome of sample C, 3D flowed by 2D growth. Triangular shapes (red lines) along the [11-20] direction were also observed, which was also found in literature [3]. It is speculated that 3D growth results in rough morphology [4-6]. In addition, the partially uncoalesced GaN morphology is usually observed on semi-polar GaN because of the anisotropic growth rates for the polar and nonpolar orientations [7].

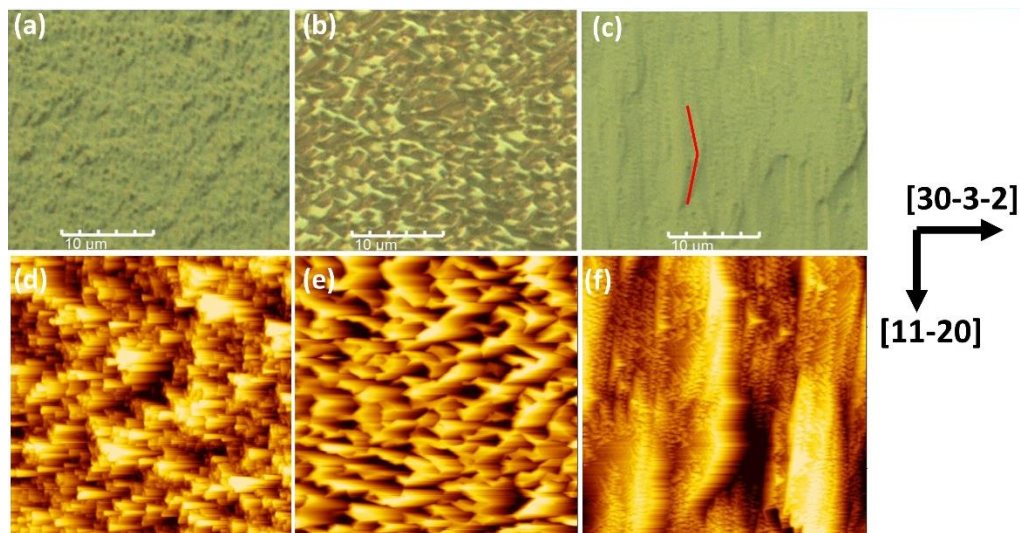


Figure 5.5 OM images of the GaN surface of (a) sample A, (b) sample B and (c) sample C. And AFM images of the GaN surface of (d) sample A, (e) sample B and (f) sample C.

Table 5.3 X-ray and RMS results of 2D, 3D and mixed 3D+2D (10-13) GaN samples.

	FWHM of X-ray rocking curve (arcsec)	RMS(nm)
(A) Only 2D growth	>2000	<30
(B) Only 3D growth	<600	>100
(C) Mixed 3D+2D growth	<600	<30

Except morphology, crystalline quality must be kept high. Table 5.3 has both FWHM values and RMS values. Compared with only 2D growth GaN layer, 3D growth GaN layer and mixed 3D+2D growth GaN layer have much narrower FWHM. It is because that TDs could be annihilated during 3D growth mode. So they have better crystalline quality. The key point is that sample C, i.e. the mixed 3D+2D grown GaN layer has both narrow FWHM and small RMS values. By 3D + 2D growth both advantage of 3D growth and 2D growth can be kept.

From this experiment, it can be seen that 2-step growth, mixed 3D and 2D growth,

is an effective way to optimize the GaN layer. But the morphology needed to be smoothed furthermore. Second, by just increasing the 2D growth, the surface will be deep yellow and adsorbing. In principle, the 2D layer can be made thinner, if the sample is smoother. But a rather thick 3D growth layer is needed to annihilate the dislocations, which makes the morphology very rough. And too long 3D growth wastes MO source. Thus optimizing the 3D growth part should be done too. If effect of 3D growth can be enhanced, 3D growth time can be decreased. Then surface may be not so rough anymore and it's easier to smoothen it by 2D growth. Of course this would influence the best ratio of 3D growth to 2D growth.

5.2.1 Optimization of 3D growth

3D growth of our (10-13) semi-polar GaN is enhanced at high temperature (1140°C-1200°C) and higher V/III ratio (>80) while 2D growth is enhanced by lower temperature (1020°C-1100°C) and low V/III ratios (<50). In this part, optimization of 3D growth is performed.

Table 5.4 Growth conditions for optimization of 3D-GaN growth.

Sample	A	B	C	D
Precursors	TMGa, NH ₃	TMGa, NH ₃	TMGa, NH ₃	TMGa, NH ₃
Chamber pressure	10kPa	10kPa	10kPa	10kPa
Carrier gas	H ₂	H ₂	H ₂	H ₂
Total flow	15000sccm	15000sccm	15000sccm	15000sccm
V/III ratio	85	100	500	1000
NH ₃ partial pressure	606Pa	707Pa	3535Pa	7050Pa
TMGa partial pressure	7.05Pa	7.05Pa	7.05Pa	7.05Pa
Growth temperature	1180°C	1180°C	1180°C	1180°C
Growth time	30min	30min	30min	30min

Several (10-13) GaN samples were fabricated to find suitable parameters. The GaN layers were grown in 3D mode with different V/III ratios from 80 to 1000, as shown in Table 5.4. The structure was same as sample B in Figure 5.4. So as the growth conditions of Al and AlN buffer layers.

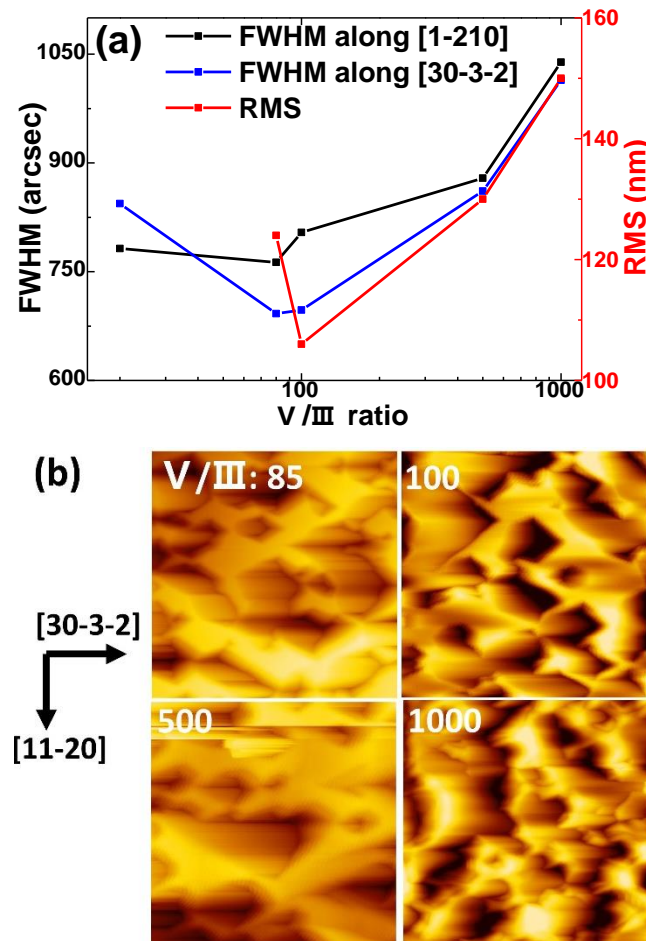


Figure 5.6 (a) FWHM values (left axis) and RMS values of $10 \times 10 \mu\text{m}$ (right axis) of 3D growth (10-13) GaN layer with different V/III ratios. AFM images are shown in (b).

Figure 5.6 shows the X-ray and AFM results. The minimum FWHM of the X-ray rocking curve was around a V/III ratio of 80-100. The RMS value show some variation, but also seems to increase at higher V/III ratios. Probably for V/III ratio larger than 100, the grain reached a number comparable to the dislocation density. Smaller grains (even

higher V/III ratio) would generate more additional dislocations at grain boundaries than are bounded to the sidewall. Figure 5.6 (b) shows the AFM images. Therefore a V/III ratio of 100 is set as the optimized 3D growth condition.

Temperature dependency was also studied, in steps of 20°C around 1180°C. But the FWHM values only changed very little. Temperature seem less important than V-III ratio in that region.

5.2.2 Ratio of 3D growth time and 2D growth time

Ratio of 3D growth time and 2D growth time is also another key parameter. The state of the surface can be know relatively easy with the in-situ monitor. Figure 5.7 shows the optical reflection at 594 nm during an optimized sequence. The reflectance signal has a contribution due to the glowing susceptor below the sample. The smoothness of the surface (or growth mode) is from oscillations of the reflectance signal. In AlN step, there is only a half oscillation, it is because the AlN layer is too thin for one whole oscillation (<120 nm). After AlN epitaxy, the surface is smooth because migration is small and the layer is thin. At the beginning of 3D GaN growth, several oscillations could be seen which disappear gradually. Since the 3D growth makes the surface rough, there is no long a single interface where the light reflected from top and bottom can form interferences. When the growth was changed into 2D mode the surface smoothens, and the oscillations appear again. Hence, it is possible to know the growth mode from the in-situ monitor.

Using the in-situ monitor, two promising sets of times were tried. The first one is

26 min 3D growth + 11 min 2D growth and the second is 34 min 3D growth + 6 min 2D growth. They were grown on same sputtered templates with otherwise the same growth parameters.

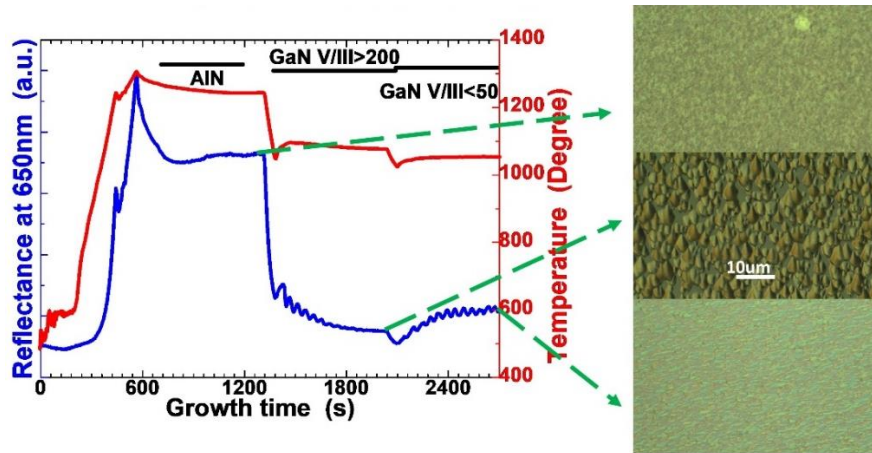


Figure 5.7 Reflectance curve of in-situ monitor and OM pictures of the different growing step.

The results were shown in Figure 5.8. The 34 min 3D growth + 6 min 2D growth one has less FWHM value and smother morphology. It is a good condition for (10-13) semi-polar GaN growth. In addition, although the 26 min 3D growth + 11 min 2D growth one has longer 2D growth time, the morphology is not good as the 34 min 3D growth + 6 min 2D growth sample. Perhaps the longer 2D growth time (which has a high growth rate of $\sim 10 \mu\text{m/h}$) causes also some negative effect on morphology if grown too thick.

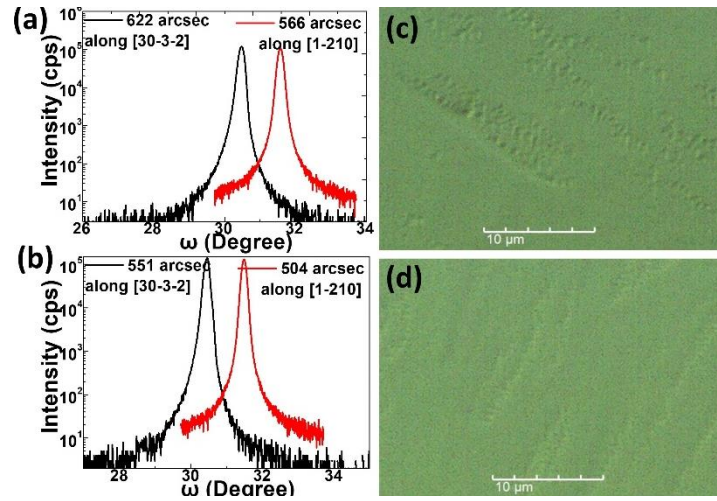


Figure 5.8 X-ray rocking curves and OM pictures of different 3D growth and 2D growth ratio. (a) and (c) from 26min 3D growth + 11min 2D growth one. (b) and (d) from 34min 3D growth + 6min 2D growth one.

After the experiments, the optimized growth parameters are listed in Table 5.5.

Table 5.5 Parameters of 3D growth and 2D growth after optimization.

Step	3D growth	2D growth
Precursors	TMGa, NH ₃	TMGa, NH ₃
Chamber pressure	10kPa	5kPa
Carrier gas	H ₂	H ₂
Total flow	15000sccm	15000sccm
V/III ratio	100	5.7
NH ₃ partial pressure	707Pa	20.2Pa
TMGa partial pressure	7.05Pa	3.53Pa
Growth temperature	1180°C	1080°C
Growth time	34min	6min

5.2.3 3D-2D sequences

As written in the previous section 5.2.1, I would like to keep the positive effect of 3D growth on dislocation reduction with a smooth surface from 2D growth. If 3D growth could be reinitialized at different positions than in the first round, then still existing dislocations could end up close to a sidewall and be annihilated. To verify this, 3D-2D sequences were attempted as sketched in Figure 5.9. A new round of 3D growth

begins each sequence, followed by 2D growth. Again, three samples were made, normal growth (1 repeat), 3 repeats and 5 repeats. The total 3D growth time and 2D growth time were the same. That means the 3D growth time was separated into 3 parts for 3 repeats and 5 parts for 5 repeats. Same for the 2D growth time.

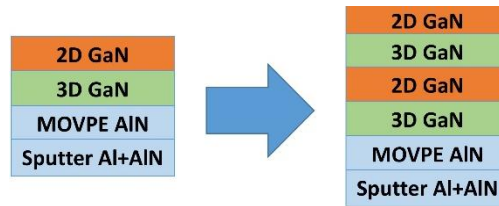


Figure 5.9 Sketch of 3D-2D loops.

As seen in Table 5.6, there is no improvement on the repeat of 3D-2D growth. So the FWHM of the initial 3D growth is most important, and later use of 3D conditions do not cause big 3D growth.

Table 5.6 X-ray (rocking curve) results of loop samples.

	No loop	3 loops	5 loops
FWHM along $[30-3-2]_{\text{GaN}}$ (arcsec)	684	830	730
FWHM along $[1-210]_{\text{GaN}}$ (arcsec)	600	824	713
Tilt angle along $[30-3-2]_{\text{GaN}}$ (Deg)	2.3	1.27	2.42

5.2.4 AlN/GaN super lattices

Reduction of the defect density has been frequently reported using super lattice (SL) [8, 9] at the transition from AlN to GaN. The SL, which consists of thin GaN layer and AlN layer, was inserted before the 3D GaN growth after the MOVPE AlN growth. Each GaN layer and AlN layer had a nominal thickness of 5 nm. There are 5 repeats of AlN/GaN super lattices in total, as shown in Figure 5.10 (a).

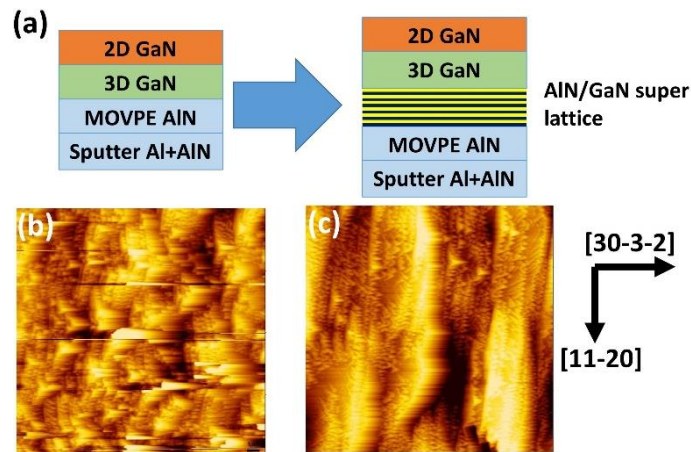


Figure 5.10 (a) Sketch of sample with AlN/GaN super lattices. (b) and (c) are AFM images of (10-13) GaN samples o/w AlN/GaN super lattices.

Table 5.7 Properties of samples w/o SL buffer layers.

	No SL	5 nm SL
XRC along $[30-3-2]_{\text{GaN}}$ (arcsec)	752	684
XRC along $[1-210]_{\text{GaN}}$ (arcsec)	730	600
Tilt angle along $[30-3-2]_{\text{GaN}}$ (Deg)	1.63	2.3
RMS (nm)	29	36.4

Table 5.7 shows that the sample with SL has a narrower X-ray rocking curve. However, the tilt angle and the RMS value (from Figure 5.10 (b) and (c)) are bigger. Apparently the SL buffer layers forms islands due the strain between AlN layers and GaN layers and therefore enhances 3D growth mode. So the effect likes extending growth time of 3D growth, but the strain also tilts the crystal more.

5.3 Characterizations of GaN layer

5.3.1 XRD measurements

Three points on the sample surface were measured by X-ray rocking curve 10-13

GaN reflection, at the center, and about 15 mm away from the center.

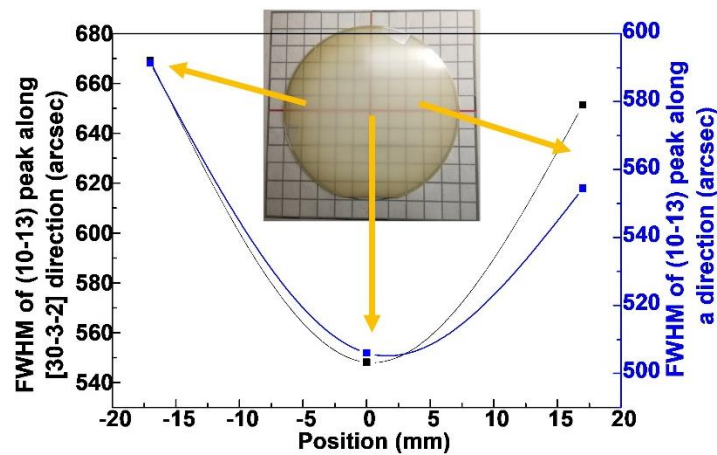


Figure 5.11 X-ray rocking curve measurement on different points of sample.

As shown in Figure 5.11, the center point has the narrowest FWHM. Compared with center point, FWHM values of edge points are about 100-150 arcsec bigger. There could be two reasons. One is that the sputtering has not the same thickness over the wafer, the sputtered layers are thicker closer to the target. Second reason may be wafer curving in the reactor, which has several origins. A showerhead reactor has a large thermal gradient from 80°C cold showerhead to 1250°C hot susceptor in 17 mm. So the sapphire surface is warmer at the top than the bottom, and the wafer forms a bowl. Then there is different strain from different expansion and lattice constants of the whole structure. The AlN is growth at 1250°C and at time relaxed on sapphire. But when cooling down, the different thermal expansion between AlN and sapphire, the wafer cause bow. Finally, when the GaN dislocation are going out in 3D growth mode, strain is increased. All this leads to a sample which is looking like a bowl, i.e. deeper in the center. Then the center would have a higher temperature than the edge. This is why the

crystalline quality of center point is a little different from edge part.

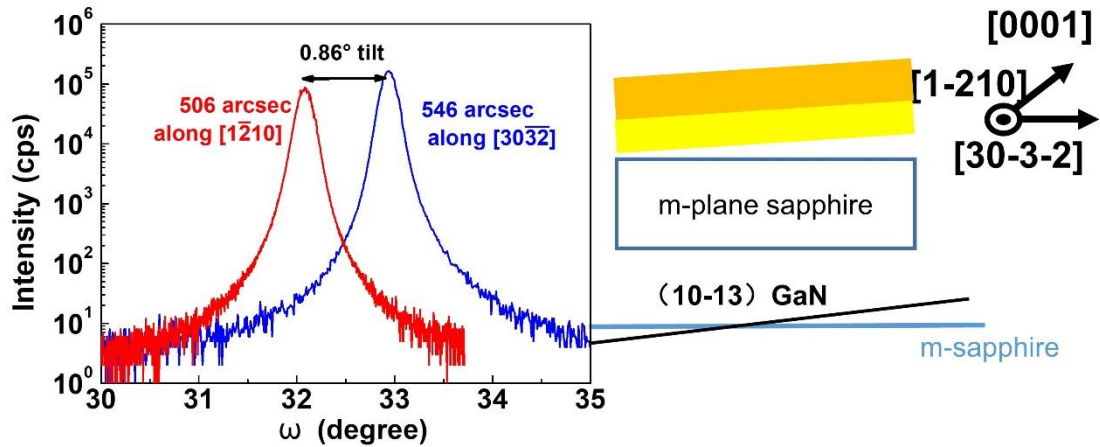


Figure 5.12 Tilt angle from X-ray rocking curve omega scans

If X-ray is scanned along and perpendicular to $[1-120]_{\text{GaN}}$, the peaks have different positions and FWHM, as shown in Figure 5.12. The main reason of the difference between peak positions scanned from $[30-3-2]_{\text{GaN}}$ and $[1-210]_{\text{GaN}}$ is that the grain always tilts along $[0001]_{\text{GaN}}$ by because of strain and dislocations [10]. Figure 5.12 indicates this.

Especially in 3D growth grains grow along $[0001]_{\text{GaN}}$. The difference of the FWHM values from different directions is caused by different number of dislocations seen by the beam along the different directions. As shown in Figure 5.13, the input X-ray is almost vertical to the dislocations, which grew along $[0001]_{\text{GaN}}$, when doing a scan along $[30-3-2]_{\text{GaN}}$. So dislocation density, which scatters the X-ray beam, is higher than the scan along $[1-210]_{\text{GaN}}$. Therefore, the FWHM along $[30-3-2]_{\text{GaN}}$ is a little wider than along $[0001]_{\text{GaN}}$.

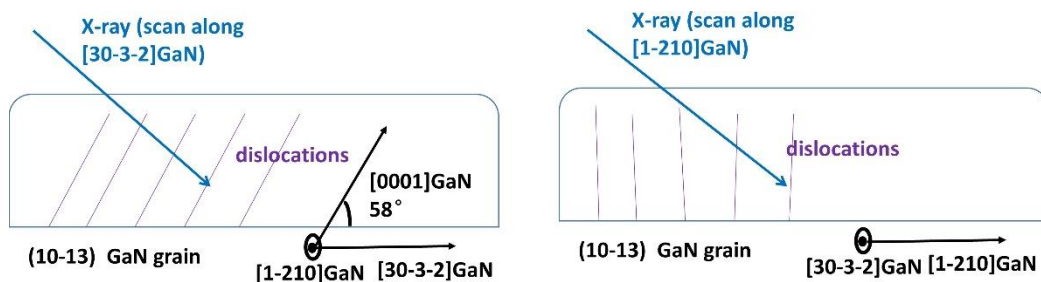


Figure 5.13 X-ray scanned from different directions

5.3.2 TEM image

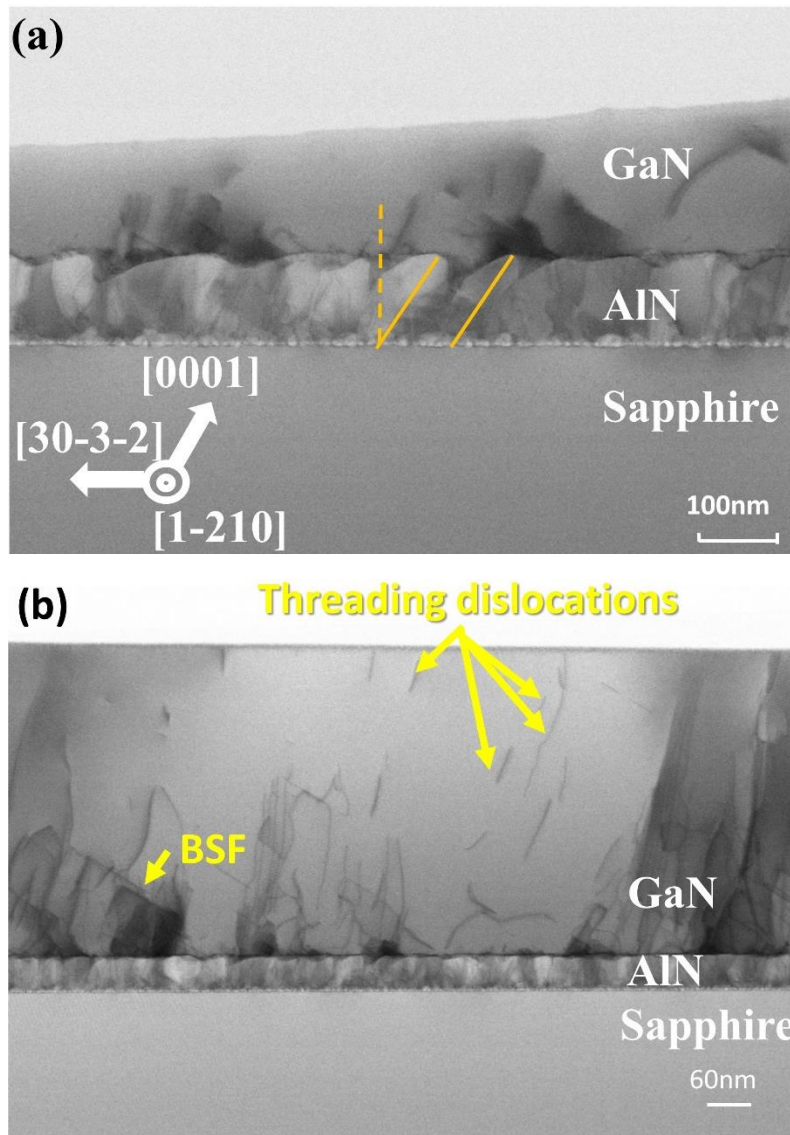


Figure 5.14 TEM cross section scan from (1-210) orientation, the very visible interface is the AlN to GaN interface, i.e. the surface at the beginning of 3D growth.

Side view scanning transmission electron microscopy (ST-TEM) was measured of a (10-13) GaN template. The cross section is from (1-210) plane. The results are shown in Figure 5.12. There are clear visible columns that are tilted by about 32° in Figure

5.14(a). This is the [0001], i.e. the initial AlN growth is mostly along the c-direction. By increasing magnification, dislocation lines could be seen (arrows in Figure 5.14(b)). There two kinds of lines. The line tilted by 32° are likely a- and a+c type threading dislocations that run along [0001] [11, 12]. From the TEM image, the threading dislocations density (TDD) is in the order of 10^9 cm^{-2} , but a side view is not suitable to give a well estimate. There is a second type of defect, which is called basal plane stacking fault (BSF). They are parallel to the (0001) surface [13-18], but should be invisible under the imaging conditions of Figure 5.14 (b). The line parallel to (0001) in Figure 5.14(b) could be only indirectly related to a BSF.

Some Al atoms has been converted into AlN during AlN sputtering, as discussed in Chapter 4.2. So there is interest to see how the MOPVE growth affects the survived Al. Because the slight grey tint after sputtering goes away after the full sequence, this is further indication that the initial Al layer is almost entirely consumed. Figure 5.15 shows a HR-STEM cross section of the interface region between AlN layer and sapphire substrate from a sample after MOVPE growth. No Al layer is visible any more, and there are no atomic columns the dark region even at higher zoom level. But atomic columns are clearly visible in the sapphire below and AlN above.

As discussed before, some part of initial Al was nitrided to AlN already during sputtering. The remaining part was likely nitrided or converted to AlN_xO_y during heating up to 1250°C under NH_3 in MOVPE prior to the AlN buffer growth [19].

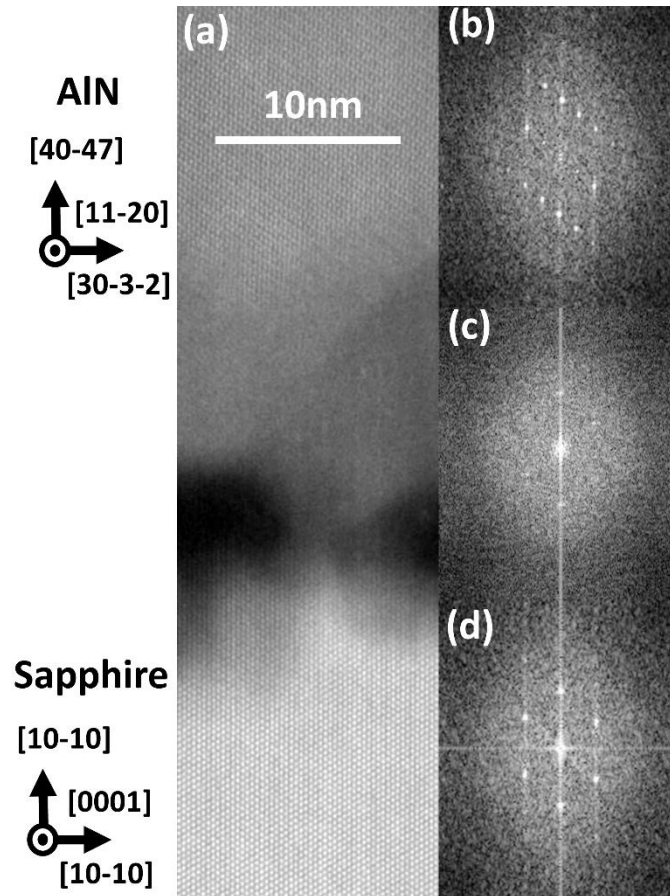


Figure 5.15 Side view of sapphire substrate and (10-13) AlN layer interface by HR-STEM. (a) is annular dark-field image. While (b), (c) and (d) are fourier transformed images of the AlN area, black area and sapphire area, respectively.

5.4 Summary

In this chapter, the epitaxy of the (10-13) GaN is studied. The (10-13) semi-polar GaN is much more difficult to smoothen than the c-plane surface. Moreover, since c-plane growth mean 3D growth for semi-polar GaN, unconventional parameters had to be used. To obtain both high crystalline quality and smooth morphology, 2 step growth is used. The first step, 3D growth is to annihilate dislocations and improve crystalline quality, and the following 2D growth is to smoothen the morphology. Optimizations have been done for 3D and 2D growth. Apart from finding good parameters for smooth or 3D growth, also the ratio of 3D growth time and 2D growth time must be adjusted.

If done correctly, (as shown in Table 5.5) both high crystalline quality and smooth samples were obtained, which could be used as templates of InGaN/GaN quantum wells.

In addition, 2D-3D loops and AlN/GaN super lattice were also tried to improve the quality of (10-13) GaN layer. The effects are shown in Table 5.8. From side view of HR-STEM, TDD is about 10^9 cm^{-2} .

Table 5.8 Methods tried to improve the quality of (10-13) GaN Layer.

Method	2D-3D loops	AlN/GaN super lattice
Effect	No improvement	Narrower FWHM but rougher surface

References

- [1] B. Leung, Q. Sun, C. D. Yerino, J. Han and M. E. Coltrin, *Semicond. Sci. Technol.* **27**, 024005 (2012)
- [2] Q. Sun, B. Leung, C. D. Yerino, Y. Zhang and J. Han, *Appl. Phys. Lett.* **95**, 231904 (2009).
- [3] H. Lee, S. Bae, K. Lekhal , T. Mitsunari, A. Tamura , Y. Honda and H. Amano, *J. Cryst. Growth* **454**, 114 (2016).
- [4] F. Schulze, A. Dadgar, J. Bläsing and A. Krost, *J. Cryst. Growth* **272**, 496 (2004).
- [5] J. C. Jeong, J. J. Jang, J. W. Hwang, C. S. Jung, J. W. Kim, K. J. Lee, H. J. Lim and O. H. Nam, *J. Cryst. Growth* **370**, 114 (2013).
- [6] T. B. Wei, Q. Hu, R. F. Duan, X. C. Wei, J. K. Yang, J. X. Wang, Y. P. Zeng, G. H. Wang and J. M. Li, *J. Electrochem. Soc.* **157**, H721 (2010).
- [7] K. Hiramatsu, K. Nishiyama, A. Motogaito, H. Miyake, Y. Iyechika and T. Maeda, *Phys. Stat. Sol. A* **176**, 535 (1999).
- [8] E. Arslan, M.K. Ozturk, A. Teke, S. Ozcelik and E. Ozbay, *J. Phys. D, Appl. Phys.* **41**, 155317 (2008).
- [9] P. Saengkaew, A. Dadgar, J. Bläsing, T. Hempel, P. Veit, J. Christen and A. Krost, *J. Cryst. Growth* **311**, 3742 (2009).
- [10] F. Oehler, M. E. Vickers, M. J. Kappers, C. J. Humphreys and R. A. Oliver, *Jpn. J. Appl. Phys.* **52**, 08JB29 (2013).
- [11] H. M. Wang, J. P. Zhang, C. Q. Chen, Q. Fareed, J. W. Yang and M. A. Khan, *Appl. Phys. Lett.* **81**, 604 (2002).

- [12] M. A. Moram, C. F. Johnston, J. L. Hollander, M. J. Kappers and C. J. Humphreys, *J. Appl. Phys.* **105**, 113501 (2009).
- [13] M. Pristovsek, Y. Han, T. Zhu, M. Frentrup, M. J. Kappers, C. J. Humphreys, G. Kozlowski, P. Maaskant and B. Corbett, *Phys. Status Solidi B* **252**, 1104 (2015).
- [14] T. Gühne, Z. Bougrioua, P. Vennéguès, M. Leroux and M. Albrecht, *J. Appl. Phys.* **101**, 113101 (2007).
- [15] J. L. Hollander, M. J. Kappers and C. J. Humphreys, *Physica B* **307**, 401 (2007).
- [16] P. de Mierry, N. Kriouche, M. Nemoz and G. Nataf, *Appl. Phys. Lett.* **94**, 191903 (2009).
- [17] T. Zhu, C. F. Johnston, M. J. Kappers and R. A. Oliver, *J. Appl. Phys.* **108**, 083521 (2010).
- [18] T. Zhu, D. Sutherland, T. J. Badcock, R. Hao, M. A. Moram, P. Dawson, M. J. Kappers and R. A. Oliver, *Jpn. J. Appl. Phys.* **52**, 08JB01 (2013).
- [19] N. Hu, D. V. Dinh, M. Pristovsek, Y. Honda and H. Amano, *Jpn. J. Appl. Phys.* **58**, SC1044 (2019).

Chapter 6 (10-13) InGaN/GaN quantum wells

6.1 Introduction

After optimizing of each layer, the (10-13) semi-polar GaN templates are good enough to grow and characterize InGaN/GaN quantum wells.

There are very few reports on (10-13) InGaN/GaN quantum wells. There were N-polar (10-1-3) InGaN/GaN LED reported at the very beginning of semi-polar GaN research in 2005 [1, 2]. Also the (10-13) orientation is included in two overview studies, e. g. when investigating the indium incorporation on various orientation. In one study [3], all InGaN/GaN quantum wells were grown simultaneously under the same condition. The templates were cut from GaN bulk. So the properties could be kept the same. The result in Figure 6.1 show that the (10-13) orientation had the lowest indium incorporation, much lower than the content of c-plane InGaN/GaN quantum well, less than 5%. In the other one [4], bulk substrates were also applied to study (10-13) and (10-1-3) InGaN/GaN quantum wells. (10-13) quantum well has much stronger PL intensity than (10-1-3) one under the same growth condition. PL wavelength of (10-13) quantum well is about 500nm while FWHM is about 52nm. Figure 1.4 (c) shows the results. Two studies did not include the (10-13), but many others including the neighboring (10-12) orientation [5, 6].

Among the different explanations step bonding configuration, strain energy, or N-H bonds are some of the origins discussed for low indium incorporation in these surface. However, there is no study how to tackle this issue.

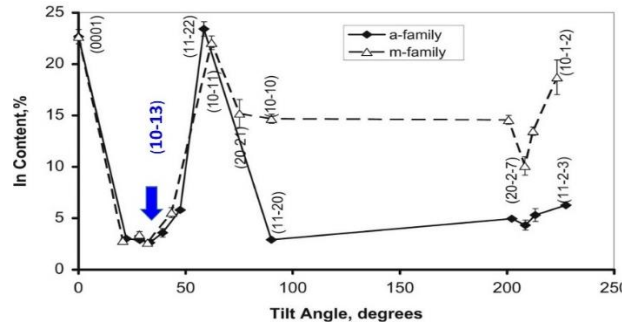


Figure 6.1 Indium content of each quantum wells on each orientation from literature.

Since the aim of this study is to make (10-13) InGaN/GaN quantum wells for green LEDs, high indium incorporation ratio is needed, especially because the weaker QCSE will blue shift emission compared to c-plane at same indium content. This is the main problem studied in this chapter.

6.2 Growth of (10-13) InGaN/GaN quantum well

The (10-13) InGaN/GaN quantum wells were grown on the (10-13) GaN templates in MOVPE. The growth conditions are listed in Table 6.1. Temperature and TEG flow were varied in the experiments. After growth, the indium incorporation ratio was measured by comparing simulations to XRD measurements. Since the strain of semi-polar InGaN/GaN quantum wells are different from c-plane InGaN/GaN quantum wells, a special calculation method is needed, which reference is given in Chapter 1.6 and an example is in Figure 1.7. C-plane InGaN/GaN quantum wells were used as control samples grown together with (10-13) InGaN/GaN quantum wells, and also to get input on the thickness of the quantum wells and barriers.

Table 6.1 Growth parameters of InGaN/GaN quantum well

Layer	High growth rate mode		Low growth rate mode	
	Well layer	Barrier layer	Well layer	Barrier layer
Precursors	TEGa, TMIIn, NH ₃	TEGa, NH ₃	TEGa, TMIIn, NH ₃	TEGa, NH ₃
Chamber pressure	26kPa	26kPa	26kPa	26kPa
Carrier gas	H ₂	H ₂	H ₂	H ₂
Total flow	15000sccm	15000sccm	15000sccm	15000sccm
V/III ratio	6150	9980	38030	93600
NH ₃ partial pressure	8667Pa	8667Pa	8667Pa	8667Pa
TEGa partial pressure	0.87Pa	0.87Pa	0.093Pa	0.093Pa
TMIIn partial pressure	0.54Pa		0.135Pa	
Growth temperature	660-720°C	850°C	660-720°C	850°C
Growth time	46s	180s	200s	480s
Repeats	5-10		5-10	

Figure 6.2 shows the growth results. Two growth rates were investigated: The standard one for (0001) which is the low growth rate of 0.8 nm/min and 3.7 nm/min for high growth rate.

For both low and high growth rate the indium content decreases with increasing growth temperature. The reason is that it is easy for indium to desorb from the surface before it is incorporated [7]. From this one would expect a higher indium incorporation at higher growth rates (since the indium has less time for desorption).

Especially for the low growth rate that the indium content of the (10-13) InGaN/GaN quantum wells is much lower, almost 50%-80% lower than the c-plane InGaN/GaN quantum wells, which is similar to literature [3].

However, at high growth rate, the indium content of (10-13) and (0001) InGaN/GaN quantum wells are almost similar. This shows that indium desorption is much higher from the (10-13) surface. This may be due to a more difficult incorporation compared to (0001), and thus the indium could stay longer on the surface at low growth

rates and thus desorb more likely. Lympherakis et al. noted that the almost vertical dangling bonds on (0001) and (11-22) surfaces coincidences with high indium incorporation, while the (10-13) only have tilted bonds [8]. Furthermore, they showed that the indium has a high activation to incorporate beyond the first atomic layer [9].

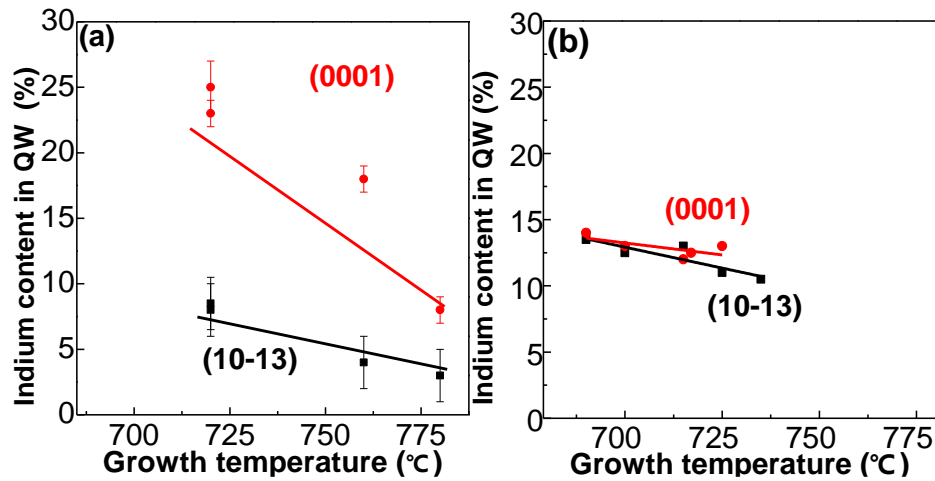


Figure 6.2 Indium content in quantum wells on both (10-13) plane and c-plane templates. (a) low growth rate mode, (b) high growth rate mode.

6.3 Characterization of (10-13) InGaN/GaN quantum wells

For application it is very important to know if the quantum well relaxed or strained. An X-ray reciprocal space map (RSM) of the 10-15 reflection was recorded in Figure 6.3, for an indium content of 17% (from the calculation which assumes a fully strained well). All the satellite reflections stay in vertical line below the GaN main reflection. Thus the (10-13) quantum is full strained [10, 11]. By X-ray check, all the (10-13) InGaN/GaN quantum wells in the experiments were full strained

Photoluminescence (PL) spectra [12, 13] of were measured at room temperature. Figure 6.4 show the dominating InGaN well emission with no yellow luminescence, which is typically associated with carbon-vacancy complexes [14-17]. Until now, the

longest PL wavelength of (10-13) InGaN/GaN quantum wells is 523nm, as shown in Figure 6.4. It's longer than the wavelength from literature [4]. The corresponding indium incorporation ratio is 17%, which is also the highest until now.

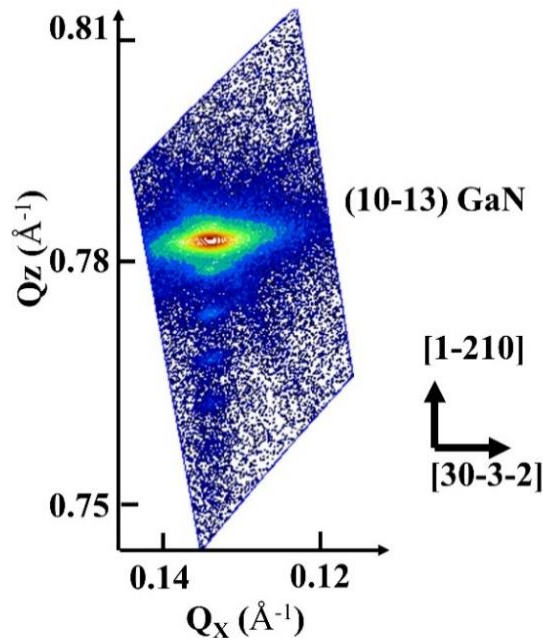


Figure 6.3 X-ray RSM of the asymmetric 10-15 GaN reflection of a (10-13) InGaN/GaN QW. ($X_{In}=17\%$)

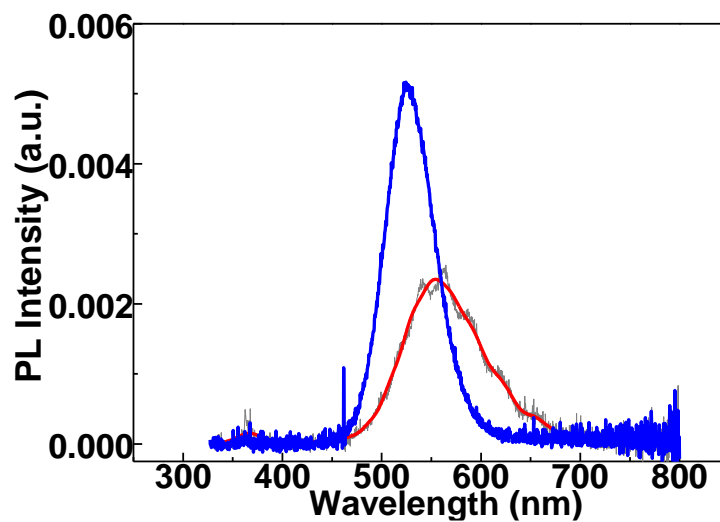


Figure 6.4 PL spectra of one (10-13) and one (0001) InGaN/GaN quantum wells grown with high growth rate.

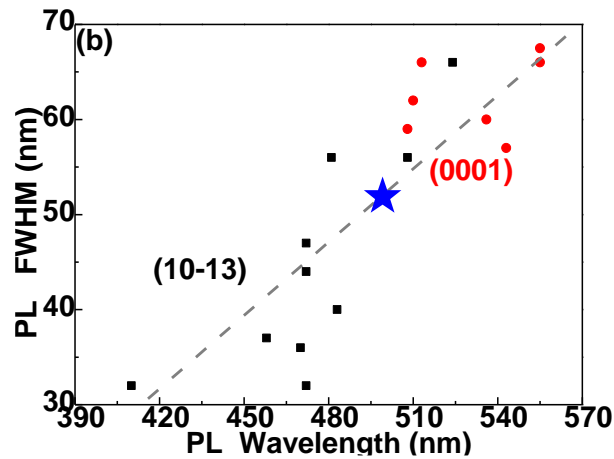


Figure 6.5 Relationship between PL wavelength and PL FWHM. Blue star is the data from literature [4].

Figure 6.5 shows relationship between PL FWHM and PL wavelength. The longer the PL wavelength, the wider is the PL FWHM. The FWHM is affected by several things, usually alloy broadening is given as one reason. Interestingly the broadening of many polar and non-polar InGaN/GaN quantum wells is mostly a function of the emission wavelength [18]. The same can be observed in Figure 6.5, the data from (10-13) and (0001) follow the same trend of wavelength over FWHM. This indicates that the (10-13) quantum wells are of the same quality than the (0001) quantum wells. Additionally, the data from literature, blue star in Figure 6.5 (b), matches to the trend of this study too. It means the samples also have similar quality with report. However, GaN bulk substrate was used in the report while hetero epitaxy layers were applied in this study.

6.4 Summary

In this chapter, (10-13) InGaN/GaN quantum well have been studied. By increasing the growth rate by five times for the InGaN layer, the indium content ratio

has been increased almost to the same content as (0001). Up to 17% Indium were incorporated fully strained in an (10-13) quantum well, which is almost 3 times higher than the value in the literature. The PL FWHM follow the same trend for (10-13) quantum wells as on (0001), indicating a comparable quality even at faster growth rates. This gives a good outlook to realize a green LED. The longest PL wavelength is 523nm, which is also longer than the value in report. The PL FWHM of this study can keep the same trend of the data in report that quantum well was grown on GaN bulk substrate. It means epitaxy quality in this work is better the quality in report. Table 6.2 shows the results from both this study and literature.

Table 6.2 Properties of (10-13) InGaN/GaN quantum wells

Property	Indium content ratio	PL wavelength	PL FWHM
This study	17%	523nm	Same trend
Literature	About 5%	About 495nm	

References

- [1] A. Chakraborty, T.J. Baker, B.A. Haskell, F. Wu, J.S. Speck, S.P. DenBaars, S. Nakamura and U.K. Mishra, *Jpn. J. Appl. Phys.* **44**, L945 (2005).
- [2] R. Sharma, P. M. Pattison, H. Masui and R. M. Farrell, *Appl. Phys. Lett.* **87**, 231110(2005).
- [3] R. Bhat and G. M. Guryanov, *J. Cryst. Growth*, **433**, 7 (2016).
- [4] D. D. Koleske, S. R. Lee, M. H. Crawford, M. E. Coltrin and P. T. Fini, Sandia Report, SAND2013-5065 (2013).
- [5] K.L. Choy, *Progress Mater. Sc.* **48**, 57 (2013).
- [6] N. Motegi, Y. Kashimoto, K. Nagatani, S. Takahashi, T. Kondo, Y. Mizusawa and I. Nakayama, *J. Vac. Sci. Technol. B* **12**, 1906 (1995).
- [7] M. Pristovsek, J. Stellmach, M. Leyer and M. Kneissl, *phys. status solidi C* **6**, S565 (2009).
- [8] J. Kioseoglou, E. Kalesaki, L. Lymperakis, T. Karakostas and P. Komninou, *J. Phys.: Condens. Matter* **25**, 045008 (2013).
- [9] A. I. Duff, L. Lymperakis and J. Neugebauer, *Phys. Rev. B* **89**, 085307 (2014).
- [10] H. Heinke, S. Einfeldt, B. Kuhn-Heinrich, G. Plahl, M. O. Moller and G. Landwehr, *J. Phys. D, Appl. Phys.* **28**, A104 (1995).
- [11] Q. Wang, J. Bai, Y. P. Gong and T. Wang, *J. Phys. D, Appl. Phys.* **44**, 395102 (2011).
- [12] S. Nagahama, T. Yanamoto, M. Sano and T. Mukai, *Jpn. J. Appl. Phys.* **40**, 3075 (2001).

- [13] D. Queren, M. Schillgalies, A. Avramescu, G. Br uderl, A. Laubsch, S. Lutgen, and U. Strau, *J. Cryst. Growth* **311**, 2933 (2009).
- [14] M. S. Jeong, Y. W. Kim, J. O. White, E. K. Suh, M. G. Cheong, C. S. Kim, C. H. Hong and H. J. Lee, *Appl. Phys. Lett.* **79**, 3440 (2001).
- [15] J. Elsner, R. Jones, M. I. Heggie, P. K. Sitch, M. Haugk, Th. Freunheim, S. Oberg, and P. R. Briddon, *Phys. Rev. B* **58**, 12571 (1998).
- [16] X. Li, P. W. Bohn, J. Kim, J. O. White and J. J. Coleman, *Appl. Phys. Lett.* **76**, 3031 (2000).
- [17] S. H. Yang, K. S. Nahm, Y. B. Hahn, Y. S. Lee, M. S. Jeong and E. K. Suh, *J. Korean Phys. Soc.* **36**, 182 (2000).
- [18] Y. Robin, M. Pristovsek¹, H. Amano, F. Oehler, R. A. Oliver and C. J. Humphreys, *J. Appl. Phys.* **124**, 183102 (2018).

Chapter 7 Summary and Outlook

7.1 Summary

As first steps towards efficient (10-13) LEDs the preparation of high quality (10-13) GaN template and InGaN/GaN quantum well growth were studied

If GaN is grown directly on m-plane sapphire, always twinned N-polar (10-1-3) GaN is obtained. The directional sputtering and following MOVPE overgrowth in this works delivered untwinned Ga-polar (10-13) GaN layers. During directional sputtering, a certain direction should be fixed towards the target without rotation. That's the reason of the name "directional sputtering". Until now, directional sputtering is the only method to achieve untwinned metal-polar (10-13) AlN layers.

Several optimizations have been done to improve the quality of (10-13) GaN templates. (10-10) m-plane sapphire was applied as substrate since low mismatch with (10-13) AlN instead of (100) Si used before. This reduced the FWHM of (10-13) GaN from 2000 to 800 arcsec. The actual procedure of directional sputtering includes Al sputtering and AlN sputtering steps. The FWHM could be further reduced to less than 550 arcsec by optimizing the Al sputtering.

Further optimization concerned the MOVPE growth. Two growth steps, 3D growth+2D growth, were used to first make a good crystalline quality and then smooth the surface. After optimization of growth condition and ratio of 3D/2D, the (10-13) GaN templates had less than 550 arcsec FWHM and 30 nm RMS.

As a further step to LEDs, (10-13) InGaN/GaN quantum well growth was studied.

The main focus of the InGaN/GaN quantum study was increasing the indium content of (10-13) quantum wells. This was achieved using a high growth rate for the InGaN layer. The Indium content ratio of (10-13) quantum well could arrive 17% fully strained, which is much higher than data in literature.

Directional sputtering could also be used to obtain (10-10), (10-13), (10-14) and even (0001) orientation AlN on m-plane sapphire by changing the thickness or temperature of the initial Al sputtering. The m-plane sapphire would lattice match to (10-10), (10-13) and to a lesser degree to (10-14) AlN. The thickness of Al initial layer was measured by optical transmission method to be only 0.8 nm for (10-13) AlN, while a thicker layer favored (10-14) and a thinner (10-10). This can be explained by Al providing mobility for AlN species in the following sputter step to find their best places (which are (10-13)).

Contributions of this work are listed as below:

Develop the directional sputtering method by using m-plane sapphire substrate.
Successfully measure the thickness of sputtered Al layer.

For the first time, control orientations of AlN/GaN epitaxy layers on m-plane sapphire by adjusting Al sputtering.

Successfully eliminate twinning crystal of (10-13) GaN by studying AlN buffer layer.

For the first time, apply two steps (3D growth + 2D growth) into (10-13) GaN hetero epitaxy and get the best (10-13) hetero epitaxy layers.

For the first time, systemically study (10-13) InGaN/GaN quantum wells and

obtain highest indium incorporation and longest PL wavelength sample.

7.2 Outlook

Many things are not fully finished in this study, especially two aspects. One is the realization of a full green LED, the main aim. The other is a better understanding of the underlying mechanism and physics.

Of course the (10-13) template can be improved more. The AlN buffer could be further optimized by high temperature annealing [1, 2]. For InGaN/GaN quantum well, higher indium content ratio and a more extensive PL characterization is needed. From literature, low temperature InGaN under layer did enhance the radiative recombination efficiency of (0001) InGaN/GaN quantum well [3]. It is interesting to see if this works on (10-13) InGaN as well, since the point defect may be very different.

For LED, doping is the foremost issue. There are no data on either p- or n-doping. Furthermore, the (10-13) surface easily starts to roughen, hence the growth conditions must be chosen with care. However, many semi-polar orientations can be doped very highly with Si, so maybe n-doping is easy on (10-13) too. Mg is tried next. However, literature cannot help, since Mg doping varies strongly with different orientations [4, 5]. Similar to Indium incorporation, growth rate may be the key parameter.

For InGaN/GaN quantum well, higher Indium content ratio is needed. It was found that higher growth rate of InGaN strongly increases Indium incorporation into the layer. However, impact of growth rate on the InGaN quality needs to be checked. Furthermore, InGaN under layers is a method still to be tried [3].

For mechanism and physics, two things are still unknown. First, what kills the twinning crystal of (10-13) GaN. At the beginning, shadow effect during AlN sputtering was thought as the reason. Then the thickness of AlN was wondered. Second, 523nm PL wavelength is too longer for 17% Indium content ratio quantum well. Both these two things needs to be checked and studied deeply in the future work.

References

- [1] H. Miyake, C. H. Lin, K. Tokoro and K. Hiramatsu, *J. Cryst. Growth*, **456**, 155 (2016).
- [2] D. D. Dinh, N. Hu, Y. Honda, H. Amano and M. Pristovsek, *J. Cryst. Growth*, **498**, 377 (2018)
- [3] C. Haller, J. F. Carlin, G. Jacopin, D. Martin, R. Butté and N. Grandjean, *Appl. Phys. Lett.* **111**, 262101 (2017).
- [4] M. Pristovsek, C. J. Humphreys, S. Bauer, M. Knab, K. Thonke, G. Kozlowski, D. O'Mahony, P. Maaskant and B. Corbett, *Jpn. J. Appl. Phys.* **55**, 05FJ10 (2016).
- [5] S. C. Cruz, S. Keller, T. E. Mates, U. K. Mishra and S. P. DenBaars, *J. Cryst. Growth* **311**, 3817 (2009).

Appendix

1. (11-22) orientation GaN

Changing the direction of sapphire during sputtering to $[0001]_{\text{sapphire}}$ towards the Al target (as Figure A1 (a)) will result in the (11-22) orientation of AlN/GaN, as shown in Figure A1 (c) and (d). Figure A1 (c) and (d) show the X-ray $2\theta-\omega$ and ω scans of (11-22) GaN sample. So orientations can be formed even with a very thin layer. From this point, Al sputtering could help to prevent the twinning. The mismatch is 16.1% along $[1-100]_{\text{GaN}} // [1-210]_{\text{sapphire}}$ is 16.1% while -6.3% along $[0001]_{\text{GaN}} // [-1-123]_{\text{sapphire}}$. To (11-22) AlN, the corresponding values are 13.3% and -9.6%. [1]

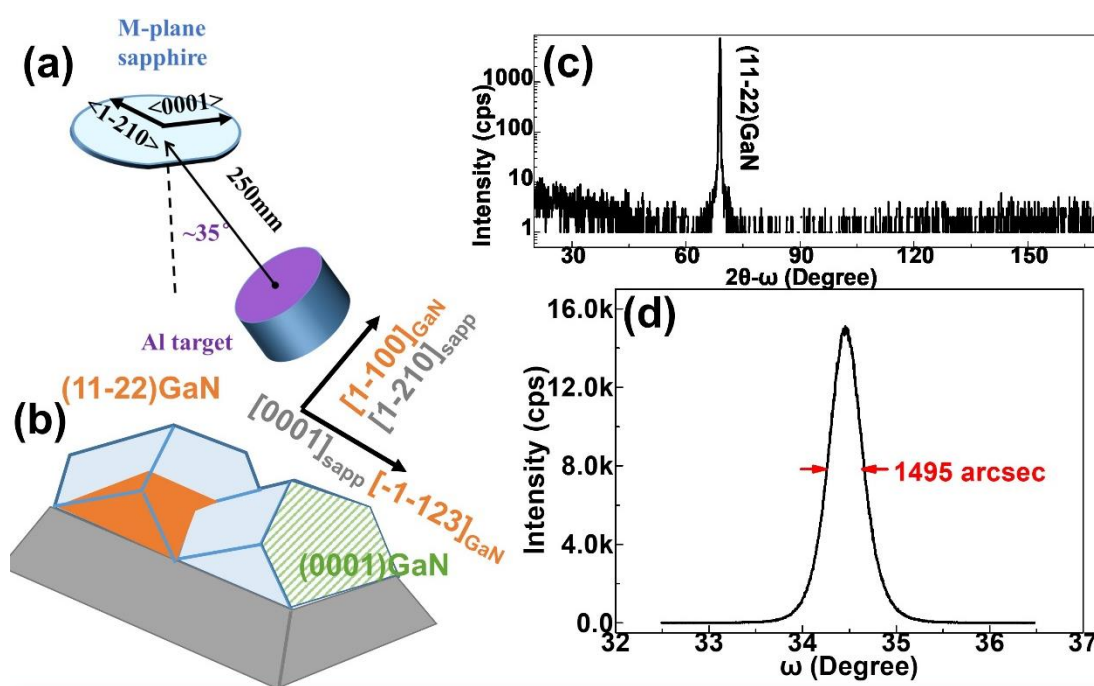


Figure A1 (a) Schematic geometry of directional sputtering for (11-22) GaN. (b) In-plane alignments of (11-22) GaN unit-cells on m-plane sapphire. X-ray (c) $2\theta-\omega$ and (d) ω scan of (11-22) GaN sample.

2. Optical transmission influenced by oxidation and roughness of Al layers

Figure A2 shows the optical transmission simulation results w/o roughness. The roughness is simulated by optical grating with structure of Al(3nm)/air(3nm). The result of the one with roughness (optical grating) is similar, no shift in energy but with a little

higher transmission ratio, to the one without roughness (optical grating). This is caused by the “air” in the grating structure.

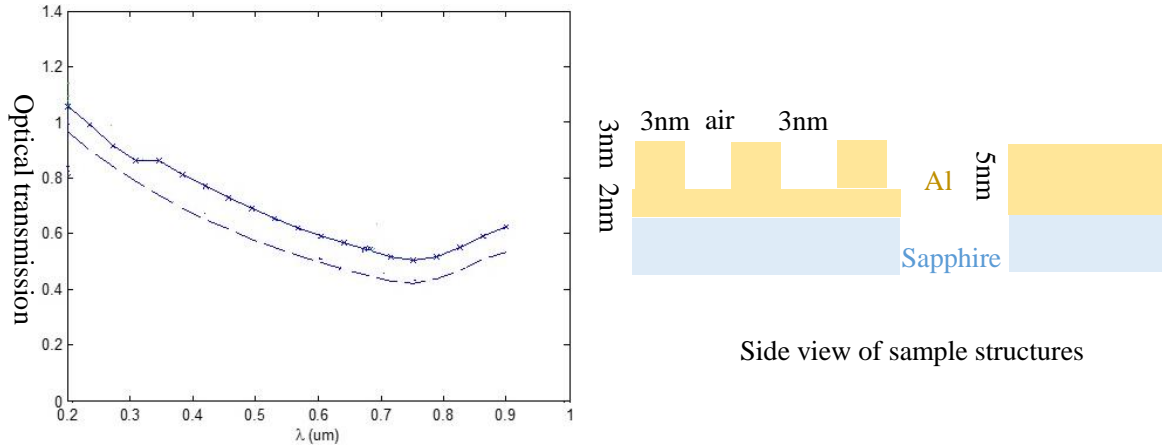


Figure A2 Optical transmission simulation results of 5nm Al layers on 380μm sapphire substrates. Solid line is the result with roughness (optical grating) while dash line is the results of pure Al layer without any structure.

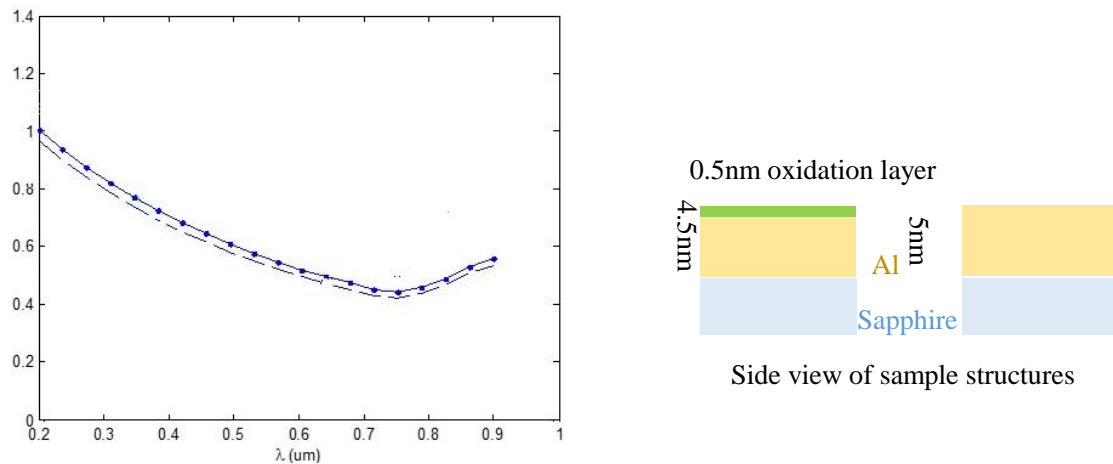


Figure A3 Optical transmission simulation results of 5nm Al layers on 380μm sapphire substrates. Dot line is a fitting with 0.5nm oxidation layer on the top while dash line is a fitting with pure Al layer without oxidation layer.

Figure A3 shows the optical transmission simulation results of Al layer w/o an oxidation layer. The oxidation layer is 0.5nm of Al_2O_3 for simplification while the Al layer is 5 nm. This oxidation layer does not influence the optic transmission much since it is very thin and the refractive index (n) and extinction coefficient (k) values of Al_2O_3 are less than the values of Al. The optical parameters (n and k) in these simulations were parameters of bulk Al too. The simulation method is from [2].

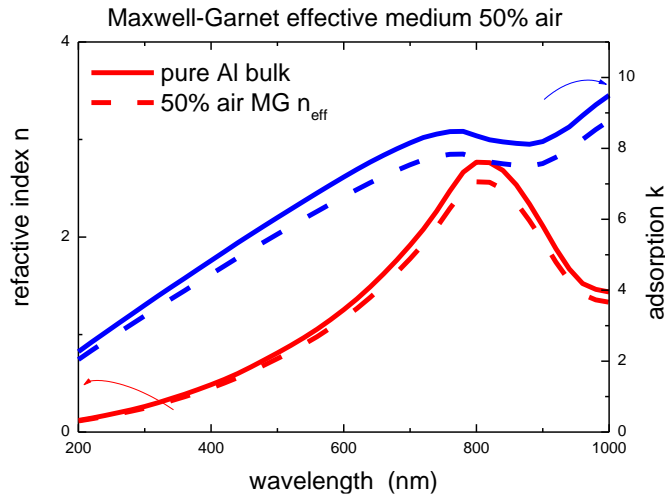


Figure A4 Change of refractive index when using effective medium (Maxwell-Garnett)

Additionally, Figure A4 shows the change of refractive index and adsorption using an effective medium approach for surface roughness. It is clearly seen that the changes are small.

From these results, it can be seen that roughness and oxidation could influence the shape and intensity of optical transmission spectra but only a little. The big deviation in Figure 3.3 (a) for thin Al layers between measured data and calculated data should be caused by variation of dielectric functions [3] in ultrathin layers.

The optical simulations of Figure A1 and A2 are done with help from Dr. Junda Zhu (Postdoctor researcher at Nankai University) and refractive index simulation is done with help from Prof. Markus Pristovsek (Designated professor at International Research Section, iMaSS, Nagoya University)

3. Twinning of (10-13)GaN

To the (10-13) GaN/AlN on m-plane sapphire, twinning occurs along the $[1-210]_{\text{sapphire}}$, as shown in the Figure A5 (a). Except the twinning, tilt of grain also occurs along this direction. The tilt of grain may also eliminate the twinning. If the twinned grains have different tilt angles (like Figure A5(b), $\angle\alpha \neq \angle\beta$), the grains with bigger tilt angle may disappear since lower growth rate with the growth going on. It could be one reason which prevents the twinning. To verify this, chi-phi mapping in X-ray can

be used to check (0002) GaN peak. (χ : $32^\circ \pm 5^\circ$, around the angle between $(10\text{-}13)_{\text{GaN}}$ and $(0001)_{\text{GaN}}$, ϕ : the angle where could find $(0002)_{\text{GaN}}$ peak+ 180°). If another peak can be found, this assumption can be verified.

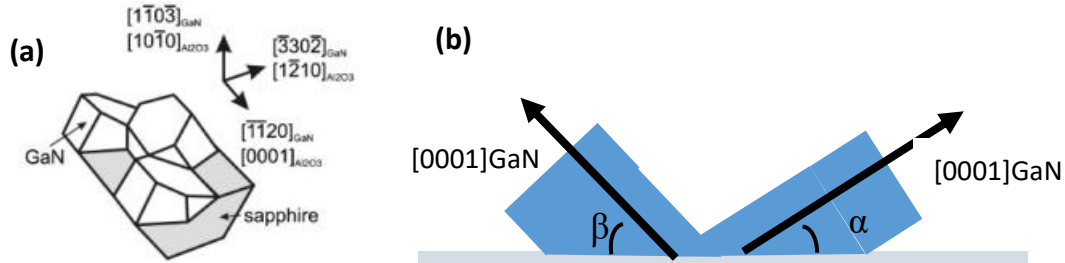


Figure A5 (a) Sketch of twinned (10-1-3) GaN on m-plane sapphire substrate [1]. (b) Sketch of twinned (10-1-3) GaN with different tilt angles. (Side view from $(1\text{-}210)_{\text{GaN}} // (0001)_{\text{sapphire}}$)

Except tilt of grain, other stuffs also could prevent the twinning. Thickness of AlN layer is the only one property found relative with twinning in this study. However, if grow on m-plane sapphire directly, no matter (10-13) AlN or GaN will be twinned [3]. And (10-13) GaN will also be twinned without AlN buffer even on directional sputtered templates. Some information could be got from literatures. Untwinned but N-polar (10-13) GaN could be grown on m-plane sapphire by HVPE [4]. Untwinned (10-13) AlN has also be achieved on m-plane sapphire directly by ammonia-free high temperature metalorganic vapor phase epitaxy (AFHT-MOVPE) at 1650°C [5]. Compared normal MOVPE growth, there are several different aspects in [4] and [5]. First, chemical reactions are different. Second, HVPE has much higher growth rate. Third, AFHT-MOVPE has much higher growth temperature. Additionally, combining results in this study and [5], it seems that it's easier for AlN to become untwinned than GaN (Fourth). Among these candidate reasons, the second one could be coincident to tilt of grain assumption. The faster crystal grows, the easier for preponderant grains to cover the other grain in Figure A5 (b). The fourth is from this study. So the second and fourth one needs to be considered firstly. Study of twinning is still ongoing.

Reference

- [1] M. Frentrup, S. Ploch, M. Pristovsek and M. Kneissl, *Phys. Status Solidi B* **248**, 583 (2011).
- [2] H. Liu and P. Lalanne, *Nature* **452**, 728 (2008).
- [3] H. V. Nguyen, I. An and R. W. Collins, *Phys. Rev. B* **47**, 3947 (1993).
- [4] T. Wernicke, C. Netzel, M. Weyers and M. Kneissl, *Phys. Status Solidi C* **5**, 1815 (2008).
- [5] X. Q. Shen, K. Kojima and H. Okumura, *Appl. Phys. Express* **13**, 035502 (2020).

Achievements list

Journal publications:

(1) “How to obtain metal-polar untwinned high-quality (1 0 –1 3) GaN on m-plane sapphire”, **Nan Hu**, Duc V. Dinh, Markus Pristovsek, Yoshio Honda and Hiroshi Amano, Journal of Crystal Growth, Vol.507, pp.205-208 (2019)

(2) “Controlling the orientations of directional sputtered non- and semi-polar GaN/AlN layers”, **Nan Hu**, Duc V. Dinh, Markus Pristovsek, Yoshio Honda and Hiroshi Amano, Japanese Journal of Applied Physics, Vol. 58, No. SC, pp. 1044-1-1044-4 (2019)

(3) “High-temperature thermal annealing of nonpolar (10-10) AlN layers sputtered on (10-10) sapphire”, Duc V. Dinh, **Nan Hu**, Yoshio Honda, Hiroshi Amano and Markus Pristovsek, Journal of Crystal Growth, Vol.498, pp.377-380 (2018)

(4) “Aluminium incorporation in polar, semi- and non-polar AlGa_{1-x}N layers: a comparative study of x-ray diffraction and optical properties”, Duc V. Dinh, **Nan Hu**, Yoshio Honda, Hiroshi Amano and Markus Pristovsek, Scientific Reports, Vol.9, p.15802 (2019)

(5) “Untwinned semipolar (10-13) Al_x Ga_{1-x}N layers grown on m-plane sapphire”, Duc V. Dinh, **Nan Hu**, Yoshio Honda, Hiroshi Amano and Markus Pristovsek,

Semiconductor Science and Technology, Vol.34, No.12, p.125012 (2019)

(6) “Indium incorporation and optical properties of polar, semipolar and nonpolar InAlN”, Duc V. Dinh, **Nan Hu**, Yoshio Honda, Hiroshi Amano and Markus Pristovsek, Semiconductor Science and Technology, Vol.33, No.3, p.035004 (2020).

International conference presentations:

(1) “Obtaining metal-polar (10-13) GaN on directionally AlN sputtered m-plane sapphire substrate”, **Nan Hu**, Duc V. Dinh, Markus Pristovsek, Yoshio Honda and Hiroshi Amano, 19th International Conference on Metalorganic Vapor Phase Epitaxy, June 3-8, Nara (Japan), 7C-1.4 (2018) (Oral)

(2) “Growth and characterization of templates and InGaN/GaN quantum wells on (0001), (10-13), (11-22) and (10-10) orientations”, **Nan Hu**, Duc V. Dinh, Markus Pristovsek, Yoshio Honda and Hiroshi Amano, International Workshop on Nitride Semiconductors (IWN 2018), November 11–16, Kanazawa (Japan), GR13-4, (2018) (Oral)

(3) “Growth and Characterization of Untwinned (10-13) GaN Templates and InGaN/GaN Quantum Wells”, **Nan Hu**, Duc V. Dinh, Markus Pristovsek, Yoshio Honda and Hiroshi Amano, 13th International Conference on Nitride Semiconductors, July 7-12, Bellevue (USA), G10.03 (2019) (Oral)

Domestic conference presentations:

(1) “Orientation control of non- and semi-polar GaN using directional AlN sputtering on (10-10) Sapphire”, **Nan Hu**, Duc V. Dinh, Yoshio Honda, Hiroshi Amano and Markus Pristovsek, 65th JSAP(Japan Society of Applied Physics) Spring Meeting, March 17-20, Tokyo (Japan), 18p-E202-12 (2018) (Oral by Markus Pristovsek)

Acknowledgement

Time always flies. My PhD course will finish very soon. I can remember details the first time I came to Nagoya University. It feels like just yesterday. I got much help during these three years. I appreciate for all the people who help me.

First and foremost, I would like to express my most heartfelt gratitude to my Professor Hiroshi Amano for his generous support, insightful guidance and indispensable encouragement throughout my doctoral course. I am deeply grateful for the opportunity he gave to my doctoral program in such amazing laboratory. At that time, I was an unemployed guy. His passionate and energetic working style and talented thinking model have brought profound influence to my attitude towards research and life. I have been extremely fortunate and honored to be his student.

I would like to thank Professor Yoshio Honda, Professor Shugo Nitta, Professor Atsushi Tanaka, Assistant Professor Maki Kushimoto, Assistant Professor Manato Deki, and Dr. Heajeong Cheong on their advice and kind assistance to my research.

Professor Takeuchi and Professor Miyazaki gave me a lot of guidance and suggestions of this thesis. Thanks for their reviewing.

I am grateful to Ms. Hosoe, Ms. Tatsumi, Ms. Fujie, Ms. Ito, Ms. Tsukada, Ms. Kinouchi and Ms. Kondo. For their assistance in many aspects in my stay in Nagoya.

Professor Markus Pristovsek, we study and work together during my PhD time. He gives me advisements on both academic and life. When I meet trouble, he help me with his goodness, erudition and optimism, like family. The same thanks to Dr. Duc

Van Dinh, Dr. Hojun Lee, Dr. Yoann Robin, Dr. Geoffrey Avit and (Dr.) Stefano Vichi.

Professor Yuhuai Liu, Professor Yongjin Wang always encourage me in these 3 years. Dr. Xu Yang, Dr. Zhibin Liu, (Dr.) Zheng Ye, (Dr.) Qiang Liu, Yaqiang Liao, Jin Yan, Hongshuo Wang, Professor Guohao Yu, Dr. Ting Liu, (Dr.) Jia Wang, (Dr.) Jian Shen, Dr. Zhe Cheng, Wentao Cai, Donglin Wu and Dr. Luke Yates. Thanks for give interest and fun to me. The relationships with you should be great experience.

Thanks to Dr. Usami, Dr. Ueoka, Ando san, Ogura san, Oyama san, Miura san, Takahashi san, Sakai san et al. I got many help from them.

My family (parents, wife and babies) always support me no matter what difficult I meet. I have a baby in my D2 time. She is an angel. (So as Miaomiao, Sansan, Simba, Panda Jr, Meimei et al.) I have meet my wife more than 12 years. We go through both happiness and sadness in these years. In my childhood, I liked to play in my father's lab. He leaded me to research.

Professor Lei Hao (SHAO) showed me the prospect of research. I would not study abroad without her points. Prof. Dexian Zhang and Prof. Hongkun Cai gave me large help in application time. Dr. Junda Zhu helped me to do the optical simulations. Thanks.